MATHEMATICAL MODELLING OF ELASTODYNAMIC PROBLEMS IN TWO TEMPERATURE THERMOELASTIC MEDIA

A Thesis Submitted for the Award of the Degree of

DOCTOR OF PHILOSOPHY

in

Mathematics

By

Gulshan Kumar

Registration Number: 41900079

Supervised By

Dr. Sachin Kaushal

Professor

Department of Mathematics,

School of Chemical Engineering and Physical Sciences

Lovely Professional University, Punjab

Co-Supervised by

Dr. Rajneesh Kumar

Professor

Department of Mathematics,

Kurukshetra University,

Kurukshetra-Haryana

LOVELY PROFESSIONAL UNIVERSITY
PHAGWARA - PUNJAB
2025

DECLARATION

I, hereby declared that the presented work in the thesis entitled "**Mathematical Modelling of Elastodynamic Problems in Two Temperature Thermoelastic Media**" in fulfilment of degree of **Doctor of Philosophy (Ph.D)** is outcome of research work carried out by me under the supervision of Dr. Sachin Kaushal, Professor, in the School of Chemical Engineering and Physical Sciences of Lovely Professional University, Punjab, India and co-supervision of Dr. Rajneesh Kumar, Professor, in the Department of Mathematics, Kurukshetra University, Kurukshetra. In keeping with general practice of reporting scientific observations, due acknowledgements have been made whenever work described here has been based on findings of other investigator. This work has not been submitted in part or full to any other University or Institute for the award of any degree.

(Signature of Scholar)

Gulshan Kumar Sharma

41900079

School of Chemical Engineering and Physical sciences

Lovely Professional University,

Punjab

CERTIFICATE

This is to certify that the work reported in the Ph.D thesis entitled "**Mathematical Modelling of Elastodynamic Problems in Two Temperature Thermoelastic Media**" submitted in fulfillment of the requirement for the award of the degree of **Doctor of Philosophy (Ph.D)** in the School of Chemical Engineering and Physical Sciences, is a research work carried out by Gulshan Kumar (41900079) is bonafide record of his original work carried out under our supervision and that no part of thesis has been submitted for any other degree, diploma or equivalent course.

Dr. Sachin Kaushal
Professor
School of Chemical Engineering and
Physical Sciences
Lovely Professional University, Punjab

Dr. Rajneesh Kumar
Professor
Department of Mathematics,
Kurukshetra University,
Kurukshetra.

ABSTRACT

The thesis entitled "**Mathematical Modelling of Elastodynamic Problems in Two Temperature Thermoelastic Media**" consists of five chapters, and a list of references is given at the end of this thesis. The subject matter is laid out in the following way:

Chapter1 is concerned with the introductory part. We have given a brief introduction of (i) Thermoelasticity (ii) Green-Lindsay (G-L) theory (iii) Green-Naghdi Thermoelasticity Theory (iv) Two temperature (TT) and Hyperbolic two temperature model (HTT) (v) Dual Phase Lag (DPL) model (vi) Non-local (N-L) theory (vii) Fractional order theory of thermoelasticity (viii) Modified Green-Lindsay (MGL) thermoelasticity (ix) Moore-Gibbson-Thomson (MGT) theory of thermoelasticity.

Chapter 2 deals with a two-dimensional deformation problem owing to the heat source and thermomechanical loading in a half-space that is homogeneous, isotropic, and thermoelastic under the modified Green-Lindsay (MGL) to study the influence of non-local (N-L) and two temperature (TT). The governing equations are converted into dimensionless form, and potential functions are used for further simplification. The problem is simplified by the integral transform technique (Laplace Transform and Fourier Transform). The approach's effectiveness is demonstrated by analyzing the normal force, the thermal source and the specific type of heat source. In the new dominion, physical field quantities (displacement components, stress components, and thermodynamic temperature and conductive temperature) are examined. The numerical inversion procedure is employed to recover the resulting quantities in original physical dominion and depicted graphically to investigate the impact of N-L, TT, heat source, and different theories of thermoelasticity on physical quantities. Some unique cases are also presented.

Chapter 3, deals with investigation of two-dimensional problem in thermoelastic half space under MGT heat equation by virtue of thermomechanical source along with heat source. After simplifying the equation with the dimensionless quantities, the potential functions and integral transform technique are applied for further simplification. The problem is inspected due to a heat source, a laser pulse decaying with time, moving with constant velocity in one direction, and thermomechanical loading. Specific types of normal distributed force (NDF) and ramp-type thermal sources (RTTS) are adopted to exemplify the effectiveness of the problem. The rational expressions of displacement components, stress components, conductive temperature, and thermodynamic temperature are computed in altered dominion. However, the numerical inversion methodology used

to obtain subsequent physical quantities in physical dominion and results are displayed graphically to illustrate the effect of N-L moving heat source, and hyperbolic two temperature parameters.

Chapter 4 deals with the axisymmetric problem in a thermoelastic half-space owing to mechanical loading in the presence of N-L and HTT parameters under the MGT heat equation and fractional-order derivatives. The solution is found using the integral transform (Laplace and Hankel Transforms) technique. Ring or disc loads are used as an application to exemplify the approach's efficacy. The transformed displacement components, stress components, conductive temperature, and thermodynamic temperature are numerically computed in the physical dominion.

Chapter 5 is concerned with the reflection problem of a plane wave in thermoelastic half-space subjected to impedance boundary under MGT heat equation with fractional order derivatives along with non-local (N-L) and HTT. The amplitude ratios of reflected waves are obtained correspond to each incident wave. The variations of amplitude ratios are shown with the help of graphs. Some limited cases are also introduced.

ACKNOWLEDGEMENT

I want to take this opportunity to express my deep sense of gratitude to all who helped me directly or indirectly during this thesis work. Firstly, I would like to thank my supervisor, Dr. Sachin Kaushal, Professor, School of Chemical Engineering and Physical Sciences of Lovely Professional University, Punjab, India, and Co-supervisor Dr. Rajneesh Kumar, Professor, Department of Mathematics, Kurukshetra University, Kurukshetra who have guided me in real sense. I wish to express my deep sense of gratitude and appreciation to them for their stimulating supervision with invaluable suggestions, keen interest, constructive criticisms, and constant encouragement during the Ph.D. I learned a lot from them in the academic area and other spheres of life. I wholeheartedly acknowledge the full cooperation that I received from the beginning of this work up to the completion of this thesis for being a great mentor and the best adviser I could ever have. His advice, encouragement, and criticism are a source of innovative ideas, inspiration, and causes behind the successful completion of this thesis work.

Reaching this stage of my life would never be possible without loads of blessings of my grandfather, Sh. Banke Bihari Lal, a teacher by profession, and my father (Sh. Surinder Kumar Sharma) and my mother (Smt. Raj Rani) for their unconditional love, encouragement, and blessings. Words can never express my feelings for them. They have been a guiding force. I have a shortage of proper words to express my abounding feelings and affection for my wife, Mrs. Nitu, for her deepest love, endless patience, and motivation. Also, I owe special thanks to my son Parth, who always stood by my decisions and provided all kinds of moral support. I also express my abounding feelings of gratitude to all those who helped me in this course but have not been listed here.

At last, I extend my heartfelt thanks to the almighty God who has given me the spiritual support and courage to carry out this work. His presence has been a constant source of strength and inspiration.

I am highly obliged to all the faculty members, Department of Mathematics and Lovely Professional University for their support and encouragement. Finally, I would like to end by paying my heartfelt thanks and praying to the Almighty for his unbound love and grace.

CONTENTS

Chapter -1

1.1 Thermoelasticity

Thermoelasticity is a field of study that examines the combined influences of change in temperature and mechanical stress on an elastic material and is deals with the prediction of thermomechanical behavior of the materials. It comprises the stress, strain theory and the heat conduction theory. Compared to the traditional elasticity theory, the influence of internal forces on the temperature field is evaluated, along with how temperature changes affect the deformation, according to the principles of thermoelasticity. On the other hand, the uncoupled theory was developed on the simplifying assumption that the effect of strain on the temperature can be ignored.

1.2 Uncoupled Thermoelasticity Theory (UCT)

Duhamel (1837) [40], was the first to propose the idea of a connection between the thermal and mechanical fields and obtained expressions to calculate the strain in a thermally changing elastic material. Later, Neumann (1841) [89] also obtained the similar outcomes. However, the concept dealt with the thermal and mechanical effects as independent effects and the overall strain was calculated by adding together the elastic strain and the thermal expansion resulting from the temperature distribution alone. Hence, the theory did not include the interactions between the strain and the temperature distributions in a specified manner. Subsequently, the thermodynamic arguments were taken into consideration by Thomson (1857) [140] was the first to use the principles of thermodynamics to study how an elastic body response to varying temperature by analyzing its stresses and strains. Later, Voigt (1928) [143] and Jefferys (1930) [58] ventured the thermodynamic documentation of the equations suggested by Duhamel (1837) [40].

1.3 Coupled Thermoelasticity Theory (CT)

Biot (1956) [24] developed the CT model to resolve the inconsistency that is intrinsic in conventional UCT theory. In this theory, the equations governing elasticity and heat conduction are coupled. However, it estimates an infinite speed of thermal wave.

1.4 Generalized Thermoelasticity Theory

Generalized thermoelasticity theories are mainly the modified forms of conventional thermoelasticity theory to address the paradox of infinite thermal propagation speed. These theories can be divided into two main categories. The first one is given by Lord-Shulman (LS) [81] by utilizing the modified Fourier's law proposed by Catteno (1958) [28] to formulate a theory of thermoelasticity incorporating a single relaxation time. Green and Lindsay (GL)

(1972) [47] provide the second generalization of the thermoelasticity theory by establishing a model that is predicated on an entropy production inequality. This model is compatible with the traditional Fourier's law for materials that have a center of symmetry at each point. However, it introduces modifications to the classical energy equation and stress-strain temperature relations by incorporating the two relaxation times.

1.5 Green-Naghdi Thermoelasticity Theory (GN)

Green and Naghdi (1991, 1992, 1993) [48-50] introduced novel theory in forms of three models, known as GN - I, GN - II, and GN - III. The linearized GN-I model is similar to the CT (1980) [38] theory but has the drawback of allowing unlimited speed of thermal waves. On the other hand, the linearized GN-II and GN-III allow the finite speed for thermal waves. GN- II is unique as it does not dissipate thermal energy, unlike other established thermoelastic models. The GN-II model has the feature of sustaining undamped thermoelastic waves in the body.

1.6 Two-Temperature (TT) and Hyperbolic Two-Temperature (HTT)Theory

The TT theory, established by Chen and Gurtin (1968) [30] and Chen et al. (1969) [31], is based on both thermodynamic and conductive temperature. The first one was the result of a mechanical process between particles and layers of elastic material, while the second one was due to a thermal process. For time-free situations, the temperature difference equals the heat supply, so removing the heat makes both temperatures the same. However, the temperatures remain different in time-dependent situations even without heat supply.

Youssef (2006) [147] utilized the generalized thermoelasticity theory to examine the uniqueness theorem in TT thermoelasticity theory, and demonstrated the finite speed of both thermal and mechanical waves. Youssef (2013) [148] explored the deformation of a semi-space induced to thermal shock by employing Laplace transform and state-space techniques for TT theory, with the boundary being traction-free. Kumar et al. (2016) [71] used GN-II and GN-III with TT to investigate the impact of Hall current and magnetic field in thermoelastic medium due to thermomechanical sources.

Youssef observed that the classical TT theory fails to account for the limited speed of thermal wave, this is not acceptable from a physical standpoint. Consequently, Youssef and El-Bary (2018) [149] improved the TT theory by introducing the HTT model for an isotropic body. This model suggests that the difference between conductive temperature and thermodynamic temperature acceleration is linked to the heat supply and it introduces a heat wave that spreads with a limited speed.

Kaur et al. (2023) [59] presented a mathematical formulation for a couple stress thermoelasticity theory for fibre-reinforced composite material under HTT. They employed it to attain the systematic solution for physical field variables owing to concentrated inclined load. Geetanjali et al. (2023) [46] examined thermoelastic diffusion half-space under the influence of various loadings (thermal, mechanical, and concentration) with dual-phase-lag model under HTT to study the impact of thermal conductivity and diffusivity on physical field quantities. Bajpai et al. (2023) [14] investigated the response of HTT and fractional order parameters on elastic circular plate. Prasad and Kumar (2024) [102] established the convolutional-type variational and reciprocity theorems under HTT model for thermoelastic material.

1.7 Dual-Phase-Lag Thermoelasticity Theory (DPL)

Tzou (1995) [142] introduced a new model to account for microscopic effects on ultra-fast heat transport. This model is known as the dual phase-lag (DPL) model, aims to modify Fourier's law by incorporating two-time phase-lags: one for heat flux and the other for temperature gradient. Kumar et al. (2021) [64] presented a dynamic dual-phase lag model to examine the effects of non-local and diffusion on waves in a bio-thermoelastic medium. In a subsequent study, Kumar et al. (2024) [75] employed the normal mode analysis to scrutinize the impact of specific heat loss and penetration depth in the DPL framework, in conjunction with memory-dependent derivatives as applied to homogeneous micropolar thermoelastic plates.

1.8 Three-Phase-Lag Thermoelasticity Theory (TPL)

Roychoudhuri (2007) [107] has further generalized the concept of phase-lag to Green-Naghdi thermoelasticity theory by incorporating three different phase-lag parameters in the constitutive relation for heat conduction given by GN-III model. One additional phase-lag parameter is incorporated here for the gradient of thermal displacement, along with the incorporation of phase-lag parameters for the heat flux as well as temperature gradient terms.

1.9 Non-Local Theory

Eringen (1972) [41] created the non-local (N-L) theory of elasticity by utilizing the second law of thermodynamics and global balance laws. In the same year, Edelen, Green, and Laws obtained constitutive relations by utilizing N-L thermodynamics. Eringen (1974) [42] evolved a N-L theory of polar elastic continua and derived constitutive relations by employing N-L thermodynamics and invariance under rigid body motion of N-L micromorphic elastic solid

and derived a set of basic equations of N-L thermoelasticity. The core concept of classical continuum mechanics is to disregard the influence of the strain field of remote points on a particular local point. In contrast, N-L elasticity theory considers this influence. Incorporating the N-L factor into heat conduction theory enhances the microscopic effects at a macroscopic scale. Balta and Suhubi (1977) [19] used N-L theory to establish field equations for homogeneous isotropic solids.

Eringen (2002) [43] established N-L continuum field theories to account for microscopic structures. Sharma (2010) [117] presented a boundary value problem in a thermodiffusive medium. Sharma (2012) [119] inspected the generation of plane waves with voids in thermoelastic and thermodiffusive medium. Sharma et al. [2013] [121] examined the propagation of Lamb waves in thermoelastic micropolar solid with two temperatures bordered with semi-spaces of inviscid liquid subjected to stress free boundary conditions.

Yu et al. (2015, 2016) [150-151] constructed a new model by integrating heat equation and N-L elasticity, with extended irreversible thermodynamics and generalized free energy. Kumar and Devi (2017) [63] explored the effects of lateral deflection, thermal moment and axial stress on the thermoelastic beam due to laser source and heat flux in a modified couple stress model. Bachher and Sarkar (2018) [12] employed the N-L model to explore deformation problem in thermoelastic medium with void. Kumar et al. (2019) [74] explored the non-local influence in bi-layer tissue used for magnetic fluid hyperthermia.

1.10 Fractional order thermoelasticity Theory (FOTT)

The FOTT is the modification of classical thermoelasticity which employed fractional calculus and has recently garnered substantial interest and attention from researcher. Over the last few decades, considerable literature has progressed in the field of FOTT. Caputo and Mainardi (1971,1971) [26-27], and Caputo (1974) [25] employed fractional order derivative (FOD) to characterize the behavior of viscoelastic materials and attempted to establish an agreement between theoretical and experimental outcomes. It was shown that constitutive relations derived in terms of time fractional order derivative were quite in agreement with results of molecular theories. For more details, one can refer to the works of the researchers mentioned: Oldham and Spanier (1974) [90], Bagley and Torvik (1983) [13], Podlubny (1998) [92], Hilfer (2000) [52].

Povstenko (2005) [93] used Caputo fractional derivatives and suggested a theory of quasi-static uncoupled thermoelasticity by incorporating a time-fractional derivative into the heat conduction equation, following this, Sherief et al. (2010) [127], and Ezzat and El-

Karamany (2011) [44] formulated new theories on generalized thermoelasticity, based on the heat conduction law with FOD. The problems based on fractional order heat conduction equation are investigated by Povstenko (2008, 2008,2009, 2009, 2010, 2011, 2011,2012) [94-101]. Sarkar and Lahiri (2012) [111] have examined a deformation problem involving a homogeneous isotropic and thermoelastic rotating medium based on a FOTT. Sherief and Hussein (2020) [128] explored the behavior of a solid sphere containing spherical cavity surface. They focused on the traction-free surface response to an axisymmetric thermal field within the scope of FOTT.

Bajpai et al. (2023) [15] explored thermodiffusion phenomenon to investigate the impact of HTT on forced vibrations under FOTT with a TPL model and examined the efficacy of the problem by considering axisymmetric thermal, mechanical, and mass concentration loading. Abbas et al. (2024) [1] employed bioheat model to investigate impact of fractional parameter in process of heat transfer in living tissues wing to magnetic hyperthermia treatment for tumors.

1.11 Modified Green-Lindsay (MGL) Thermoelasticity Theory

The GL model was applied to certain problems, and it was observed that the displacement experiences finite leaps. This is in contradiction with the postulates of continuum mechanics Dhaliwal and Rokne (1989) [39], Ignaczak and Mr´owka-Matejewska (1990) [54], Chandrasekharaiah (1998) [29]. Considering this, Yu et al. (2018) [152] recently established a modified version of the GL thermoelasticity theory, including strain-rate and temperature-rate terms. This theory is called modified Green-Lindsay theory and has evolved with the help of the principle of thermodynamics.

The strain-rate term is usually neglected in constitutive relations of linear theory by assuming it to be relatively small. This is not an appropriate assumption for extreme conditions such as ultra-fast heating. Based on these factors, a novel thermoelasticity model was introduced using extended thermodynamics theory and generalized dissipation inequality.

1.12 Moore-Gibson-Thompson (MGT) thermoelasticity theory

The MGT thermoelastic theory has been the focus of extensive research and stems from a third-order differential equation. Thompson (1972) [139] originated the idea based on fluid mechanics principles. It has relevance in diverse fields, including fluid mechanics, nanostructures, and thermoelasticity. Furthermore, the MGT thermoelastic model is the generalization of the LS (1967) [81] and (GN-III) (1993) [50] theories of thermoelasticity.

1.13 Literature Review

Quintanilla (2018) [104] presented qualitative findings related to the MG-L thermoelasticity model. Sarkar and De (2020) [109] investigated wave problem in the thermoelastic medium by employing the MGL model using the harmonic plane wave technique at stress-free and isothermal surfaces. In the context of MGL, Sarkar et al. (2020) [110] examined the propagation of waves in thermoelastic medium and reported that both MGL and G-L significantly impact the amplitude ratios of reflected waves (ARRW). Sarkar and Mondal (2020) [112] presented mathematical expressions for analyzing the behavior of a wave in thermoelastic medium at free surface and obtained ARRW. Shakeriaski and Ghodart. (2020) [113] performed a nonlinear study on the temporary response of elastic medium exposed to laser pulse using the L-S model. Sarkar et al. (2020) [108] examined the behavior of plane waves in thermoelastic semi-space and obtained reflection coefficients and their respective energy ratios within the framework of MGL thermoelasticity.

Shakeriaski et al. (2021) [114] analyzed the wave propagation phenomenon in elastic material induced by thermal shock under MGL model. Sharma and Kumar (2021) [122] explored the photothermoelastic properties of semiconducting materials under distributed loads. Mohamed et al. (2021) [88] contributed to the literature a semiconducting material by demonstrating the stimulus of a absorption coefficient owing to laser using the MGL model. Kumar et al. (2022) [66] adopted MGL model to study reflection phenomenon in micropolar thermoelastic media to explore the bearing of impedance parameters on various reflection coefficients of reflected wave. Further, Mirparizi and Razavinasab (2022) [87] utilized the MGL model to analyze stress and thermal wave propagation in a functionally graded medium exposed to thermal shock and electromagnetic influences.

Sharma and Kumari (2022) [116] utilized classical theory and L-S theory (1967) with FOTT to study impressions of N-L parameter on the reflection coefficient of plane waves. Malik et al. (2022) [83] obtained a fundamental solution of plane wave propagation for functionally graded solid with diffusion and void based on couple stress micropolar thermoelasticity. Abouelregal and Alesemi (2022) [4] studied the viscoelastic behavior of the fibre-reinforced material in modified thermo-viscoelastic MGT model. Kumar et.al (2023) [76] investigated the waves under the impact of memory-dependent derivatives by applying insulated thermal restriction at the boundary surface of the plate in the micropolar thermoelastic medium.

Kumar et al. (2023) [65] presented the axisymmetric study using thick circular plate exposed to specific type of heat source within the framework of modified couple stress model and examined the various impacts (void, diffusion, phase lags parameter) on physical field quantities. Liang et al. (2023) [80] adopted MGL model to examine the phenomenon of reflection at imperfect boundary of thermoelastic solid half-space to study the impact of relaxation time and the interface effect on amplitude ratios (AR). Singh and Mukhopadhyay (2023) [135] explored problem in thermoelastic medium to investigate the impact of both strain and temperature rate owing to continuous line heat source with MGL model. Kaushal et al. (2024) [60] studied the waves in thermoelastic medium to explore the impact of N-L and TT and impedance parameters on AR of reflected wave.

Quintanilla (2019) [105] developed new thermoelastic model by using the MGT heat equation, focusing on TT. The research confirmed the well-posedness and exponential decay of the solution for dipolar structure. Quintanilla (2020) [106] formulated the MGT with TT. Marin et al. (2020)[85] investigated thermoelastic dipolar structure based on MGT heat equation and proved domain of influence theorem for mixed boundary value problem (BVP) for bounded functions. Conti et al. (2019) [34] established MGT thermoelastic theory results by transition of the heat equation into integro-differential equation.

Conti et al. (2020, 2021) [35,33] explored some problems in MGT thermoelastic heat equation. Jangid et al. (2021)[57] discussed the harmonic plane waves propagation with the MGT model and derived dispersion relation for longitudinal wave. Bazarra et al. (2021) [22] proved existence and uniqueness for thermoelastic problem using theory of linear semi group and obtained exponential decay solution using MGT model. Singh and Mukhopadhyay (2021) [132] presented a Galerkin-type solution under the MGT theory. Jangid and Mukhopadhyay (2021) [55] utilized MGT model to discuss results for domain of influence. Sharma and Khator (2021, 2022) [124,125] studied power generation challenges associated with renewable sources and delved into micro-grid planning within the renewable inclusive prosumer market. Al-Lehaibi (2022) [8] used MGT thermoelasticity theory to investigate a thermomechanical deformation due to ramp type heating thermal loading

Bazarra et al. (2022)[23] presented the MGT thermoelasticity theory for thermoelastic dielectrics. Lotfy et al. (2022) [82] examined photothermoelasticity with MGT model for semiconductor material and illustrated the interaction between thermal, plasma and elastic wave propagation owing to the impact of laser beam within semiconductor materials. Kumar et al. (2023) [77] explored thermomechanical interaction in a homogeneous, isotropic, photo-viscothermoelastic plate with fractional order derivative under MGT model. Conti et al.

(2024) [32] examined the stability condition with constraints of the problem in MGT heat equation.

Yadav (2024) [145] investigated reflection problem of thermoelastic and microstretch semi-space to explore the impact of the impedance boundary due to magnetic diffusion. Kumar et al. (2024) [67] analyzed reflection phenomenon in propagation of plane wave in micropolar thermoelastic medium to investigate the effect of N-L, HTT and impedance parameter on reflection coefficients within the framework of MGT heat equation. Kumar et al. (2024) [68] explored axisymmetric problem in micropolar model using MGT heat equation to explore the effect of N-L and HTT due to mechanical loading.

1.14 Research Gaps

In the past decade, serious attention has been paid towards generalized thermoelasticity theories with different models and numerous research have been done in this field. As the work in this field is motivated by the need to analyse the vibration of structure such as rail/road tracks and bridges that is caused by moving vehicles. During the literature review, it has been observed that mathematical modelling by using modified G-L theory and using non local parameter was not explored to great extent so there is a requirement for interdisciplinary communication that motivates much of work in this field. The motivation behind this study lies in the increasing demand for advanced mathematical models that accurately predict thermoelastic behavior in modern engineering materials, aerospace components, and biological tissues. By integrating nonlocality, fractional calculus, and hyperbolic heat conduction, this research aims to enhance the fundamental understanding of thermoelasticity and contribute to the development of more precise predictive tools for scientific and industrial applications. Therefore, we will intend to work on framing new mathematical model in context of modified G-L theory in thermoelasticity, and thermoelastic model with and without energy dissipation with two temperature by considering various parameter such as non-local, diffusion, void and viscosity with different set of boundary conditions depending upon the nature of problem or model framed. The characteristics of new model will be discussed by comparing the numerical results with previous model. Also, the effect of parameters such as relaxation times, two temperature, diffusion, void and non local parameter will be calculated numerically for a particular model and their influence will be shown graphically

1.15 Organization of the thesis

The present thesis works deals with "**Mathematical Modelling of Elastodynamic Problems in Two Temperature Thermoelastic Media**" and it consists of five chapters, and a list of references is given at the end of this thesis. The subject matter is laid out in the following way:

Chapter1 is deals with the historical background and introductory part of thermoelasticity theories from where it comes into existence. We have given a brief introduction of (i) Thermoelasticity (ii) Green-Lindsay theory (iii) Green-Naghdi thermoelasticity theory (iv) Two temperature and Hyperbolic two temperature model (v) DPL model (vi) Non-local theory (vii) Fractional order theory of thermoelasticity (viii) Modified Green-Lindsay (MGL) thermoelasticity (ix) Morre-Gibbson Thomson (MGT) theory of thermoelasticity.

Chapter 2 deals with a two-dimensional deformation problem with heat source and thermomechanical loading in a half-space that is homogeneous, isotropic, and thermoelastic under the modified Green-Lindsay (MGL) to study the effects of non-local (N-L) and two temperature (TT). The governing equations are rendered dimensionless for two-dimensional problem, and potential functions are used for further simplification. The problem is simplified by the integral transform technique (Laplace Transform and Fourier Transform). The approach's usefulness is demonstrated by analyzing the normal force, the thermal source and the specific type of heat source. In the transformed domain, physical field quantities (displacement components, stress components, thermodynamic temperature and conductive temperature) are examined. The numerical inversion procedure is employed to recover the resulting quantities in original physical dominion and depicted graphically to investigate the influence of N-L, TT, heat source, and different theories of thermoelasticity on physical quantities. Some unique cases are also presented.

Chapter 3, concerned with investigation of two-dimensional problem in thermoelastic half space under MGT heat equation by virtue of thermomechanical source along with heat source. After simplifying the equation with the dimensionless quantities, the potential functions and integral transform technique are applied for further simplification. The problem is studied due to a heat source, a laser pulse decaying with time, moving with constant velocity in one direction, and thermomechanical loading. Specific types of normal distributed force (NDF) and ramp-type thermal sources (RTTS) are assumed to illustrate the usefulness of the problem. The rational expressions of displacement components, stress components,

conductive temperature, and thermodynamic temperature are computed in altered dominion. However, the numerical inversion methodology used to obtain subsequent physical quantities in physical dominion and results are displayed graphically to illustrate the effect of N-L moving heat source, and hyperbolic two temperature parameters.

Chapter 4 concerned with the axisymmetric problem in a thermoelastic half-space owing to mechanical loading in the presence of N-L and HTT parameters under the MGT heat equation and fractional-order derivatives (FOD). The solution is found using the integral transform (Laplace and Hankel Transforms) technique. Ring or disc loads are used as an application to exemplify the approach's efficacy. The transformed displacement components, stress components, conductive temperature, and thermodynamic temperature are numerically computed in the physical dominion.

Chapter 5 deals with the reflection problem of a plane wave in thermoelastic half-space subjected to impedance boundary under MGT heat equation with fractional order derivatives along with non-local (N-L) and HTT. For the assumed model when a wave (P-wave, T-wave, SV-wave) is incident on the surface $x_3 = 0$, three varieties of reflected waves are produced: P-wave, T-wave and SV-wave. The amplitude ratios for these reflected waves are obtained numerically and displayed graphically to investigate the influence of specific parameters (N-L, HTT, and impedance). Additionally, special cases are inferred from the current investigation.

Chapter 2

Deformation in a Thermoelastic Medium with Modified Green-Lindsay Model Incorporating Non-local and Two-Temperature Effects

2.1 Introduction

Sharma (2011) [118] explored the deformation in thermoelastic diffusive semi- space due to inclined load based on G-L (1972) and CT (1980) theory. Sharma and Sharma (2014) [123] explored the response of relaxation time and heat sources in viscoelastic medium using bio heat equation. Bajpai et al. (2021) [17] constructed mathematical model of generalized thermoelasticity with fractional order derivatives to study the impacts of two temperature (TT) and diffusion in thermoelastic plate owing to thermomechanical loading.

Abbas et al. (2022) [2] studied wave propagation in thermoelastic material under L-S (1967) model of thermoelasticity to explore effect of relaxation and non-local (N-L) parameters. Jangid and Mukhopadhyay (2022) [56] used the MGL theory proposed by Yu et al. (2018) [152] to investigate the effects of temperature and strain rate in an isotropic, thermoelastic medium by virtue of continuous line heat source. Othman et al. (2023) [91] analyzed various impacts (Hall current, TT, viscosity, and gravity) on physical field quantities in fiber reinforced visco-thermoelastic material under magnetic field in the context of the modified Green-Lindsay (MGL) model.

Ailawalia and Gupta (2024) [9] investigated photothermoelastic interactions in a semiconducting material to study the effect of thermal conductivity under MGL model of thermoelasticity by applying normal mode analysis. Yadav et al. (2024)[146] used MGL theory of thermoelasticity and normal mode technique to examine the influence of N-L parameter in thermoelastic solid half-space subjected to moving thermal load. Tayel and Almuqrin (2024) [138] investigated two-dimensional axi-symmetric problem due to specific causes in photothermoelastic semi-space under MGL model.

The investigation of thermoelastic materials incorporating non-local (N-L) and two-temperature (TT) effects is crucial for advancing the theoretical framework of thermoelasticity. Therefore, this research is motivated by the need to bridge gaps in existing theories by exploring the combined effects of heat sources and thermomechanical loading, providing deeper insights into stress distribution in complex thermoelastic media.

In this chapter, heat source and thermomechanical loading are taken to study the effect of N-L and TT in thermoelastic semi-space under MGL model. The governing equations are made dimensionless, and potential functions are employed to facilitate further simplification. The problem is resolved by applying the Laplace transform (L.T) w.r.t time variable t and Fourier transform (F.T) w.r.t space variable x_1. The problem's utility is illustrated using specific categories of heat sources, including thermal source and normal force. The components of displacement, normal stress, tangential stress, thermodynamic temperature and conductive temperature are obtained in the transformed domain. The subsequent quantities are attained in actual dominion using a numerical inversion method and represented explicitly to investigate the impact of N-L, TT, heat source, and different theories of thermoelasticity on physical quantities. Some unique cases are also presented.

2.2 Basic Equations

Following (Eringen (1974) [42],Youssef (2006) [147] and Yu et al. (2018) [152]) the basic equations and constitutive relations under MGL model with heat source, without body forces, taking into accounts N-L, and TT are

$$\left(1+\eta_1\tau_1\frac{\partial}{\partial t}\right)[(\lambda+\mu)\nabla(\nabla\cdot\vec{u})+\mu\Delta\vec{u}]-\beta_1\left(1+\eta_2\tau_1\frac{\partial}{\partial t}\right)\nabla\mathrm{T}=\rho(1-\xi_1^2\Delta)\frac{\partial^2\vec{u}}{\partial t^2}, \tag{2.1}$$

$$K_1\Delta\phi=\left(1+\eta_3\tau_0\frac{\partial}{\partial t}\right)\left(\beta_1T_0\frac{\partial}{\partial t}\mathrm{e_{kk}}-Q\right)+\left(1+\eta_4\tau_0\frac{\partial}{\partial t}\right)\rho C_e\,\dot{\mathrm{T}}\,, \tag{2.2}$$

$$t_{ij}=\left(1+\eta_1\tau_1\frac{\partial}{\partial t}\right)\left[\lambda e_{kk}\delta_{ij}+2\mu\,\mathrm{e_{ij}}\right]-\beta_1\left(1+\eta_2\tau_1\frac{\partial}{\partial t}\right)T\delta_{ij}\ , \tag{2.3}$$

$$T=(1-a\Delta)\phi, \tag{2.4}$$

where λ,μ -Lame's constants, $\vec{u}$ -displacement vector, ρ, C_e -density and specific heat, t -time, β_1=$(3\lambda+2\mu)\alpha_t$, α_t -coefficient of linear thermal expansion, K_1-thermal conductivity, ϕ -conductive temperature, T -thermodynamic temperature , ξ_1 – N-L parameter, t_{ij} -components of stress tensor, Q -heat source, T_0 -reference temperature, τ_0,τ_1- the relaxation times, δ_{ij}- Kronecker delta, $\eta_1,\eta_2,\eta_3,\eta_4$- constants, a - two temperature parameter, Δ - Laplacian operator , ∇- nable (gradient) operator, e_{kk} - dilatation, $e_{ij}=\frac{1}{2}\left(u_{i,j}+u_{j,i}\right)$ (i, j = 1,2,3).

The equations (2.1) - (2.4) reduce to the following model

$\eta_1=\eta_2=\eta_3=\eta_4=1$: MGL model (2018) [152],

$\eta_1 = \eta_4 = 0,\ \eta_2 = \eta_3 = 1$: Green-Lindsay (G-L) model, (1972) [47],

$\eta_1 = \eta_2 = 0, \eta_3 = \eta_4 = 1$: Lord -Shulman, (L-S) model, (1967) [81],

$\eta_1 = \eta_2 = \eta_3 = \eta_4 = 0$: Coupled thermoelasticity(C-T) model, (1980) [38],

Equations (2.1) - (2.4) in components form for cartesian coordinates (x_1, x_2, x_3) are written as

$$\left(1 + \eta_1\tau_1 \frac{\partial}{\partial t}\right)\left[(\lambda + \mu)\frac{\partial e}{\partial x_1} + \mu\, \Delta u_1\right] - \beta_1 \left(1 + \eta_2\tau_1 \frac{\partial}{\partial t}\right)\frac{\partial T}{\partial x_1} = \rho(1 - \xi_1^2\Delta)\frac{\partial^2 u_1}{\partial t^2}, \tag{2.5}$$

$$\left(1 + \eta_1\tau_1 \frac{\partial}{\partial t}\right)\left[(\lambda + \mu)\frac{\partial e}{\partial x_2} + \mu\, \Delta u_2\right] - \beta_1 \left(1 + \eta_2\tau_1 \frac{\partial}{\partial t}\right)\frac{\partial T}{\partial x_2} = \rho(1 - \xi_1^2\Delta)\frac{\partial^2 u_2}{\partial t^2}, \tag{2.6}$$

$$\left(1 + \eta_1\tau_1 \frac{\partial}{\partial t}\right)\left[(\lambda + \mu)\frac{\partial e}{\partial x_3} + \mu\, \Delta u_3\right] - \beta_1 \left(1 + \eta_2\tau_1 \frac{\partial}{\partial t}\right)\frac{\partial T}{\partial x_3} = \rho(1 - \xi_1^2\Delta)\frac{\partial^2 u_3}{\partial t^2}, \tag{2.7}$$

$$K_1\Delta\phi = \left(1 + \eta_3\tau_0 \frac{\partial}{\partial t}\right)\left[\beta_1 T_0 \frac{\partial e}{\partial t} - Q\right] + \left(1 + \eta_4\tau_0 \frac{\partial}{\partial t}\right)\rho C_e \frac{\partial T}{\partial t}, \tag{2.8}$$

$$t_{11} = \left(1 + \eta_1\tau_1 \frac{\partial}{\partial t}\right)[\lambda\, e + 2\,\mu\, \mathrm{e}_{11}] - \beta_1 \left(1 + \eta_2\tau_1 \frac{\partial}{\partial t}\right)T, \tag{2.9}$$

$$t_{22} = \left(1 + \eta_1\tau_1 \frac{\partial}{\partial t}\right)[\lambda\, \mathrm{e} + 2\,\mu\, \mathrm{e}_{22}] - \beta_1 \left(1 + \eta_2\tau_1 \frac{\partial}{\partial t}\right)T, \tag{2.10}$$

$$t_{33} = \left(1 + \eta_1\tau_1 \frac{\partial}{\partial t}\right)[\lambda\, e + 2\,\mu\, \mathrm{e}_{33}] - \beta_1 \left(1 + \eta_2\tau_1 \frac{\partial}{\partial t}\right)T, \tag{2.11}$$

$$t_{31} = 2\left(1 + \eta_1\tau_1 \frac{\partial}{\partial t}\right)\mu\, e_{31}, \tag{2.12}$$

$$t_{32} = 2\left(1 + \eta_1\tau_1 \frac{\partial}{\partial t}\right)\mu\, e_{32}, \tag{2.13}$$

$$t_{21} = 2\left(1 + \eta_1\tau_1 \frac{\partial}{\partial t}\right)\mu\, e_{21}, \tag{2.14}$$

$$T = (1 - a\Delta)\phi, \tag{2.15}$$

where $\Delta = \frac{\partial^2}{\partial \mathrm{x}_1^2} + \frac{\partial^2}{\partial \mathrm{x}_2^2} + \frac{\partial^2}{\partial \mathrm{x}_3^2}$, $e = \frac{\partial \mathrm{u}_1}{\partial \mathrm{x}_1} + \frac{\partial \mathrm{u}_2}{\partial \mathrm{x}_2} + \frac{\partial \mathrm{u}_3}{\partial \mathrm{x}_3}$. (2.16)

2.3 Problem Statement

A homogeneous, isotropic, generalized thermoelastic solid semi - space MGL model besides the N-L and TT effects occupy a region $x_3 \geq 0$ in rectangular cartesian coordinate system $(\mathrm{x}_1, \mathrm{x}_2, \mathrm{x}_3)$ with x_3 - axis pointing into the medium. The surface of the semi-space ($x_3 = 0$) is underneath the influence of thermomechanical loading and heat source. We define x_1-x_3 as plane of incidence for our investigation, allowing the various quantities to be expressed as functions of x_1 , x_3 and t.

Therefore, the displacement vector, thermodynamic temperature and conductive temperature are taken as

$$\vec{u} = (\, u_1(x_1, x_3, t), 0, u_3(x_1, x_3, t)),\ \mathrm{T} = \mathrm{T}(x_1, x_3, t),\ \phi = \phi(x_1, x_3, t). \qquad (2.17)$$

Equations (2.5) - (2.8), (2.11), (2.12) and (2.15) with the aid of (2.17) reduce to two dimensions form as follows:

$$\left(1 + \eta_1\tau_1 \frac{\partial}{\partial t}\right)\left[(\lambda + \mu)\frac{\partial e}{\partial x_1} + \mu\, \Delta u_1\right] - \beta_1 \left(1 + \eta_2\tau_1 \frac{\partial}{\partial t}\right)\frac{\partial T}{\partial x_1} = (1 - \xi_1^2\Delta)\frac{\partial^2 u_1}{\partial t^2}, \qquad (2.18)$$

$$\left(1 + \eta_1\tau_1 \frac{\partial}{\partial t}\right)\left[(\lambda + \mu)\frac{\partial e}{\partial x_3} + \mu\, \Delta u_3\right] - \beta_1 \left(1 + \eta_2\tau_1 \frac{\partial}{\partial t}\right)\frac{\partial T}{\partial x_3} = (1 - \xi_1^2\Delta)\frac{\partial^2 u_3}{\partial t^2}, \qquad (2.19)$$

$$K_1\Delta\phi = \left(1 + \eta_3\tau_0 \frac{\partial}{\partial t}\right)\left[\beta_1 T_0 \frac{\partial e}{\partial t} - Q\right] + \left(1 + \eta_4\tau_0 \frac{\partial}{\partial t}\right)\rho C_e \frac{\partial\, T}{\partial t}\,, \qquad (2.20)$$

$$t_{33} = \left(1 + \eta_1\tau_1 \frac{\partial}{\partial t}\right)\left[\lambda\, e + 2\,\mu\, \frac{\partial u_3}{\partial x_3}\right] - \beta_1 \left(1 + \eta_2\tau_1 \frac{\partial}{\partial t}\right) T\,, \qquad (2.21)$$

$$t_{31} = \left(1 + \eta_1\tau_1 \frac{\partial}{\partial t}\right)\mu\, \left(\frac{\partial u_3}{\partial x_1} + \frac{\partial u_1}{\partial x_3}\right), \qquad (2.22)$$

$$T = (1 - a\,\Delta)\phi, \qquad (2.23)$$

where

$$\Delta = \frac{\partial^2}{\partial \mathrm{x}_1^2} + \frac{\partial^2}{\partial \mathrm{x}_3^2},\ \mathrm{e} = \frac{\partial \mathrm{u}_1}{\partial \mathrm{x}_1} + \frac{\partial \mathrm{u}_3}{\partial \mathrm{x}_3}. \qquad (2.24)$$

For further simplifications, following dimensionless quantities are taken as

$$(x_i', u_i', \xi_1') = \frac{\omega_1}{\mathrm{c}_1}(x_i, \mathrm{u_i}, \xi_1),\ t_{3i}' = \frac{t_{3i}}{\beta_1 T_0}, \qquad (\phi', \mathrm{T}') = \frac{1}{\mathrm{T}_0}(\phi, \mathrm{T}),$$

$$(t', \tau_0', \tau_1') = \omega_1(t, \tau_0, \tau_1),\ a' = \frac{\omega_1^2}{c_1^2}a, \qquad Q' = \frac{c_1^2}{K_1\omega_1 T_0}Q,$$

$$F_{10}' = \frac{1}{\beta_1 T_0}F_{10}, \qquad F_{20}' = \frac{c_1}{\omega_1 T_0}F_{20}, \qquad (i = 1,3). \qquad (2.25)$$

where

$c_1^2 = \frac{\lambda+2\mu}{\rho}$, $\omega_1 = \frac{\rho\, C_e c_1^2}{K^*}$, and ω_1, c_1 being the characteristic frequency and longitudinal wave velocity respectively.

Using the dimensionless quantities defined by equations (2.25), in equations (2.18) - (2.23), after removing the primes give,

$$\left(1 + \eta_1\tau_1 \frac{\partial}{\partial t}\right)\left[a_1 \frac{\partial e}{\partial x_1} + a_2\Delta u_1\right] - a_3 \left(1 + \eta_2\tau_1 \frac{\partial}{\partial t}\right)\frac{\partial T}{\partial x_1} = (1 - \xi_1^2\Delta)\frac{\partial^2 u_1}{\partial t^2}, \qquad (2.26)$$

$$\left(1 + \eta_1\tau_1 \frac{\partial}{\partial t}\right)\left[a_1 \frac{\partial e}{\partial x_3} + a_2\Delta u_3\right] - a_3 \left(1 + \eta_2\tau_1 \frac{\partial}{\partial t}\right)\frac{\partial T}{\partial x_3} = (1 - \xi_1^2\Delta)\frac{\partial^2 u_3}{\partial t^2}\,, \qquad (2.27)$$

$$\Delta\phi = \left(1 + \eta_3\tau_0 \frac{\partial}{\partial t}\right)\left[a_4 \left(\frac{\partial \dot{u}_1}{\partial x_1} + \frac{\partial \dot{u}_3}{\partial x_3}\right) - Q\right] + \left(1 + \eta_4\tau_0 \frac{\partial}{\partial t}\right)\frac{\partial T}{\partial t}, \qquad (2.28)$$

$$t_{33} = \left(1 + \eta_1\tau_1\frac{\partial}{\partial t}\right)\left[a_5\frac{\partial u_1}{\partial x_1} + a_6\frac{\partial u_3}{\partial x_3}\right] - \left(1 + \eta_2\tau_1\frac{\partial}{\partial t}\right)T, \qquad (2.29)$$

$$t_{31} = a_7\left(1 + \eta_1\tau_1\frac{\partial}{\partial t}\right)\left(\frac{\partial u_3}{\partial x_1} + \frac{\partial u_1}{\partial x_3}\right), \qquad (2.30)$$

$$T = (1 - a\Delta)\phi\,, \qquad (2.31)$$

where

$$a_1 = \frac{\lambda+\mu}{\rho c_1^2}, \qquad a_2 = \frac{\mu}{\rho {c_1}^2}, \qquad a_3 = \frac{\beta_1 T_0}{\rho c_1^2}, \qquad a_4 = \frac{\beta_1 c_1^2}{K^*\omega_1},$$

$$a_5 = \frac{\lambda}{\beta_1 T_0}, \qquad a_6 = \frac{\lambda+2\,\mu}{\beta_1\, T_0}, \qquad a_7 = \frac{\mu}{\beta_1\, T_0}.$$

2.4 Solution Procedure

Following Helmholtz's decomposition, $u_1(x_1, x_3, t)$ and $u_3(x_1, x_3, t)$ relate to potential functions $q\ (x_1, x_3, t)$ and $\Psi\ (x_1, x_3, t)$ in dimensionless form are expressed as

$$\mathrm{u_1} = \frac{\partial \mathrm{q}}{\partial \mathrm{x_1}} - \frac{\partial \Psi}{\partial \mathrm{x_3}}, \qquad u_3 = \frac{\partial \mathrm{q}}{\partial \mathrm{x_3}} + \frac{\partial \Psi}{\partial \mathrm{x_1}}. \qquad (2.32)$$

Equations (2.26) - (2.28) along with (2.31) reduce to the following equations after using (2.32).

$$\left(1 + \eta_1\tau_1\frac{\partial}{\partial t}\right)\Delta \mathrm{q} - a_3\left(1 + \eta_2\tau_1\frac{\partial}{\partial t}\right)(1 - a\Delta)\phi = (1 - \xi_1^2\Delta)\frac{\partial^2 \mathrm{q}}{\partial t^2}, \qquad (2.33)$$

$$a_2\left(1 + \eta_1\tau_1\frac{\partial}{\partial t}\right)\Delta\Psi = (1 - \xi_1^2\Delta)\frac{\partial^2\Psi}{\partial t^2}, \qquad (2.34)$$

$$\Delta\phi = \left(1 + \eta_3\tau_0\frac{\partial}{\partial t}\right)(a_4\Delta\dot{q} - Q) + \left(1 + \eta_4\tau_0\frac{\partial}{\partial t}\right)\frac{\partial}{\partial t}(1 - a\Delta)\phi. \qquad (2.35)$$

The L.T of a function $f(x_1, x_3, t)$ following [Debnath (1995)] [37] w.r.t variable '*t*' and '*s*' as the L.T parameter is defined as

$$\hat{\mathrm{f}}(\mathrm{x_1}, \mathrm{x_3}, \mathrm{s}) = \mathrm{L}\{\mathrm{f}(\mathrm{x_1}, \mathrm{x_3}, \mathrm{t})\} = \int_0^\infty \mathrm{e}^{-\mathrm{st}}\mathrm{f}(\mathrm{x_1}, \mathrm{x_3}, \mathrm{t})\ \mathrm{dt}. \qquad (2.36)$$

With following basic properties

(i) $$\mathrm{L}\left(\frac{\partial \mathrm{f}}{\partial \mathrm{t}}\right) = \mathrm{s}\ \hat{\mathrm{f}}(\mathrm{x_1}, \mathrm{x_3}\ \mathrm{s}) - \mathrm{f}(\mathrm{x_1}, \mathrm{x_3}, 0), \qquad (2.37)$$

(ii) $$\mathrm{L}\left(\frac{\partial^2 \mathrm{f}}{\partial \mathrm{t}^2}\right) = \mathrm{s}^2\ \hat{\mathrm{f}}(\mathrm{x_1}, \mathrm{x_3}\ \mathrm{s}) - \mathrm{s}\ \mathrm{f}(\mathrm{x_1}, \mathrm{x_3}, 0) - \left(\frac{\partial \mathrm{f}}{\partial \mathrm{t}}\right)_{\mathrm{t=0}}. \qquad (2.38)$$

Initial conditions are as follows:

$$\mathrm{u_1}(\mathrm{x_1}, \mathrm{x_3}, 0) = \left(\frac{\partial \mathrm{u_1}}{\partial \mathrm{t}}\right)_{\mathrm{t=0}} = 0, \qquad \mathrm{u_3}(\mathrm{x_1}, \mathrm{x_3}, 0) = \left(\frac{\partial \mathrm{u_3}}{\partial \mathrm{t}}\right)_{\mathrm{t=0}} = 0,$$

$$\mathrm{q}(\mathrm{x_1}, \mathrm{x_3}, 0) = \left(\frac{\partial \mathrm{q}}{\partial \mathrm{t}}\right)_{\mathrm{t=0}} = 0, \qquad \mathrm{T}(\mathrm{x_1}, \mathrm{x_3}, 0) = \left(\frac{\partial \mathrm{T}}{\partial \mathrm{t}}\right)_{\mathrm{t=0}} = 0,$$

$$\Psi(\mathrm{x_1}, \mathrm{x_3}, 0) = \left(\frac{\partial \Psi}{\partial \mathrm{t}}\right)_{\mathrm{t=0}} = 0, \qquad \phi(\mathrm{x_1}, \mathrm{x_3}, 0) = \left(\frac{\partial \phi}{\partial \mathrm{t}}\right)_{\mathrm{t=0}} = 0, \qquad (2.39)$$

and the regularity conditions are

$$\mathrm{u_1}(\mathrm{x_1}, \mathrm{x_3}, \mathrm{t}) = \mathrm{u_3}(\mathrm{x_1}, \mathrm{x_3}, \mathrm{t}) = \mathrm{q}(\mathrm{x_1}, \mathrm{x_3}, \mathrm{t}) = \mathrm{T}(\mathrm{x_1}, \mathrm{x_3}, \mathrm{t}) = \Psi(\mathrm{x_1}, \mathrm{x_3}, \mathrm{t}) = 0,$$

$$\phi(\mathrm{x_1}, \mathrm{x_3}, \mathrm{t}) = 0, \text{ for } t > 0, x_3 \to \infty \quad . \qquad (2.40)$$

Following Sneddon (1979) [137], the F.T of function a $\tilde{f}$ (x_1 , x_3 , s) w.r.t space variable x_1 is defined as

$$\tilde{f}(\xi, x_3, s) = \int_{-\infty}^{\infty} e^{-\iota \xi x_1} \hat{f}(x_1, x_3, s)\, dx_1 \,. \qquad (2.41)$$

where ξ is the Fourier transform variable and ι denote iota.

Applying L.T and F.T defined by equations (2.36) and (2.41) on equations (2.33) - (2.35) and with the aid of basic properties and initial conditions given by equation (2.37) - (2.39) yield

$$\left[R_1\left(\frac{d^2}{dx_3^2} - \xi^2\right) - \left(\mathrm{R}_2 - \xi_1^2 \frac{d^2}{dx_3^2}\right) s^2\right] \tilde{q} \; - \left(R_3 \mathrm{R}_4 - a\, \mathrm{R}_3 \frac{d^2}{dx_3^2}\right) \tilde{\phi} = 0, \qquad (2.42)$$

$$\left[(a_2\, \mathrm{R}_1 + \xi_1^2\, s^2) \frac{d^2}{dx_3^2} - (a_2\, \xi^2 \mathrm{R}_1 + \mathrm{R}_2\, s^2)\right] \tilde{\Psi} = 0, \qquad (2.43)$$

$$\left(R_5 \xi^2 - \; R_5 \frac{d^2}{dx_3^2}\right) \tilde{q} + \left[(1 + a\, R_6) \frac{d^2}{dx_3^2} - (\xi^2 + R_7)\right] \tilde{\phi} = -R_8\, \tilde{Q}, \qquad (2.44)$$

where

$R_1 = 1 + \eta_1 \tau_1 s$, $R_2 = 1 + \xi_1^2 \xi^2$, $R_3 = a_3(1 + \eta_2 \tau_1 s)$,

$R_4 = 1 + a\xi^2$, $R_5 = a_4 s(1 + \eta_3 \tau_0 s)$, $R_6 = s + \eta_4 \tau_0 s^2$,

$R_7 = R_4 R_6$, $R_8 = 1 + \eta_3 \tau_0 s$.

Solving equations (2.42) and (2.44) yield

$$\left(\frac{d^4}{dx_3^4} + B_{01} \frac{d^2}{dx_3^2} + B_{02}\right)(\tilde{\mathrm{q}}, \tilde{\phi}) = \left(B_{03} \frac{d^2}{dx_3{}^2} + B_{04}\,, B_{03}^* \frac{d^2}{dx_3{}^2} + B_{04}^*\right) \tilde{\mathrm{Q}}\,, \qquad (2.45)$$

where

$B_{01} = \frac{B_2}{B_1}$, $B_{02} = \frac{B_3}{B_1}$, $B_{03} = \frac{B_4}{B_1}$, $B_{04} = \frac{B_5}{B_1}$, $B_{03}^* = \frac{B_4^*}{B_1}$, $B_{04}^* = \frac{B_5^*}{B_1}$,

$B_1 = (1 + aR_6)(R_1 + \xi_1^2 s^2) + aR_3 R_5$,

$B_2 = -[R_3 R_4 R_5 + aR_3 R_5 \xi^2 + (R_1 \xi^2 + R_2 s^2)(1 + aR_6) + (\xi^2 + R_7)(R_1 + \xi_1^2 s^2)]$,

$B_3 = (\xi^2 + R_7)(R_1 \xi^2 + R_2 s^2) + \; R_3 R_4 R_5 \xi^2$, $B_4 = \mathrm{a} R_3 R_8$, $B_5 = -R_3 R_4 R_8$,

$B_4^* = -(aR_8\, R_1 + R_8 \xi_1^2 s^2)$, $B_5^* = R_8\, (R_1 \xi^2 + R_2 s^2)$.

Simplification of equation (2.43) give

$$\left(\frac{d^2}{dx_3^2} - \mathrm{B}_{05}\right) \tilde{\Psi} = 0, \qquad (2.46)$$

where

$B_{05} = \frac{B_6}{B_7}$, $B_6 = a_2\, \xi^2 R_1 + \mathrm{R}_2\, s^2$, $B_7 = \; a_2\, R_1 + \xi_1^2\, s^2$.

The bounded solution of equations (2.45) and (2.46) satisfying the regularity conditions given by (2.40) can be written as:

$$\tilde{\mathrm{q}} = \mathrm{A}_1 \mathrm{e}^{-\lambda_1 \mathrm{x}_3} + \mathrm{A}_2 \mathrm{e}^{-\lambda_2 \mathrm{x}_3} - \frac{\mathrm{R}_3 \mathrm{R}_4 \mathrm{R}_8}{(\xi^2 + \mathrm{R}_7)(\mathrm{R}_1 \xi^2 + \mathrm{R}_2 s^2) + \mathrm{R}_3 \mathrm{R}_4 \mathrm{R}_5 \xi^2} \tilde{\mathrm{Q}}\,, \qquad (2.47)$$

$$\tilde{\phi} = d_1 A_1 e^{-\lambda_1 x_3} + d_2 A_2 e^{-\lambda_2 x_3} + d_3 \tilde{Q}\,, \qquad (2.48)$$

$$\tilde{\Psi} = A_3 e^{-\lambda_3 x_3}, \qquad (2.49)$$

where A_i $(i = 1,2,3)$ are the random constants to be determined and λ_i (i = 1,2,3) are roots of subsequent characteristic equations

$$\left(\frac{d^4}{dx_3^4} + B_{01}\frac{d^2}{dx_3^2} + B_{02}\right) = 0,$$

$$\left(\frac{d^2}{dx_3^2} - B_{05}\right) = 0,$$

and coupling constants are given by

$$d_i = \frac{(R_1+\xi_1^2 s^2)\lambda_i^2 - (R_1\xi^2 + R_2 s^2)}{R_3 R_4 - a R_3 \lambda_i^2}, \qquad d_3 = \frac{(R_1\xi^2 + R_2 s^2)R_8}{(\xi^2+R_7)(R_1\xi^2+R_2 s^2) + R_3 R_4 R_5 \xi^2}\,, \quad (i = 1,2).$$

2.5 Heat source

Here, we consider the concentrated ramp-type heat source as

$$Q = Q_1 \delta(x_1),$$

where

$$Q_1 = Q_0 \begin{cases} 0, t \le 0 \\ \frac{t}{t_0}, 0 < t \le t_0 \\ 1, t > t_0 \end{cases}, \qquad (2.50)$$

where Q_0 is constant, t_0 is the Ramp type parameter and $\delta(\,)$ is Dirac delta function.

2.6 Boundary Conditions

We take distributed exponentially decaying normal force and concentrated thermal source in addition the vanishing of the tangential stress at $x_3 = 0$, Mathematically, these are expressed as

(i) $t_{33} = F_1(x,t)$, (ii) $t_{31} = 0$, (iii) $\frac{\partial \phi}{\partial x_3} = F_2(x,t)$, $\qquad (2.51)$

where

$$F_1(x,t) = \frac{F_{10} t^2}{16 t_p^2} \exp\left(\frac{-t}{t_p}\right) H(a_1^* - |x_1|)\,, \qquad (2.52)$$

$$F_2(x,t) = F_{20} \exp(-b x_1)\, H(x_1) x_3^2 \delta(t). \qquad (2.53)$$

F_{10} , F_{20} signifies immensity of the force and steady temperature applied on the boundary respectively. a_1^* and b are constants, H( ) is Heaviside step function.

Using non-dimensional defined in equation (2.25) on equation (2.51) yield the non-dimensional boundary conditions and applying L.T and F.T defined by equations (2.36) and (2.41) on resulting non-dimensional boundary conditions along with (2.52) - (2.53), determine

(i) $\tilde{t}_{33} = \tilde{F}_1(\xi, s)$, (ii) $\tilde{t}_{31} = 0$, (iii) $\frac{\partial \tilde{\Psi}}{\partial x_3} = \tilde{F}_2\ (\xi, s)$, (2.54)

where

$\widetilde{F_1}\ (\xi\ , s\ ) = F_{10}\frac{t_p}{\left(1+st_p^2\right)^3}\frac{\sin a_1\xi}{\xi}$, $\widetilde{F_2}(\xi\ , s\ ) = a_8\ F_{20}\frac{x_3^2}{b-\iota\ \xi}$, (2.55)

where

$a_8 = \frac{\beta_1\ c_1}{\omega_1}$.

Using L.T and F.T defined by equation (2.36) and (2.41) on (2.29) - (2.32) and (2.50) yield

$\widetilde{u_1} = -\iota\ \xi\ \tilde{\mathrm{q}}\ - \frac{\mathrm{d}\ \tilde{\Psi}}{\mathrm{dx_3}}$, (2.56)

$\widetilde{\mathrm{u_3}} = \frac{\mathrm{d}\ \tilde{\mathrm{q}}}{\mathrm{dx_3}}\ -\ \iota\ \xi\ \tilde{\Psi}$, (2.57)

$\widetilde{t_{33}} = \mathrm{R_1}(\mathrm{a_5}\iota\xi\ \widetilde{\mathrm{u_1}} + a_6\iota\xi\ \widetilde{\mathrm{u_3}}) - \mathrm{R_1}\ \widetilde{T}$, (2.58)

$\widetilde{t_{31}} = \mathrm{a_7}R_1\left(-\iota\xi\widetilde{u_3} + \frac{\mathrm{d}\ \widetilde{\mathrm{u_1}}}{\mathrm{dx_3}}\right)$, (2.59)

$\tilde{T} = \left(1 - a\left(\frac{d^2}{dx_3^2} - \xi^2\right)\right)\tilde{\Phi}$, (2.60)

$\tilde{Q} = a_9\ Q_0$, (2.61)

where

$a_9 = \frac{(\ 1-e^{t_0\ S}\ )}{t_0\ s^2}$.

Inserting the value of $\tilde{\mathrm{q}}, \tilde{\Phi}, \tilde{\Psi}$ from equations (2.47) - (2.49) in the transformed boundary conditions (2.54) and with aid of equations (2.56) -(2.61), determine the expressions for components of displacement, stresses, thermodynamic temperature and conductive temperature as

$$\tilde{u}_1 = -\frac{1}{\Delta_0}\left[\iota\xi\ \sum_{k=1}^{3}\begin{pmatrix}\tilde{F}_1(\xi,s)\Delta_{k1}e^{-\lambda_k x_3} + \tilde{F}_2(\xi,s)\Delta_{k2}e^{-\lambda_k x_3}\\ +\Delta_{k3}e^{-\lambda_k x_3}\end{pmatrix} - \frac{a_9 R_8 R_4 R_3}{B_3}\ Q_0\right], \quad (2.62)$$

$$\tilde{u}_3 = -\frac{1}{\Delta_0}\left[\begin{matrix}\left(\sum_{k=1}^{2}\left(\tilde{F}_1(\xi,s)\lambda_k\Delta_{k1}e^{-\lambda_k x_3} + \tilde{F}_2(\xi,s)\Delta_{k2}e^{-\lambda_k x_3} + \lambda_k\Delta_{k3}e^{-\lambda_k x_3}\right)\right)\\ +\iota\xi\left(\tilde{F}_1(\xi,s)\Delta_{31}e^{-\lambda_3 x_3} + \tilde{F}_2(\xi,s)\Delta_{32}e^{-\lambda_3 x_3} + \ \mathrm{a_{13}}(a_{11}Q_0 + a_{10})e^{-\lambda_3 x_3}\right)\end{matrix}\right], \quad (2.63)$$

$$\tilde{t}_{33} = \frac{1}{\Delta_0}\left[\begin{matrix}\left(\sum_{k=1}^{3}\left(\tilde{F}_1(\xi,s)H_k\Delta_{k1}e^{-\lambda_k x_3} + \tilde{F}_2(\xi,s)H_k\Delta_{k2}e^{-\lambda_k x_3} + H_k\Delta_{k3}e^{-\lambda_k x_3}\right)\right)\\ +(a_{11}Q_0 + a_{10})\Delta\end{matrix}\right],$$

$$(2.64)$$

$$\tilde{t}_{31} = \frac{1}{\Delta_0}\left[\sum_{k=1}^{3}\left(\tilde{F}_1(\xi,s)H_{k+4}\Delta_{k1}e^{-\lambda_k x_3} + \tilde{F}_2(\xi,s)H_{k+4}\Delta_{k2}e^{-\lambda_k x_3}\right) + \right.$$

$$\left. \mathrm{H_5H_7H_9}(a_{11}Q_0 + a_{10}) + \sum_{k=2}^{3} H_{k+4}\Delta_{k3}e^{-\lambda_k x_3}\right], \qquad (2.65)$$

$$\tilde{T}$$

$$= \frac{1}{\Delta_0}\left[\sum_{k=1}^{2}\begin{pmatrix}\tilde{F}_1(\xi,s)\left[(1+a\xi^2) - a\lambda_k^2\right]d_k\Delta_{k1}e^{-\lambda_k x_3} \\ +\tilde{F}_2(\xi,s)\left[(1+a\xi^2) - a\lambda_k^2\right]d_k\Delta_{k2}e^{-\lambda_k x_3} + d_k\Delta_{k3}e^{-\lambda_k x_3}\end{pmatrix} + a_9 d_3\,(1+a\xi^2)\,Q_0\Delta_0\right]$$

$$(2.66)$$

$$\tilde{\Phi} = \frac{1}{\Delta_0}\left[\left(\sum_{k=1}^{2}\left(\tilde{F}_1(\xi,s)d_k\Delta_{k1}e^{-\lambda_k x_3} + \tilde{F}_2(\xi,s)d_k\Delta_{k2}e^{-\lambda_k x_3} + d_k\Delta_{k3}e^{-\lambda_k x_3}\right)\right) + a_9 d_3\;Q_0\Delta_0\right]$$

$$(2.67)$$

where

$\Delta_0 = \mathrm{H_8(H_2H_7 - H_3H_6) + H_9(H_3H_5 - H_1H_7)}$, $\Delta_{11} = -\mathrm{H_9H_7}$, $\Delta_{21} = \mathrm{H_7H_8}$,

$\Delta_{31} = \mathrm{H_5H_9 - H_6H_8}$, $\Delta_{12} = \mathrm{a_8(H_2H_7 - H_3H_6)}$, $\Delta_{22} = \mathrm{(H_3H_5 - H_1H_7)a_8}$,

$\Delta_{32} = \mathrm{(H_1H_6 - H_2H_5)a_8}$, $\Delta_{13} = \mathrm{a_{12}H_7H_9}$, $\Delta_{23} = -\mathrm{a_{12}H_7H_8}$,

$\Delta_{33} = \mathrm{a_{13}\,(a_9H_4Q_0 + a_{10})}$, $\mathrm{H_i = R_1(-a_5\xi_1^2 + a_6\lambda_i^2) - R_1[(1 + a\xi^2) + a\lambda_i^2]d_i}$,

$\mathrm{H_3 = i\xi\lambda_3R_1(a_6 - a_5)}$, $\mathrm{H_4 = \frac{a_5\xi^2R_8R_4R_3R_1}{B_3}\,(1 + \eta_1\tau_1 s)}$,

$\mathrm{H_{i+4} = 2ia_7\xi\lambda_iR_1}$, $\mathrm{H_7 = a_7R_1(\xi^2 + \lambda_3^2)}$, $\mathrm{H_{i+7} = \lambda_i d_i}$,

$\mathrm{a_{10} = -R_1(1 + a\xi^2)d_3}$, $\mathrm{a_{11} = a_9H_4}$, $\mathrm{a_{12} = a_{11}Q_0 + a_{10}}$,

$\mathrm{a_{13} = (H_6H_8 - H_5H_9)}$, $\mathrm{(i = 1,2)}$

and $\widetilde{F_1}(\xi, s), \widetilde{F_2}(\xi, s)$ are given by equation (2.55).

2.7 Validations

(i) Modified Green-Lindsay model with two temperature

Taking $\xi_1 = 0$, in equations (2.62) - (2.67) yield the corresponding expressions for MGL with TT and a heat source.

(ii) Non-local Modified Green-Lindsay model

Neglecting two temperature parameters, i.e. $a = 0$, in equations (2.62) - (2.67) yield the resulting expressions for the N-L, MGL model involving heat source.

(iii) Non-local L-S model without two temperature

Taking $\eta_1 = \eta_2 = 0, \eta_3 = \eta_4 = 1$, $a = 0$ along with absence of heat source in equations (2.62) - (2.67) yield the expressions for the N-L, L-S model and results are same as those obtained by Abbas et al. (2022) [2].

(iv) Non-local G-L model without two temperature

Taking $\eta_1 = \eta_4 = 0, \eta_2 = \eta_3 = 1, a = 0$ in equations (2.62) - (2.67) yield the expressions for N-L, G-L model without TT and the resulting equations are same as obtained by Bayones (2020) [20] as special cases.

(v) Non-local L-S model with two temperature

Taking $\eta_1 = \eta_2 = 0, \eta_3 = \eta_4 = 1$, in equations (2.62) - (2.67) determines the resulting expressions for L-S model with TT and in addition to the without heat source, the outcomes are the same as those attained by Lata and Singh (2020) [79].

2.8 Inversion of the Transformation

In this section we shall illustrate the method to invert the transformed components to physical dominion. The transformed components of transforms for the equations (2.62) - (2.67) CD, NS, TS, conductive temperature and thermodynamic temperature. These expressions are functions of x_3, s and ξ where s is the parameter of L.T and ξ is the F.T parameter. The function $f(x_1, x_3, t)$ attained from the $\tilde{f}(\xi, x_3, s)$ in the actual dominion, we find inverse of the F.T as

$$\hat{f}(x_1, x_3, s) = \frac{1}{2\pi}\int_{-\infty}^{\infty} \tilde{f}(\xi, x_3, s) \exp(-i\xi x_1)\, d\xi = \frac{1}{\pi}\int_0^{\infty} |\cos(\xi x_1) f_e - i \sin(\xi x_1) f_0|\, d\xi, \quad (2.68)$$

where

f_0 - odd parts of $\tilde{f}(\xi, x_3, s)$, f_e - even part of $\tilde{f}(\xi, x_3, s)$.

Consequently equation (2.68) yields the L.T, $\hat{f}(x_1, x_3, s)$ of $f(x_1, x_3, t)$.

$\hat{f}(x_1, x_3, s)$ in the expression (2.68) may be taken as the L.T $\hat{g}(s)$ of g(t) for the static values of the variables x_1 and x_3. The inverse function g(t) of transformed function $\hat{g}(s)$ is written [Honig and Hirdes(1984)][53] as

$$g(t) = \frac{1}{2\pi i}\int_{A-i\infty}^{A+i\infty} \hat{g}(s) \exp(st)\, ds, \quad (2.69)$$

where $s = A + \iota x_3$, A is a freely chosen real number that surpasses the real parts of all singularities of $\tilde{g}(s)$.

Substituting the value in equation (2.69) yield

$$g(t) = \frac{\exp(At)}{2\pi}\int_{-\infty}^{\infty} \hat{g}(A + \iota x_3) \exp(\iota \xi x_3)\, dx_3, \quad (2.70)$$

by defining $h(t) = \exp(At)g(t)$ and expanding it using a Fourier series over the interval [0, 2M], we drive the following approximation formula

$$g(t) = E_D + g_\infty(t), \quad (2.71)$$

where

$$g_\infty(t) = \frac{A_0}{2} + \sum_{i=1}^{\infty} A_k, \qquad 0 \le t \le 2M, \quad (2.72)$$

$$A_k = \frac{\exp(At)}{M} \mathrm{Re}\left[\hat{g}\left(A + \frac{\iota k\pi}{M}\right) \exp\left(\frac{\iota k\pi t}{M}\right)\right]. \qquad (2.73)$$

By choosing a suitably large number for A, the discretization error E_D can be made arbitrarily tiny. The criterion to select the value of A and M is given by Honig and Hirdes (1984) [53].

In addition to discretization error E_D there occur truncation error E_T.

In equation (2.71), the infinite series can be truncated after a finite number of N terms. Consequently, g(t)'s approximate value

$$g_N(t) = \frac{A_0}{2} + \sum_{k=1}^{N} A_k, \qquad 0 \le t \le 2M, \qquad (2.74)$$

The approximate formula to evaluate the function g(t) by "Korrecktur method" is

$$g(t) = g_\infty(t) - \exp(-2AM)\, g_\infty(2M + t) + E'_D, \qquad (2.75)$$

where

$|E'_D| \ll |E_D|$,

Now $\epsilon -$ algorithm the approximate value of $g(t)$ as follows

$$g_{N_k}(t) = g_N(t) - \exp(-2AM)\, g_{N'}(2M + t), \qquad (2.76)$$

where N' is an integer such that $N' < N$.

Define the sequence of partial sums of the series in the equation (2.73) as

$S_m = \sum_{k=1}^{m} A_k$ and $\epsilon -$sequence by

$\varepsilon_{0,m} = 0, \varepsilon_{1,m} = s_m$,

and

$$\varepsilon_{n+1,m} = \varepsilon_{n-1,m+1} + \frac{1}{\varepsilon_{n,m+1} - \varepsilon_{n,m}}, \; n, m \in N\,. \qquad (2.77)$$

Thus the sequence $\ldots\varepsilon_{1,1}, \varepsilon_{3,1}, \ldots \varepsilon_{N,1}$ (where N is a natural number) converges to $g(t) + E_D - \frac{A_0}{2}$ much quicker than the $\langle S_m \rangle$, $m \in N$[(Honig and Hirdes, (1984)] [53].

The actual process is to find inversion of L.T of equation (2.76) using the ε-algorithm. Choosing the right free parameter N is crucial for accuracy, the Korrecktur technique, and the ε-algorithm. The final stage is evaluating the integral in equation (2.76). Press et al. (1986) [103] propose a technique to calculate this integral.

2.9 Computational Interpretation and discussion

For numerical calculations, we take case of magnesium crystal type material, the physical constants are following Dhaliwal and Singh (1980) [38], as

$\lambda = 2.17 \times 10^{10}\mathrm{Nm}^{-2}$, $\mu = 3.278 \times 10^{10}\mathrm{Nm}^{-2}$, $K_1 = 1.7 \times 10^{2}\mathrm{Wm}^{-1}\,\mathrm{K}^{-1}$,

$\omega_1 = 3.58 \times 10^{11}\mathrm{S}^{-1}$, $\beta_1 = 2.68 \times 10^{6}\mathrm{Nm}^{-2}\mathrm{K}^{-1}$, $\rho = 1.74 \times 10^{3}\mathrm{Kgm}^{-3}$,

$\mathrm{C_e} = 1.04 \times 10^{3}\mathrm{JKg}^{-1}\mathrm{K}^{-1}$, $\mathrm{T_0} = 298\mathrm{K}$, $\tau_0 = 0.1\mathrm{s}$, $\tau_1 = 0.2\mathrm{s}$.

To investigate the impact of different factors, numerical calculations are computed using a mathematical software Force 2.0 and Grapher for four distinct scenarios: (i) nonlocal (ii) heat source (iii) two-temperature, and (iv) various thermoelasticity theories (MGL, G-L, and L-S theories)

2.9.1 Non-Local Parameter

Figures 2.1-2.4 show that the computation are carried out for t_0 = 0.25, a = 0.0104, and nonlocal parameter values ξ_1 = 0, 0.5, and 0.75. for $0 \le x_1 \le 10$.

i. The solid black line (——) represents NLMGL ($\xi_1 = 0.75$).
ii. Small dashed red line (. . .) stands for NLMGL ($\xi_1 = 0.5$).
iii. Long dashed blue line (− − −) represents the case of NLMGL ($\xi_1 = 0$).

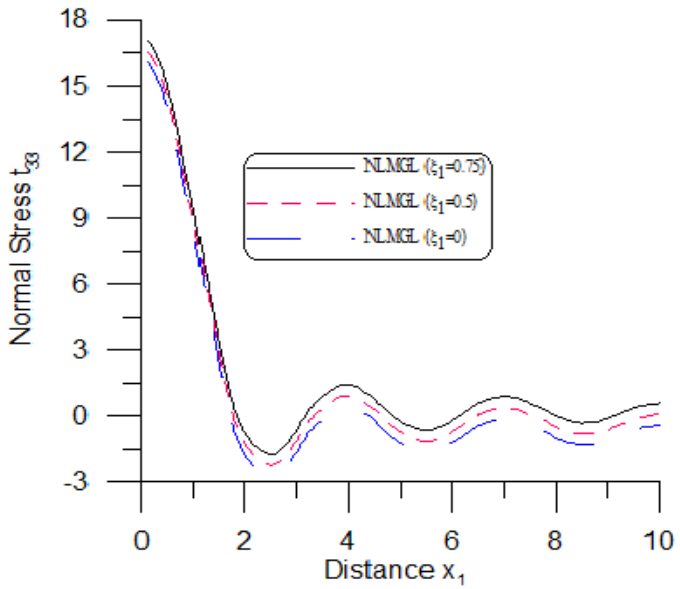

Figure 2.1 Profile of t_{33} vs $\mathbf{x_1}$

Figure 2.1 illustrates the behavior of the normal stress t_{33} vs x_1 . The value of t_{33} decreases sharply for all values of ξ_1 in the bounded range, $0 \le x_1 \le 2.5$ and as x_1 increases further, it shows a similar oscillatory behavior for remaining range.

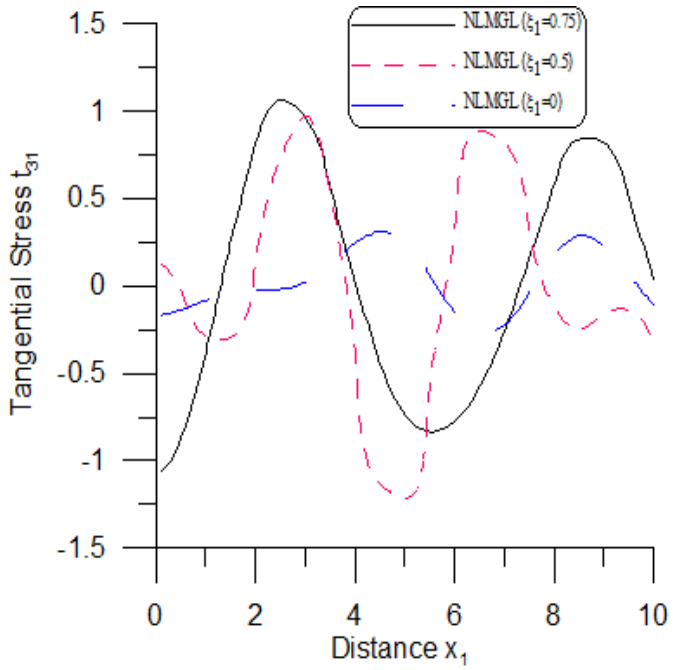

Figure 2.2 Profile of t_{31} vs x_1

Figure 2.2 displays the trend of t_{31} vs x_1 . Initially, the values of t_{31} for $\xi_1 = 0.75$ are lesser in contrast to other values of ξ_1 . The N-L parameter considerably impacts t_{31} as for higher values of $\xi_1 = 0.75$, t_{31} has high oscillatory pattern whereas for the value of $\xi_1 = 0$, the magnitude of oscillation is small.

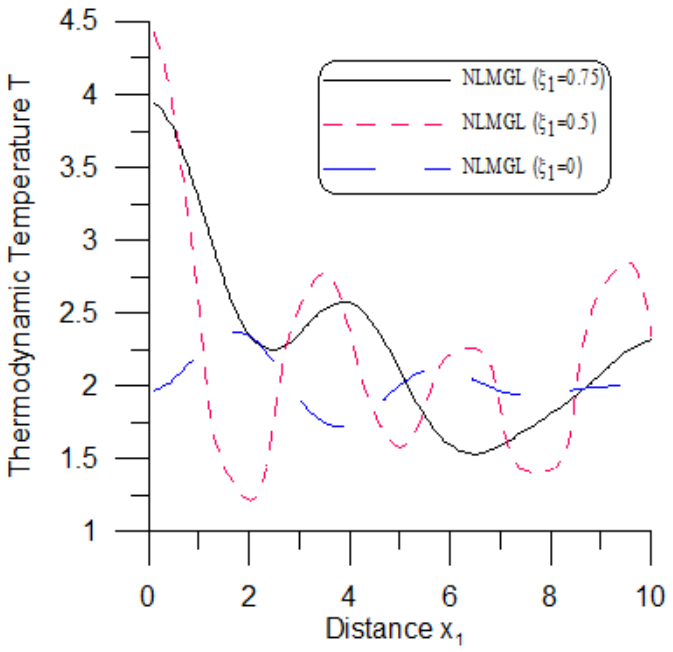

Figure 2.3 Profile of T vs x_1

Fig. 2.3 predicts T vs x_1. The behavior of T for all the values ξ_1 of is oscillatory in the entire interval. The curve corresponds to T for intermediate value of ξ_1=0.5, remains on higher side as compared to others considered values of ξ_1.

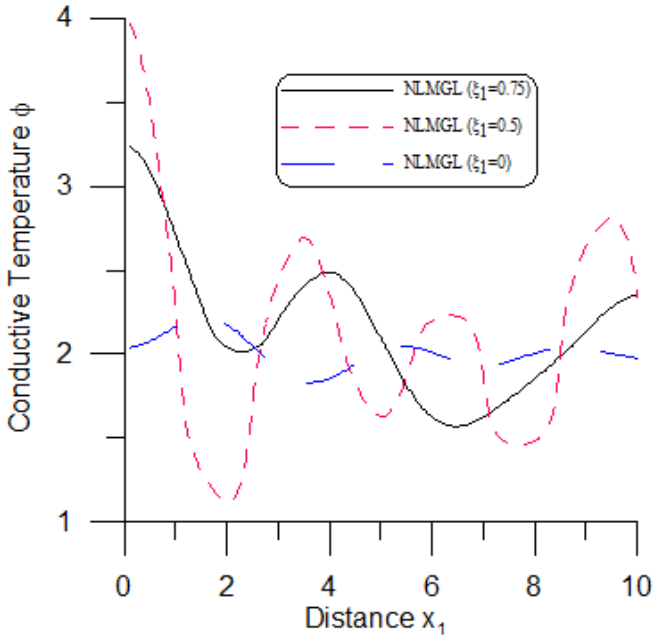

Figure 2.4 Profile of ϕ vs x_1

Figure 2.4 shows the trend of conductive temperature ϕ vs x_1. It is seen that the behaviour and variations for T and ϕ are alike with small difference in magnitude.

2.9.2 Heat Source Parameter

Figures 2.5-2.8 show the results computed for ξ_1 = 0.5, a = 0.0104, and t_0 = 0.01, 0.25, and 0.75.

i. The solid black line (——) represents HSMGL $t_0 = 0.75$.
ii. Small dashed red line (. . .) related to HSMGL $t_0 = 0.25$.
iii. Long dashed blue line (− − −) stands for HSMGL $t_0 = 0.01$.

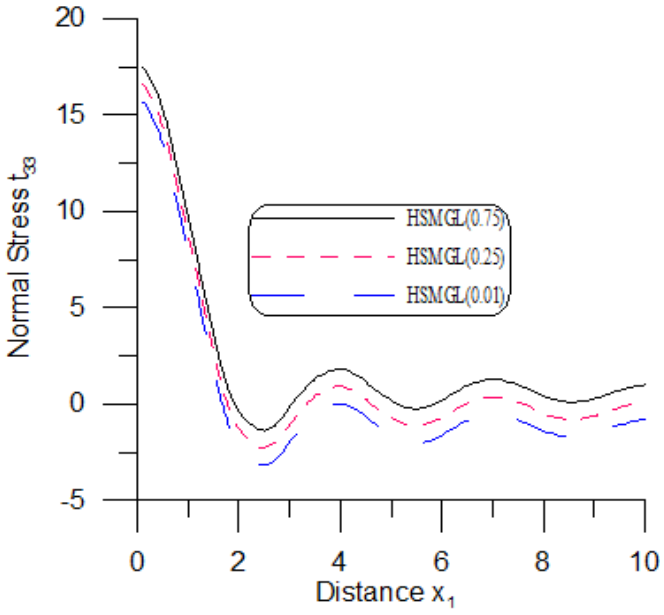

Figure 2.5: Profile of t_{33} vs x_1.

Fig. 2.5 displays the trend of t_{33} vs x_1. It is notice that all the curve corresponding to t_{33} decreases abruptly for $0 \leq x_1 \leq 2$ and after that follows similar oscillatory behavior. Also, immensity t_{33} is enhanced due to higher value of ramp time parameter t_0.

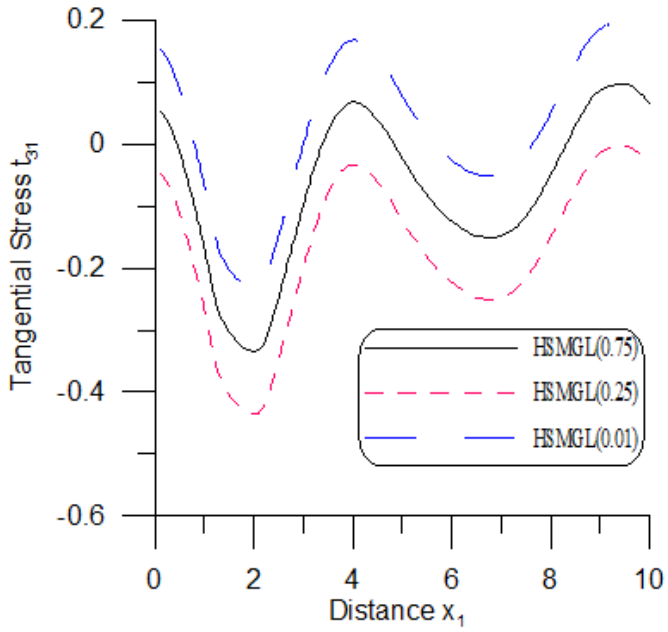

Figure 2.6: Profile of t_{31} vs $\mathbf{x_1}$

Fig. 2.6 displays the variation of t_{31} vs x_1 It is seen that t_{31} exhibit similar pattern for all assumed cases. The values of t_{31} shows increasing trend for $2 \leq x_1 \leq 4$ and $7 \leq x_1 \leq 9$ and decreasing trend for remaining range. Moreover, immensity of t_{31} increases for the smaller value of t_0

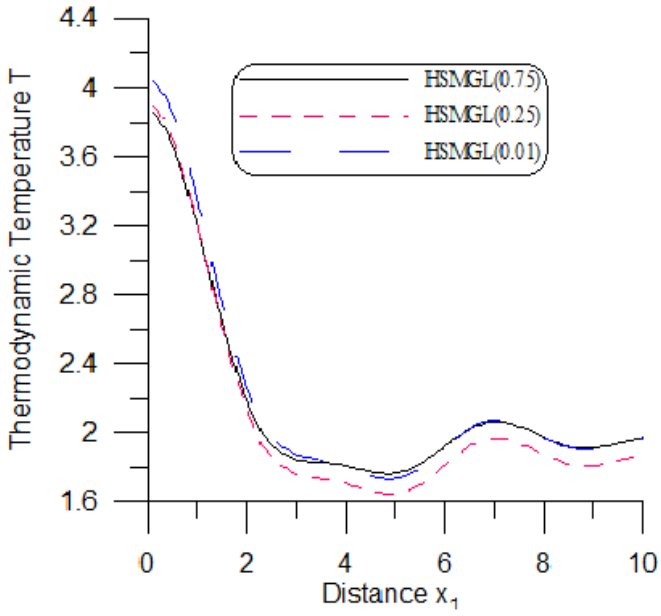

.

Figure 2.7: Profile of T vs $\mathbf{x_1}$.

Fig. 2.7 represents the T vs x_1. The values of T exhibit decreasing behaviour for all

assumed t_0 in the range $0 \leq x_1 \leq 2$ and shows oscillatory trend in the left-over domain.

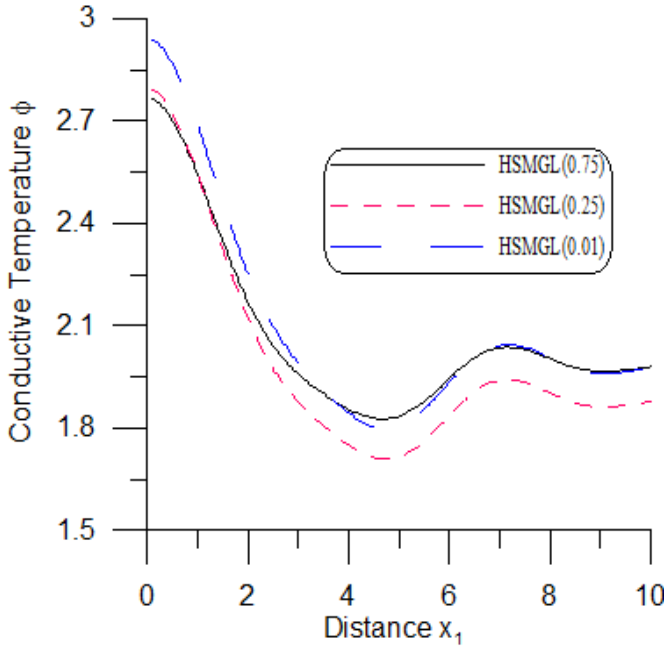

Figure 2. 8: Profile of ϕ vs x_1

Figure. 2.8 shows that all the curve corresponding to ϕ vs x_1 decreases in the interval $0 \leq x_1 \leq 4$ and follows an oscillatory behavior with increase in x_1.

2.9.3 Two Temperature Parameter

Figures 2.9-2.12 show the results computed for t_0 = 0.25, ξ_1 = 0.5, and a = 0, 0.0104, and a = 0.5.

i. The solid black line (——) represents TTMGL ($a = 0.5$).
ii. Small dashed red line (. . .) related to TTMGL ($a = 0.0104$).
iii. Long dashed blue line ($- - -$) represents the case of TTMGL ($a = 0.0$).

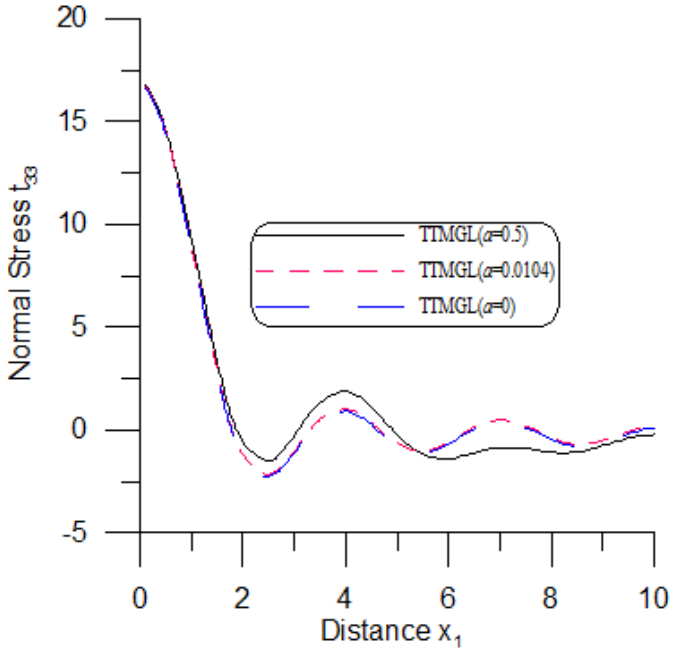

Figure 2.9: Profile of t_{33} vs x_1

Figure 2.9 illustrates the behavior of the t_{33} vs x_1 . The magnitude of t_{33} display sharp decreasing tendency for $0 \leq x_1 \leq 2$. Also, the magnitude of value of t_{33} is greater for $a = 0.5$ as compared to those obtained for other values of this parameter; for $x_1 > 2$, the value of t_{33} tends to zero.

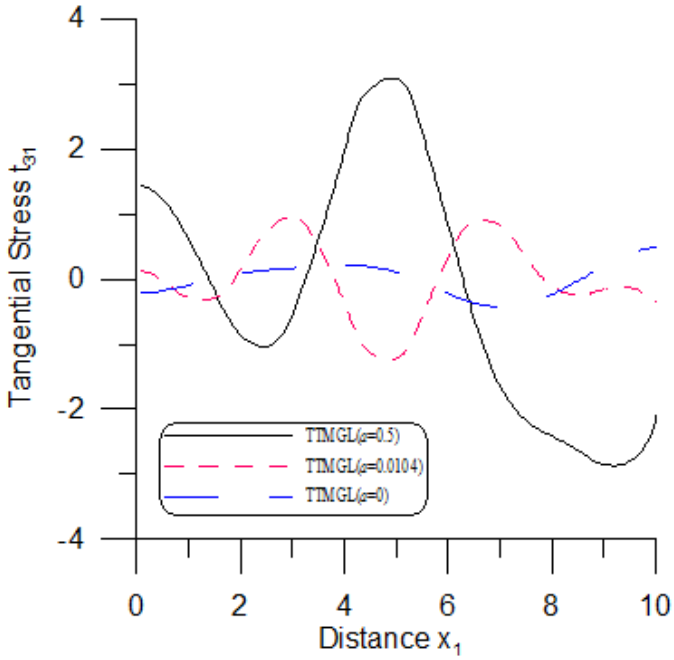

Figure 2.10: Profile of t_{31} vs x_1

Figure 2.10 displays the stress t_{31} vs x_1 . The behavior and variation of t_{31} is opposite to each other for $a = 0.5$ and $a = 0.0104$ in the range $2 \leq x_1 \leq 6$ and exhibit alike decreasing pattern in the left-over region, whereas in absence of two temperature

parameter, the values of t_{31}shows small variations about origin, which reveals the impact of two temperature parameter.

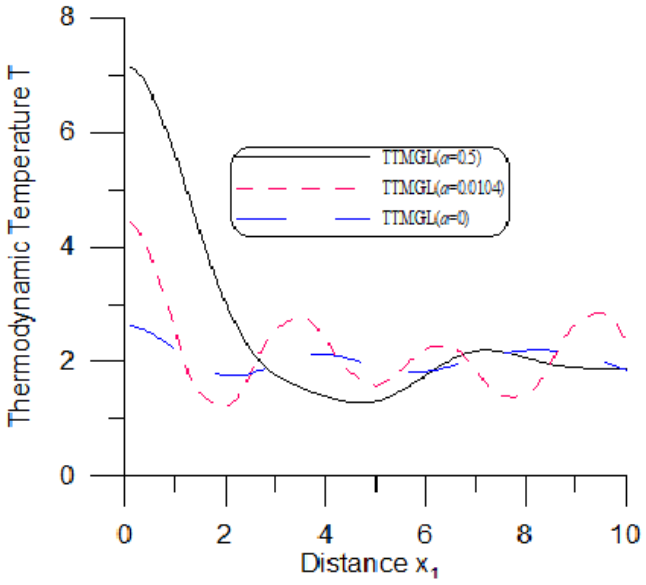

Figure 2.11: Profile of T vs x_1

Fig. 2.11 is a plot of T vs x_1. Initially, the values of T for $a = 0.5$, 0.0104 shows decrement behaviour for $0 \leq x_1 \leq 3$ and shows the oscillatory trend in the left-over domain with the difference in the magnitude of oscillation. Also, the curve corresponding to T for a = 0.5 remains on higher side as compared all considered cases.

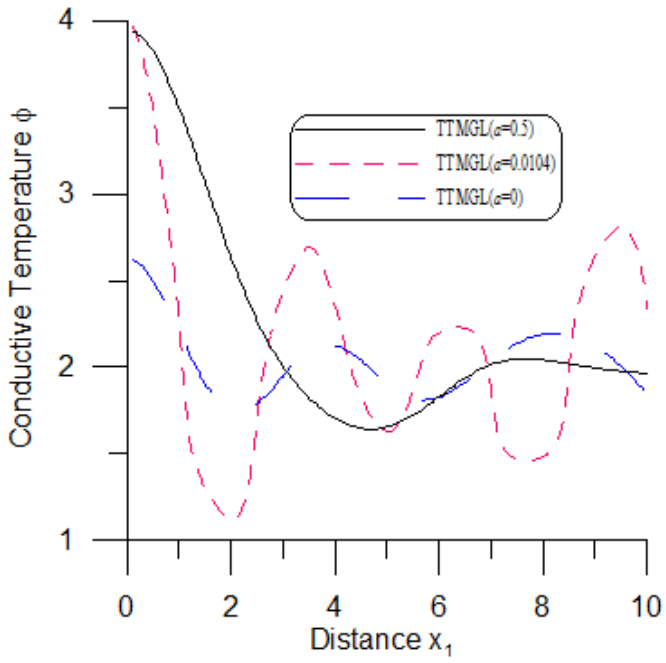

Figure 2.12: Profile of ϕ vs x_1

Figure 2.12 illustrates that the values of ϕ for a= 0.5 decreases for the first half of the

range and in left over range, it shows steady state about '2', whereas the trend of ϕ for a = 0.0104 and a = 0.0 displays alike oscillatory trend in the whole region except for $5 \leq x_1 \leq 8$.

2.9.4 Comparison of MGL, G-L and L-S models

Figures (2.13) -(2.16) show the comparison of different theories MGL, G-L and L-S with $a = 0.0104$, $t_0 = 0.25$, $\xi_1 = 0.5$ as fixed values for $0 \leq x_1 \leq 10$.

i. The solid black line (——) represents the MGL theory of thermoelasticity.
ii. Small dashed red line (. . .) related to G-L theory of thermoelasticity.
iii. Long dashed blue line (− − −) represents the case of L-S theory of thermoelasticity.

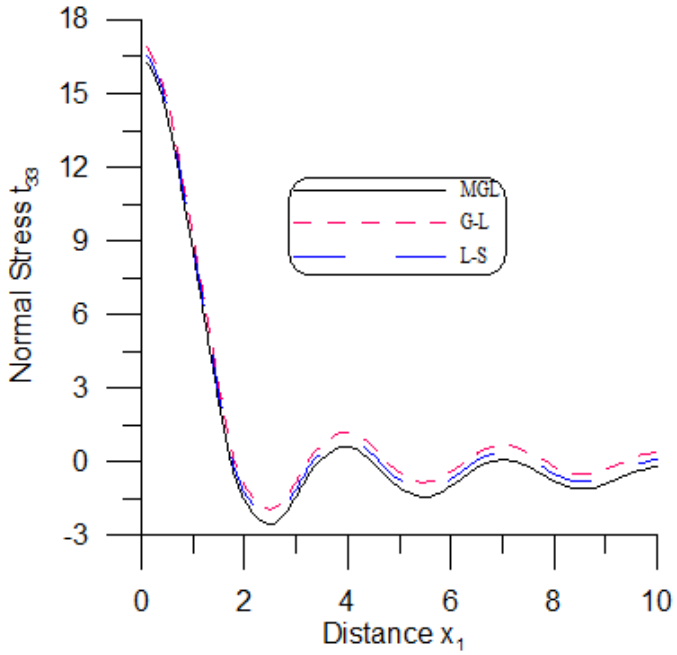

Figure 2.13: Profile of t_{33} vs x_1

Figure 2.13 illustrates the behavior of the t_{33} vs x_1 . Initially the values of t_{33} for MGL theory are smaller than those observed for G-L and L-S theory, which is accounted as the impact of relaxation times. Also, the values of t_{33} decreases sharply for $0 \leq x_1 \leq 3$ and attains minimum value at x_1 = 2.5 for L-S theory.

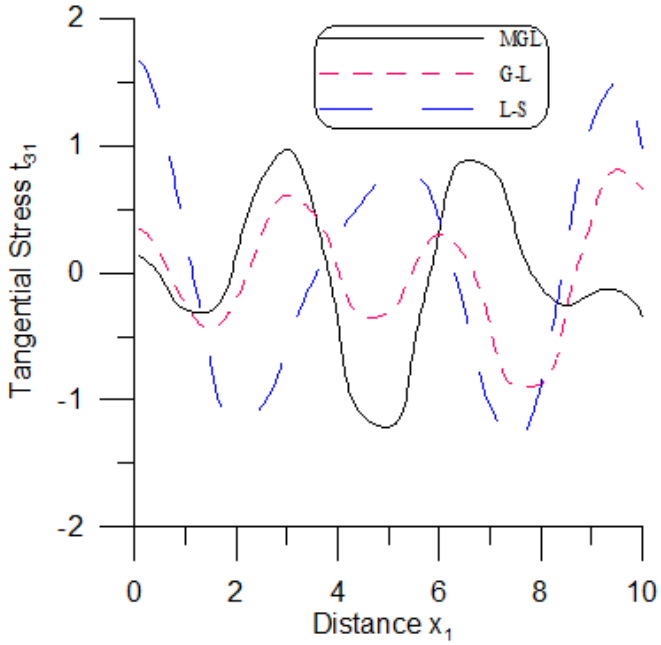

Figure 2. 14: Profile of t_{31} vs x_1

Figure 2.14 shows t_{31} vs x_1 . It is seen that the trend of t_{31} for MGL theory and G-Ltheory exhibits opposite behavior as seen for L-S theory in the interval $0 \leq x_1 \leq 8$ and similar behavior is observed in rest of the interval, which signifies the impact of different theories of thermoelasticity.

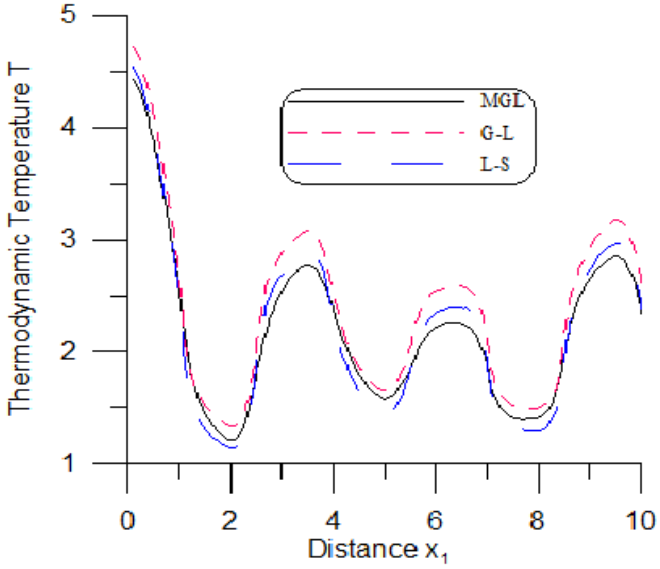

Figure 2.15: Profile of T vs x_1

Fig. 2.15 exhibits the plot for T vs x_1. The curve corresponding to T for GL theory is on higher side as compared to MGL and L-S theories in the entire range. Moreover, the magnitude of T shows abrupt decreasing pattern for $0 \leq x_1 \leq 2$, then, for the remaining interval, it exhibits the oscillatory behavior with large amplitude for GL theory.

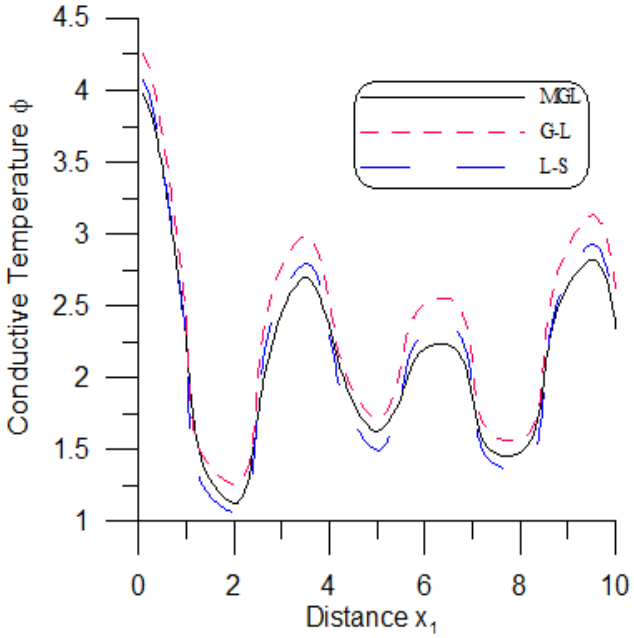

Figure 2. 16: Profile of ϕ vs x1

Figure 2.16 represent the ϕ vs x_1. It is noticed that initially magnitude of values of ϕ for MGL is higher as in comparison to G-L and L-S theory Also, the value of ϕ decreases sharply in limited range of $0 \leq x_1 \leq 2$. For remaining interval, ϕ exhibits the oscillatory behavior with large amplitude for MGL in the entire range.

2.10 Conclusions

In this chapter, a mathematical MGL model of thermoelasticity with non-local and two-temperature has been presented to solve deformation problem in homogenous, isotropic, thermoelastic semi-space. The governing equations are simplified with dimensionless and potential functions. The integral transform (L.T and F.T) technique has been employed to work out the problem. The exponentially decaying normal force, concentrated thermal source, and concentrated ramp-type heat source are taken to study the impact of N-L and TT. Numerical inversion methodology has been employed to attain the transformed expressions in original dominion and presented graphically to investigate the impact of N-L, TT, heat source, and different theories of thermoelasticity on obtained physical quantities. From Numerically computed results the conclusions are summarized as

i. Presence of the non-local parameter intensify the amplitude of stress component, thermodynamic and conductive temperature and behaviour of normal stress, tangential stress, thermodynamic temperature and conductive temperature is oscillatory for all the assumed cases in most of the range different physical quantities

exhibit oscillatory behavior in most of the range. With the increase of the N-L parameter, thermodynamic and conductive temperature as well as stress component increases which demonstrates the stimulus of the N-L parameter on the physical field quantities.

ii. The behavior of normal stress, tangential stress, thermodynamic temperature and conductive temperature for various values of the heat source parameter are qualitatively similar. However, the amplitudes of oscillations of these quantities are different. Even small values of the heat source parameter enhance the values of normal stress, T, and ϕ .

iii. The immensity of conductive temperature gets enhanced with presence of TT parameter, whereas the values of normal stress and tangential stress remain unchanged.

iv. The values of the stresses and the conductive temperature predicted by the G-L model are greater than those determined by the M G-L and L-S models.

The physical applications of the model can be found in mechanical engineering and geophysics

Chapter 3

The Influence of Non-Local and Heat Source in the Moore-Gibson-Thompson Heat Equation Using the Hyperbolic Two-Temperature Model

3.1 Introduction

Abouelregal et al. (2022) [5] analyzed problem in thermoelastic half-space medium owing to periodic heat source with modified MGT thermoelastic heat equation to explore the impact of a magnetic field on different physical quantities. Kumar et al. (2022) [73] presented photothermoelastic model based on MGT theory for orthotropic plate to explore the impact of velocity, ramp type and periodic loading parameters on physical field quantities. Gupta et al. (2023) [51] employed Eringen (1974) non-local (N-L) elasticity theory to analyze thermomechanical response for micropolar thermoelastic material with voids using MGT heat conduction equation with memory-dependent derivative.

Srivastava and Mukhopadhyay (2023) [136] studied wave problem in thermoelastic medium owing to heat source and discussed analytical method to solve the problem under MGT model. Abouelregal et al. (2023) [3] studied the magneto-thermoelastic interactions in viscoelastic medium under fourth-order MGT model and analyzed the effect of Hall current. Kumar et al. (2024) [69] employed the integral transform technique to examine the influence of N-L and HTT on stress components and temperature distribution in thermoelastic half-space with the MGT and micropolar models.

Abouelregal et al. (2024) [6] used fourth-order MGT model along with fractional order derivative to explore thermoelastic behavior of a functionally graded medium containing a spherical gap subjected to uniform electromagnetic field. Bazzara et al. (2024) [21] proved existence and uniqueness relations for poro-thermoelastic medium under MGT heat equation with microtemperature.

Temperature changes affect the mechanical behavior of materials, including stress and strain, and play a significant role in analyzing deformation, particularly in investigations related to earthquakes and other phenomena in seismology and engineering. Therefore, this research is motivated to explore the influence of a moving heat source and thermomechanical loading,

providing deeper insights into stress distribution and temperature evolution in complex thermoelastic media and contributing to the development of more accurate and efficient models,

In this chapter, the deformation problem of thermoelastic half -space under MGT heat equation with N-L and HTT is presented. After simplifying the equations with the dimensionless quantities, the potential functions and integral transform (L.T and F.T) technique is used for further simplification. The problem is examined due to a heat source which is taken as a laser pulse decaying with time and moving with constant velocity in one direction along with thermomechanical loading. Specific kinds of normal distributed force and ramp type thermal source (RTTS) are adopted to establish the effectiveness of the problem. The physical field quantities, component of displacement (CD), normal stress (NS), tangential stress (TS), thermodynamic temperature and conductive temperature are computed numerically and illustrated graphically for specific model to study the influence of N-L, HTT and moving heat source (MVS). Particular cases are also deduced from the present investigation.

3.2 Basic Equations

Following [(Quintanilla (2019) [105], Eringen (1974) [42], Youseff and El-Bary (2018) [149]] the field equations and constitutive relations in thermoelastic solid in the context of MGT heat equation with N-L, HTT and without body forces are written as:

$$(\lambda+\mu)\nabla(\nabla\cdot\vec{u})+\mu\Delta\vec{u}-\beta_1\nabla T=\rho\left(1-{\xi_1}^2\Delta\right)\frac{\partial^2\vec{u}}{\partial t^2}, \qquad (3.1)$$

$$\left(1+\tau_0\frac{\partial}{\partial t}\right)\left[\rho C_e\ddot{T}+\beta_1 T_0\ddot{e}-\dot{Q}\right]=K^*\frac{\partial}{\partial \mathrm{t}}\Delta\phi+K_1\Delta\phi, \qquad (3.2)$$

$$\ddot{\phi}-\ddot{T}=\beta^*\Delta\phi, \qquad (3.3)$$

$$t_{ij}=\lambda e_{kk}\delta_{ij}+2\mu\, \mathrm{e_{ij}}-\beta_1 T\delta_{ij}, \qquad (3.4)$$

where e_{ij} is same as defined in section 2.2 [Chapter 2], $\mathrm{K^*}=\frac{\mathrm{C_e}(\lambda+2\mu)}{4}$ is rate of the thermal conductivity, β^*- HTT parameter constant, $\mathrm{e_{ij}}$ and other symbols λ, μ , β_1,ρ, ξ_1,$\mathrm{C_e}$, K_1, $\mathrm{T_0}$, T, ϕ are same as defined in section 2.2 [Chapter 2].

The equations (3.1) - (3.4) yield to the following special cases.

$\mathrm{K^*}=\tau_0=0$: CT model, (1980) [38],

$\mathrm{K^*}=0$, $\tau_0\neq 0$: L-S model, (1967) [81],

$\mathrm{K_1}=\tau_0=0$, $\mathrm{K^*}\neq 0$: GN-II model, (1993) [49],

$\tau_0=0$, $\mathrm{K^*}\neq 0, K_1\neq 0$: GN-III model, (1992) [50].

Equations (3.1) - (3.4), in components form for cartesian coordinates (x_1, x_2, x_3) can be written as:

$$(\lambda+\mu)\frac{\partial e}{\partial x_1}+\mu\,\Delta u_1-\beta_1\frac{\partial T}{\partial x_1}=\rho(1-\xi_1^2\Delta)\frac{\partial^2 u_1}{\partial t^2}, \qquad (3.5)$$

$$(\lambda+\mu)\frac{\partial e}{\partial x_2}+\mu\,\Delta u_2-\beta_1\frac{\partial T}{\partial x_2}=\rho(1-\xi_1^2\Delta)\frac{\partial^2 u_2}{\partial t^2}, \qquad (3.6)$$

$$(\lambda+\mu)\frac{\partial e}{\partial x_3}+\mu\,\Delta u_3-\beta_1\frac{\partial T}{\partial x_3}=\rho(1-\xi_1^2\Delta)\frac{\partial^2 u_3}{\partial t^2}, \qquad (3.7)$$

$$\frac{\partial^2 T}{\partial\, t^2}=\left(\frac{\partial^2}{\partial\, t^2}-\beta^*\Delta\right)\phi, \qquad (3.8)$$

$$\left(1+\tau_0\frac{\partial}{\partial t}\right)\left[\rho C_e\frac{\partial^2 T}{\partial t^2}+\beta_1 T_0\frac{\partial^2 e}{\partial t^2}-\frac{\partial Q}{\partial t}\right]=K^*\Delta\dot{\phi}+K_1\Delta\phi, \qquad (3.9)$$

$$t_{11}=\lambda\, e+2\,\mu\, e_{11}-\beta_1 T, \qquad (3.10)$$

$$t_{22}=\lambda\, e+2\,\mu\, e_{22}-\beta_1 T, \qquad (3.11)$$

$$t_{33}=\lambda\, e+2\,\mu\, e_{33}-\beta_1 T, \qquad (3.12)$$

$$t_{31}=2\mu\, e_{31}, \qquad (3.13)$$

$$t_{32}=2\mu\, e_{32}, \qquad (3.14)$$

$$t_{21}=2\mu\, e_{21}, \qquad (3.15)$$

where Δ, e are same as defined by equation (2.24) Section 2.2 [Chapter 2].

3.3 Formulation and Solution of the Problem

A domain of solid half-space being homogeneous, isotropic thermoelastic under the MGT heat equation along with the impact of N-L and HTT parameters in an undisturbed state without body forces is considered. The starting point of rectangular cartesian coordinate system (x_1, x_2, x_3) is situated on the surface when x_3 =0. Also, x_3-axis directing vertically downward into the semi-space. The scenario includes a specific kind of forces/sources such as NDF and RTTS, with a heat source (HS) in the form of laser pulse decaying with time and moving with constant velocity in one direction is considered.

For the assumed model, we take

$$\vec{u}=(u_1(x_1,x_3,t),0,u_3(x_1,x_3,t)),\quad T=T(x_1,x_3,t),\qquad \phi=\phi(x_1,x_3,t). \qquad (3.16)$$

Using equation (3.16) in (3.5) - (3.9) and (3.12) - (3.13), we get

$$(\lambda+\mu)\frac{\partial e}{\partial x_1}+\mu\Delta u_1-\beta_1\frac{\partial T}{\partial x_1}=\rho\left(1-{\xi_1}^2\Delta\right)\frac{\partial^2 u_1}{\partial t^2}, \qquad (3.17)$$

$$(\lambda+\mu)\frac{\partial e}{\partial x_3}+\mu\Delta u_3-\beta_1\frac{\partial T}{\partial x_3}=\rho\left(1-{\xi_1}^2\Delta\right)\frac{\partial^2 u_3}{\partial t^2}, \qquad (3.18)$$

$$\left(1+\tau_0\frac{\partial}{\partial t}\right)\left[\rho C_e\frac{\partial^2 \mathrm{T}}{\partial t^2}+\beta_1 T_0\frac{\partial^2 \mathrm{e}}{\partial t^2}-\frac{\partial Q}{\partial t}\right]=K^*\Delta\dot{\phi}+K_1\Delta\phi, \qquad (3.19)$$

$$\frac{\partial^2 T}{\partial t^2}=\left(\frac{\partial^2}{\partial t^2}-\beta^*\Delta\right)\phi, \qquad (3.20)$$

$$t_{33}=\lambda\,\mathrm{e}+2\mu e_{33}-\beta_1 T, \qquad (3.21)$$

$$t_{31}=2\mu e_{31}, \qquad (3.22)$$

where

e and Δ are same as defined in Section 2.3 [Chapter 2].

The following dimensionless quantity is taken in addition to dimensionless quantities defined by equation (2.23) [Chapter 2]

$$\beta^{*\prime}=\frac{1}{c_1^2}\beta^*. \qquad (3.23)$$

Equations (3.17) - (3.22), with the help of equations (2.23) and (3.23) simplify to the following equations after suppressing the primes,

$$a_1\frac{\partial e}{\partial x_1}+a_2\Delta u_1-a_3\frac{\partial T}{\partial x_1}=\left(1-{\xi_1}^2\Delta\right)\frac{\partial^2 u_1}{\partial t^2}, \qquad (3.24)$$

$$a_1\frac{\partial e}{\partial x_3}+a_2\Delta u_3-a_3\frac{\partial T}{\partial x_3}=\left(1-{\xi_1}^2\Delta\right)\frac{\partial^2 u_3}{\partial t^2}, \qquad (3.25)$$

$$\left(1+\tau_0\frac{\partial}{\partial t}\right)\left(\frac{\partial^2 T}{\partial t^2}+a_4\frac{\partial e}{\partial t^2}-\frac{\partial Q}{\partial t}\right)=\left(\frac{\partial}{\partial t}+k_0\right)\Delta\phi, \qquad (3.26)$$

$$\ddot{\phi}-\ddot{T}=\beta^*\Delta\phi, \qquad (3.27)$$

$$t_{33}=a_5\frac{\partial u_1}{\partial x_1}+a_6\frac{\partial u_3}{\partial x_3}-T, \qquad (3.28)$$

$$t_{31}=a_7\left(\frac{\partial u_3}{\partial x_1}+\frac{\partial u_1}{\partial x_3}\right), \qquad (3.29)$$

where

$\mathrm{k}_0=\frac{K_1}{K^*\omega_1}$, a_i = (1-7) are same as defined in [Chapter2].

3.4 Solution Procedure

The relation between displacement components and scalar potentials is same as given by equation (2.32) [Chapter 2].

Using (2.32) in equations (3.24) - (3.26) give,

$$\Delta q-a_3 T=\left(1-{\xi_1}^2\Delta\right)\frac{\partial^2 q}{\partial t^2}, \qquad (3.30)$$

$$\left[a_2\Delta-(1-\xi_1^2\Delta)\frac{\partial^2}{\partial\, t^2}\right]\psi=0\,, \qquad (3.31)$$

$$\left(1+\tau_0\frac{\partial}{\partial t}\right)\left(\frac{\partial^2 T}{\partial t^2}+a_4\frac{\partial}{\partial t^2}\Delta q-\frac{\partial Q}{\partial t}\right)=\left(\frac{\partial}{\partial t}+k_0\right)\Delta\phi\,. \qquad (3.32)$$

Applying L.T and F.T defined by (2.36) and (2.41) on equations (3.30) - (3.32) and (3.27) along with the help of initial conditions (2.39) yield

$$\left(\frac{d^2}{d\,x_3^2}-\xi^2\right)\tilde{q}-a_3\,\tilde{T}=\left(1+\xi^2\xi_1^2-{\xi_1}^2\frac{d^2}{d\,x_3^2}\right)s^2\tilde{q}\,, \qquad (3.33)$$

$$\left[(\mathrm{a}_2+s^2\xi_1^2)\frac{d^2}{d\,x_3^2}-\left((1+\xi^2\xi_1^2)s^2+a_2\,\xi^2\right)\right]\widetilde{\Psi}=0\,, \qquad (3.34)$$

$$(1+\tau_0 s)\left(\mathrm{s}^2\widetilde{\mathrm{T}}+a_4\,s^2(\frac{d^2}{d\,x_3^2}-\xi^2)-\mathrm{s}\widetilde{\mathrm{Q}}\right)=(\mathrm{s}+k_0)\left(\frac{d^2}{d\,x_3^2}-\xi^2\right)\widetilde{\Phi}\,, \qquad (3.35)$$

$$\tilde{T}=\widetilde{\Phi}-\varsigma\left(\frac{\mathrm{d}^2}{\mathrm{dx_3}^2}-\xi^2\right)\widetilde{\Phi}\,, \qquad (3.36)$$

where $\varsigma=\begin{cases}0,\text{for one temperature (1T)}\\ a,\text{for two temperature (TT)}\\ \frac{\beta^*}{s^2},\text{for hyperbolic two temperature (HTT)}\end{cases}$.

Using equation (3.36) in equation (3.33) and (3.35) give

$$\left(R_1+R_2\,\frac{d^2}{d\,x_3^2}\right)\widetilde{\Phi}+\left(R_4+R_3\frac{d^2}{dx_3^2}\right)\tilde{\mathrm{q}}\;-\;R_5\,\widetilde{\mathrm{Q}}\;=0\,, \qquad (3.37)$$

$$\left(R_9+R_8\,\frac{d^2}{d\,x_3^2}\right)\widetilde{\Phi}+\left(R_7+R_6\,\frac{d^2}{d\,x_3^2}\right)\tilde{\mathrm{q}}\;=0, \qquad (3.38)$$

where

$R_1=(1+\tau_0 s)[s^2(1+\varsigma\xi^2)+(s+a_8)\xi^2]$, $\quad R_2=(s+k_0)-s^2\varsigma(1+\tau_0 s)$,

$R_3=a_4 s^2(1+\tau_0 s)$, $\quad R_4=-a_4 s^2\xi^2(1+\tau_0 s)$, $\quad R_5=s(1+\tau_0 s), R_6=1+{\xi_1}^2 s^2$,

$R_7=-\left(s^2\left(1+{\xi_1}^2\xi^2\right)+\xi^2\right)$, $\quad R_8=a_3\varsigma$, $\quad R_9=-a_3(1+\varsigma\xi^2)$.

Solving equation (3.37) - (3.38), after algebraic simplication's, yield

$$\left(\frac{d^4}{dx_3^4}+B_{01}\frac{d^2}{dx_3^2}+B_{02}\right)(\tilde{q},\tilde{\phi})=\left(B_{03}\frac{d^2}{dx_3{}^2}+B_{04}\,,B_{03}^*\frac{d^2}{dx_3{}^2}+B_{04}^*\right)\tilde{Q}, \qquad (3.39)$$

$B_{01}=\frac{B_2}{B_1}$, $\quad B_{02}=\frac{B_3}{B_1}$, $\quad B_{03}=\frac{B_4}{B_1}$, $\quad B_{04}=\frac{B_5}{B_1}$, $\quad B_1=R_2R_6-R_3R_8$,

$B_2=(R_1R_6+R_2R_7-R_8R_4-R_9R_3)$, $\quad B_3=(R_1R_7-R_9R_4)$, $\quad B_4=-R_5R_8$,

$B_5=-R_5R_9$, $\; B_{03}^*=\frac{B_4^*}{B_1}$, $\quad B_{04}^*=\frac{B_5^*}{B_1}$, $\quad B_4^*=R_5\,R_6$, $\quad B_5^*=R_5\,R_7$.

Equation (3.34), after simplification gives

$$\left(\frac{d^2}{dx_3^2}-\lambda_3^2\right)\overline{\Psi}=0\,, \qquad (3.40)$$

where

$\lambda_3^2 = \frac{a_2\,\xi^2+(1+\xi_1^2\xi^2)s^2}{a_2+\xi_1^2\,s^2}$.

The bounded solution of equations (3.39) and (3.40) satisfying the regularity conditions given by (2.40) determine the following

$$\tilde{q} = A_1 e^{-\lambda_1 x_1} + A_2 e^{-\lambda_2 x_3} + \frac{R_5 R_9}{R_9 R_4 - R_1 R_7}\tilde{\mathrm{Q}}, \qquad (3.41)$$

$$\tilde{\Phi} = d_1 A_1 e^{-\lambda_1 x_3} + d_2 A_2 e^{-\lambda_2 x_3} + d_3\tilde{\mathrm{Q}}, \qquad (3.42)$$

$$\tilde{\Psi} = A_3 e^{-\lambda_3 x_3}. \qquad (3.43)$$

$\lambda_l (i = 1,2)$ being the roots of the characteristic equation $\left(\frac{d^4}{dx_3^4} + B_{01}\frac{d^2}{dx_3^2} + B_{02}\right) = 0$ and coupling constants are given by

$d_i = -\frac{\lambda_i^2 R_3 + R_4}{R_1 + R_2\lambda_i^2}$, $\qquad d_3 = \frac{R_5 R_7}{R_1 R_7 - R_9 R_4}$, (i = 1,2).

3.5 Heat Source

Here, we take exponentially decaying heat source with velocity *v* as

$$Q = Q_0\, exp\left(-\frac{t}{t_p}\right)\delta(x_1 - vt), \qquad (3.44)$$

where Q_0 is constant, t_p is the time duration of laser pulse decaying, v is the velocity of moving heat source, *t* is time, δ ( ) symbolizes the Dirac delta function.

3.6 Boundary Conditions

The boundary restrictions for thermoelastic semi- space which is exposed to specific normal force (distributed normal force) and thermal source (ramp type) are considered as

$$(i)\ t_{33} = F_1(x_1, t), \quad (ii)\ t_{31} = 0, \quad (iii)\ \frac{\partial\phi}{\partial x_3} = F_2(x_1, t), \quad \text{at } x_3 = 0\,. \qquad (3.45)$$

where

$$F_1(x_1, t) = F_{10}\begin{cases} sin\frac{\pi t}{\eta}\delta(x) & 0 \le t < \eta \\ 0 & t > \eta \end{cases}, \qquad (3.46)$$

$$F_2(x, t) = F_{20}\,\delta_{t_0}(t)\,\delta(x)\,, \quad \delta_{t_0}(t) = \begin{cases} \frac{t}{t_0} & 0 \le t < t_0 \\ 0 & t > t_0 \end{cases}, \qquad (3.47)$$

F_{10} , F_{20} are as defined in section 2.6 [Chapter 2].

Using non-dimensional equation (2.25) on equation (3.44) and (3.45) give the non-dimensional boundary condition and applying L.T and F.T defined by (2.36) and (2.41) [Chapter 2], on resulting non-dimensional boundary conditions along with (3.46) - (3.47), determine

$$\tilde{Q} = Q_0\, a_9, \qquad (3.48)$$

where

$a_9 = e^{-\left(s+\frac{1}{t_p}\right)\frac{x_1}{v}}$ and

$$(i)\ \tilde{t}_{33} = \tilde{F}_1(\xi, s), \qquad (ii)\ \tilde{t}_{31} = 0, \quad (iii)\ \frac{\partial\tilde{\phi}}{\partial x_3} = \tilde{F}_2(\xi, s) \text{ at } x_3 = 0. \qquad (3.49)$$

where

$$\tilde{F}_1(\xi, s) = F_{10}\, a_{10}\,,\ \tilde{F}_2(\xi, s) = F_{20}\, a_{11}\,. \qquad (3.50)$$

$a_{10} = \frac{(1-e^{-st_0})}{t_0 s}, a_{11} = \frac{\pi\,\eta(1+e^{-\eta s})}{\pi^2+s^2\eta^2}$.

Invoking L.T and F.T on equations (3.28) and (3.29) yield

$$\widetilde{t_{33}} = a_5 \iota\xi\, \widetilde{u_1} + a_6 \frac{\partial\widetilde{u_3}}{\partial x_3} - \widetilde{T}\,, \qquad (3.51)$$

$$\widetilde{t_{31}} = a_7\left(-\iota\xi\widetilde{u_3} + \frac{d\widetilde{u_1}}{dx_3}\right). \qquad (3.52)$$

Inserting the values of $\tilde{q}\,, \widetilde{\psi}, \tilde{\phi}$ from equations (3.41) - (3.43) in the transformed boundary conditions (3.49) and using equations (2.32), (3.48), (3.50) - (3.52), yield the expressions of physical field quantities (displacement components, stresses, conductive temperature and thermodynamic temperature) as

$$\tilde{u}_1 = \frac{1}{\Delta}\begin{bmatrix} F_{10}\left[(-\iota\xi)\sum_{i=1}^{2}\Delta_{i1}\, e^{-\lambda_i x_3} + \Delta_{31} e^{-\lambda_3 x_3}\right] + F_{20}\left[(-\iota\xi)\sum_{i=1}^{2}\Delta_{i2} e^{-\lambda_i x_3} + \Delta_{32}\, e^{-\lambda_3 x_3}\right] \\ -i\xi\left(\sum_{i=1}^{2}\Delta_{i3}\, e^{-\lambda_i x_3} + \frac{R_5 R_9}{R_9 R_4 - R_1 R_7} Q_0 a_9\right) + \Delta_{33} e^{-\lambda_3 x_3} \end{bmatrix}, \qquad (3.53)$$

$$\tilde{u}_3 = \frac{-1}{\Delta}\begin{bmatrix} F_{10}\left(\sum_{i=1}^{2}\lambda_i\Delta_{i1}\, e^{-\lambda_i x_3} + i\xi\Delta_{31} e^{-\lambda_3 x_3}\right) + F_{20}\left(\sum_{i=1}^{2}\lambda_i\Delta_{i2}\, e^{-\lambda_i x_3} + i\xi\Delta_{32} e^{-\lambda_3 x_3}\right) \\ +\left(\sum_{i=1}^{2}\lambda_i\Delta_{i3}\, e^{-\lambda_i x_3} + i\xi\Delta_{33}^{*} a_9 Q_0 e^{-\lambda_3 x_3}\right) \end{bmatrix}, \qquad (3.54)$$

$$\widetilde{t_{33}} = \frac{1}{\Delta}\left[F_{10}\sum_{i=1}^{3} H_i^{*}\,\Delta_{i1} e^{-\lambda_i x_3} + F_{20}\sum_{i=1}^{3} H_i^{*}\Delta_{i2}\, e^{-\lambda_i x_3} + \sum_{i=1}^{3} H_i^{*}\Delta_{i3} e^{-\lambda_i x_3} + H_4^{*} Q_0 a_9 \Delta\right], \qquad (3.55)$$

$$\hat{t}_{31} = \frac{1}{\Delta}\left[F_{10}\sum_{i=1}^{3} H_{i+4}^{*}\Delta_{i1}\, e^{-\lambda_i x_3} + F_{20}\sum_{i=1}^{3} H_{i+4}^{*}\Delta_{i2} e^{-\lambda_i x_3} + \sum_{i=1}^{2} H_{i+4}^{*}\Delta_{i3} e^{-\lambda_i x_3} + H_7^{*}\Delta_{33}^{*}\, a_9 Q_0 e^{-\lambda_3 x_3}\right], \qquad (3.56)$$

$$\widetilde{\phi} = \frac{1}{\Delta}\left[F_{1_0}\sum_{i=1}^{2} H_{i+7}^{*}\Delta_{i1} e^{-\lambda_i x_3} + F_{20}\sum_{i=1}^{2} H_{i+7}^{*}\Delta_{i2} e^{-\lambda_i x_3} + \sum_{i=1}^{2} H_{i+7}^{*}\Delta_{i3} e^{-\lambda_i x_3} + H_{10}^{*} Q_0 a_9\right], \qquad (3.57)$$

$$\widehat{T} = \frac{1}{\Delta}\left[F_{1_0}\sum_{i=1}^{2} d_i\Delta_{i1}\, e^{-\lambda_i x_3} + F_{20}\sum_{i=1}^{2} d_i\Delta_{i2}\, e^{-\lambda_i x_3} + \sum_{i=1}^{2} d_i\Delta_{i3}\, e^{-\lambda_i x_3} + d_3 Q_0 a_9\right], \tag{3.58}$$

where

$H_i^* = -a_5\xi^2 + a_6{\lambda_i}^2 - (1+\varsigma\xi^2)d_i + \varsigma d_i{\lambda_i}^2$, $H_3^* = \lambda_3 i\xi(a_5 + a_6)$,

$H_4^* = -d_3(1+\varsigma\xi^2) - a_5\xi^2\frac{R_5R_9}{R_4R_9 - R_1R_7}$, $H_{i+4}^* = -2ia_7\xi\lambda_i$,

$H_7^* = -(\lambda_3^2 - \xi^2)$, $H_{i+7}^* = d_i\left(1 + \varsigma\xi^2 - \varsigma{\lambda_i}^2\right)$, $H_{10}^* = d_3(1+\varsigma\xi^2)$,

$\Delta = d_1(H_2^*H_7^* - H_3^*H_6^*) + d_2(H_3^*H_5^* - H_1^*H_7^*)$, $\Delta_{11} = -d_2H_7^*a_{10}$,

$\Delta_{12} = (H_2^*H_7^* - H_3^*H_6^*)a_{11}$, $\Delta_{13} = (H_4^*H_7^*d_2 + H_3^*H_6^*d_3 - H_2^*H_7^*d_3)a_9Q_0$,

$\Delta_{21} = d_1H_7^*a_{10}$, $\Delta_{22} = (H_3^*H_5^* - H_1^*H_7^*)a_{11}$, $\Delta_{23} = (H_1^*d_3 - H_4^*d_1)H_7^*a_9Q_0$,

$\Delta_{31} = (d_2H_5^* - d_1H_6^*)a_{10}$, $\Delta_{32} = (H_1^*H_6^* - H_2^*H_5^*)a_{11}$,

$\Delta_{33} = (H_2^*H_5^*d_3 - H_1^*H_6^*d_3 - H_4^*H_5^*d_2 + H_4^*H_6^*d_1)a_9Q_0$, $(i = 1,2)$.

3.7 Validation and Special Cases

(i) MGT thermoelasticity with HTT

if $\boldsymbol{\xi_1 \to 0}$ in equations (3.53) - (3.58), determine the resulting expressions for MGT with HTT with the changed value of constants $\boldsymbol{R_6 = 1}$, $\boldsymbol{R_7 = \xi^2 s^2}$.

(ii) Non-Local Lord Shulman Model (L-S model) with HTT

Letting $\boldsymbol{K^* = 0}$**,** in equations (3.53) - (3.58), give the expressions for generalized thermoelasticity, which involve one relaxation time under N-L and HTT with changed value of $\boldsymbol{k_0 = 0}$.

(iii) GN-II model with HTT

Taking $\boldsymbol{K_1 = \tau_0 = 0}$, $\boldsymbol{K^* > 0}$, in equations (3.53) - (3.58), will explore the resulting quantities for GN type-II model under N-L theory and HTT.with change value of constants

$R_1 = (s^2(1+\varsigma\xi^2) + (s+k_0)\xi^2)$, $R_3 = a_4s^2$, $R_4 = -a_4s^2\xi^2$, $R_5 = s$.

(iv) Green- Naghdi-III model (GN-III model) with HTT

Taking $K^*, K_1 > 0$, $\tau_0 = 0$, in equations (3.53) - (3.58), determine the expressions for the GN type III model under the influence of N-L and HTT.

(v) Lord Shulman model (L-S model) with TT

Letting $K^* = 0, \xi_1 = 0$ and $\varsigma = a$ in equations (3.53) - (3.58), gives the expression of generalized thermoelasticity, which involve one relaxation time under N-L and TT.

3.7.1 Sub Cases:

3.7.1.1 For $\varsigma = \boldsymbol{a}$, in equations (3.53) - (3.58) yield resulting expressions for MGT thermoelasticity with TT and N-L effect.

3.7.1.2 Putting $\mathbf{K}^{*} = \mathbf{0}, \varsigma = \mathbf{0}$, $\boldsymbol{\xi_1} = \mathbf{0}$ in equations (3.53) - (3.58), determine the resulting expressions for L-S thermoelasticity model with moving heat source then results agree with those obtained by Amin et al. (2017) [10] for a special case.

3.8 Inversion of the Transforms

To solve the problem in the physical realm, we must find the inverse of the transformations in equations (3.53) - (3.58). The inverse of the L.T and F.T can be found using the method explained in section 2.8 of [Chapter 2].

3.9 Numerical Result and Discussion

For numerical computations, following Dhaliwal and Singh (1980) [38], we take material magnesium and the value of material constants are same as given by section 2.9[Chapter 2].

3.9.1 Non-Local

In this case, we consider N-L parameter as $\xi_1 = 0$, $\xi_1 = 0.20$, $\xi_1 = 0.50$, $\xi_1 = 0.75$, HTT parameter $\varsigma = 0.5$ and $v = 1$ for $0 \leq x_1 \leq 10$.

i. The solid line (——) represents ($\xi_1 = 0.75$).
ii. Small dashed line (. . .) stands for ($\xi_1 = 0.50$).
iii. Solid line with center symbol Diamond ' $\diamond$ ' ($- \diamond -$) related to ($\xi_1 = 0.20$).
iv. Small dashed line with center symbol Circle 'o ' ($-\mathrm{o}-$) represents the case of ($\xi_1 = 0$).

3.9.1.1 Normal Distributed Force

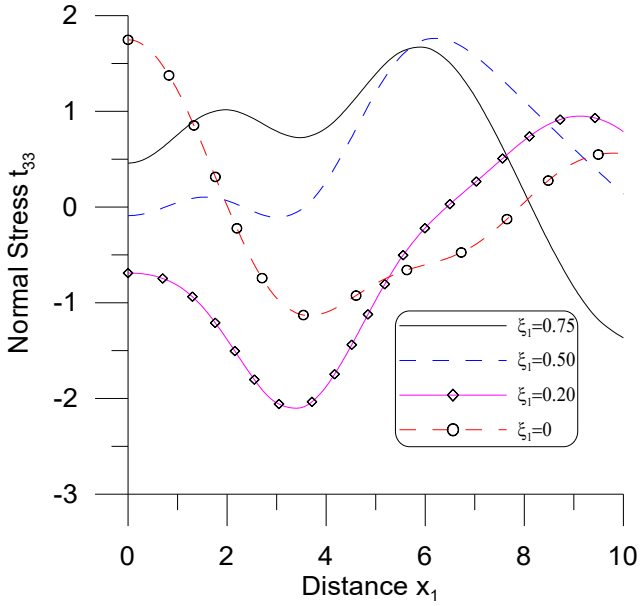

Fig. 3.1: **Variation of t_{33} vs x_1**

Figure 3.1 shows the behaviour of t_{33} vs x_1. It is noticed that the behavior of t_{33} for $\xi_1 = 0.75$ and 0.5 are reverse in nature as that of $\xi_1 = 0.20$ and $\xi_1 = 0$ for the range $0 \leq x_1 \leq 2$ and $6 \leq x_1 \leq 10$ respectively, while similar trends are noticed in the left-over interval. It is also seen that near the boundary surface, t_{33} attains minima for $\xi_1 = 0.20$ at $x_1 = 4$.

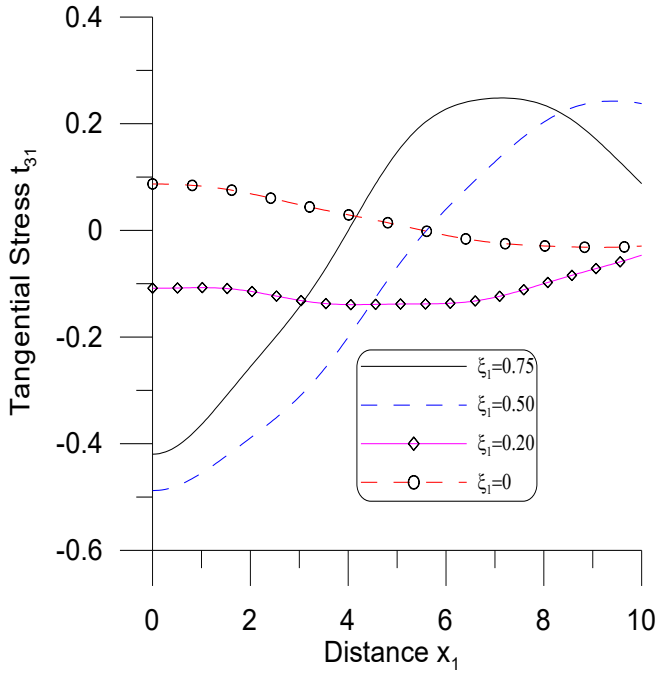

Fig. 3.2: Variation of t_{31} vs x_1

Figure 3.2 is plot of t_{31}vs x_1, which demonstrates that for $\xi_1 = 0.0$, the values of $t_{31}$are higher in contrast to those obtained for $\xi_1 = 0.20$for the entire range. It is also seen that for a higher value ($\xi_1 = 0.75, \xi_1 = 0.50$), the values increase in the entire range with a significant difference in their magnitude.

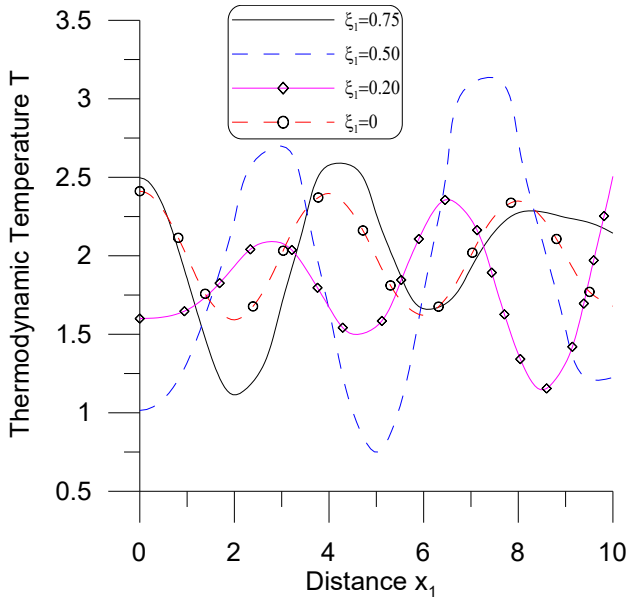

Fig. 3.3: Variation of T vs x_1

Figure 3.3 predicts T vs x_1. It is seen that the magnitude of T for intermediate values of the N-L parameter ($\xi_1 = 0.50, \xi_1 = 0.20$) are opposite in nature to those for the other value of ξ_1 ($\xi_1 = 0.75, \ \xi_1 = 0.0$) Moreover, T shows oscillatory behaviour with more variations for $\xi_1 = 0.50$ than other lesser values of $\xi_1$which is accounted as impact of N-L parameter.

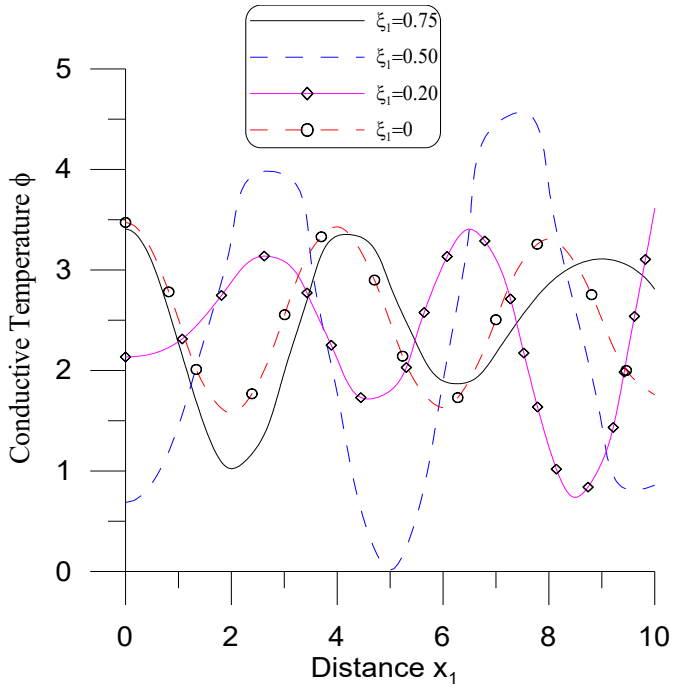

Fig. 3.4: Variation of ϕ vs x_1

The graphical representation of ϕ with x_1 is represented in figure 3.4. It is noticed that ϕ exhibits similar pattern in the range $0 \leq x_1 \leq 2$ and $4 \leq x_1 \leq 6$ for ξ_1 ($\xi_1 = 0.75$,$\xi_1 = 0.0$), whereas ϕ shows reverse trend for other considered values of ξ_1, which is accounted as the impact of N-L parameter.

3.9.1.2 Ramp Type Thermal Source

Figure 3.5 represents the variations of t_{33} vs x_1. t_{33} begins with large value in absence of N-L parameter. As the value of N-L parameter increases, the magnitude of t_{33} increases and attain maxima at $x_1 = 5$ for $\xi_1 = 0.75$ and decreases thereafter.

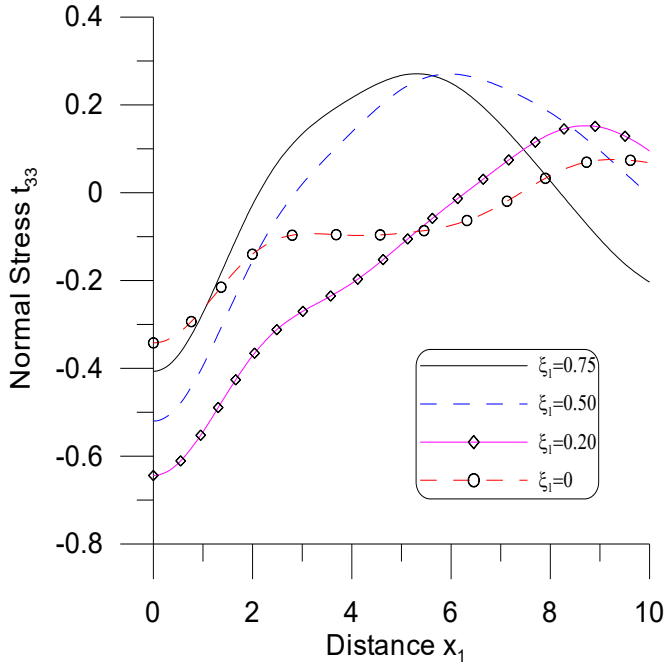

Fig. 3.5: Variation of t_{33} vs x_1

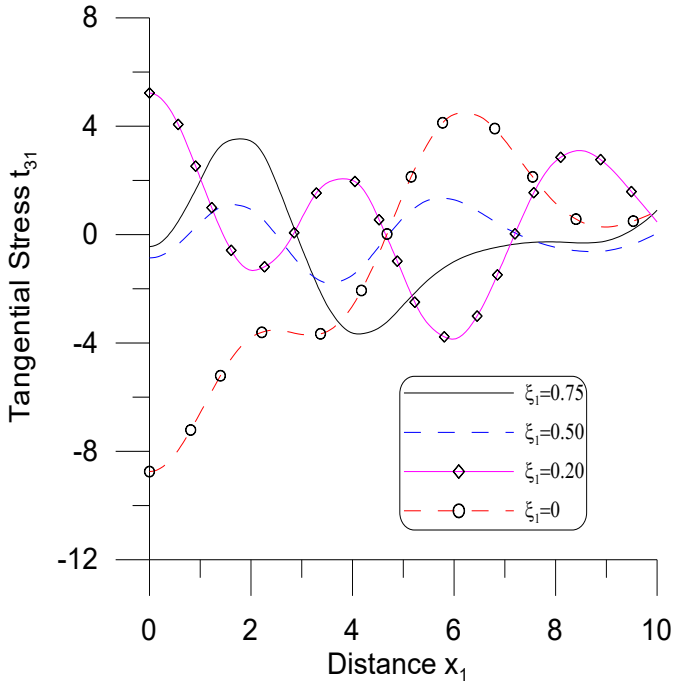

Fig. 3.6: Variation of t_{31} vs x_1

The plot of t_{31}vs x_1 is represented by figure 3.6. It is seen that the trend of t_{31} for $\xi_1 = 0.20$and $\xi_1 = 0.0$ are inverse in nature in the entire range, whereas for higher values of ξ_1 ($\xi_1 = 0.50$, $\xi_1 = 0.75$) the behaviour of t_{31} is similar in nature in the entire range, although ,magnitude of values are greater for higher value of ξ_1.

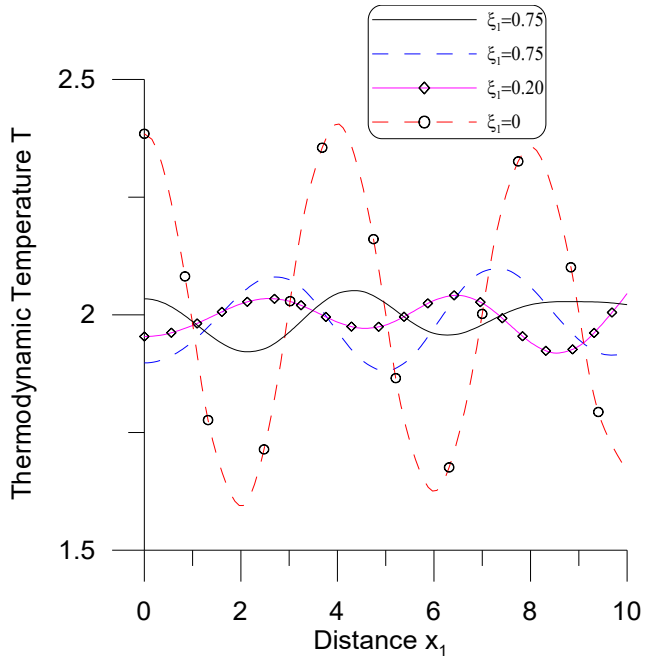

Fig. 3.7: Variation of T vs x_1

Figure 3.7 shows the variations of T vs x_1. It is noticed that T exhibits oscillatory behaviour for all values of ξ_1, magnitude of oscillation is greater in absence of N-L parameter i.e. for $\xi_1 = 0$, while for other values of ξ_1 , T shows small variations about ' 2 '.

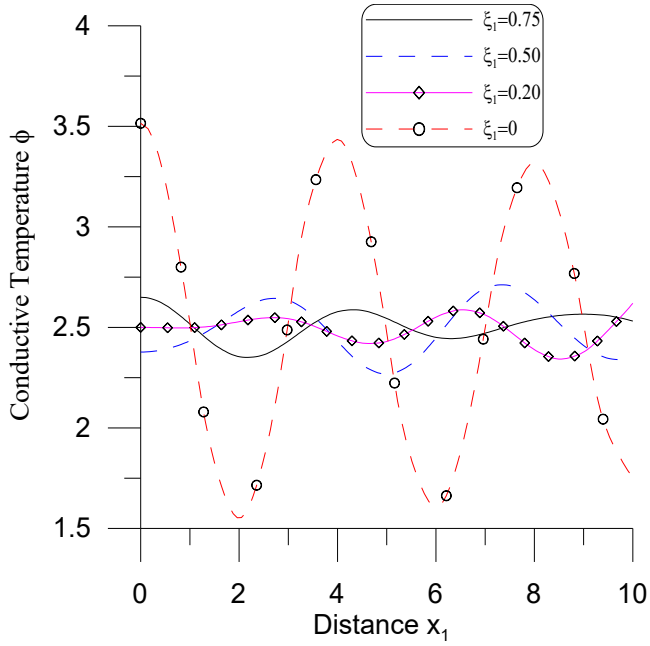

Fig. 3.8: Variation of ϕ vs x_1

Figure 3.8 exhibits the plot for ϕ vs x_1. The behaviour and variations of ϕ is similar with that for T with significant difference in their magnitude.

3.9.2 Moving Heat Source

In this case, we consider moving heat source parameter, $v = 0.25$, $v = 1$ and $v = 1.75$, N-L parameter $\xi_1 = 0.50$ and HTT parameter $\varsigma = 0.5$ for range $0 \leq x_1 \leq 10$.

i. The solid black line (——) corresponds to ($v = 1.75$).

ii. Small dashed blue line (. . .) corresponds to ($v = 1$).

iii. The solid violet line (——) represents the case of $v = 0.25$.

3.9.2.1 Normal Distributed Force

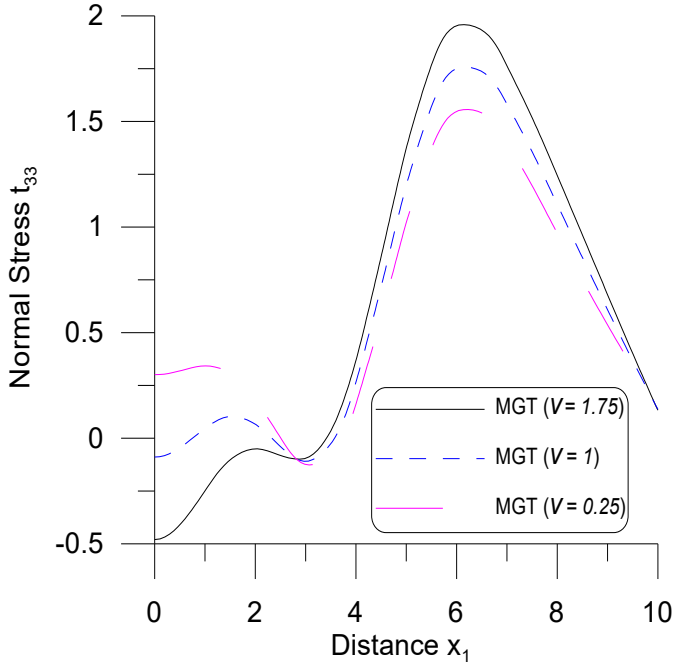

Fig. 3.9: Variation of t_{33} vs x_1

Figure 3.9 demonstrates the variations of t_{33} vs x_1. It is noticed that the value of t_{33} decreases in the ranges $2 \leq x_1 \leq 3$ and $6 \leq x_1 \leq 10$ and increase in the rest of the interval for all considered values of v. Moreover, the value of t_{33} is the highest when ($v = 1.75$).

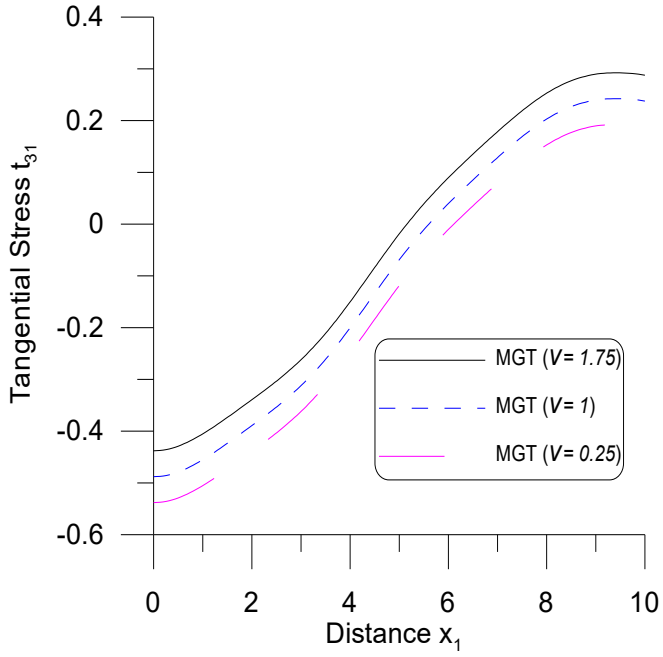

Fig. 3.10: Variation of t_{31} vs x_1

The variation of t_{31} vs x_1 is represented in figure 3.10. t_{31} shows an increasing trend for the entire range for all considered values of v. Moreover, the magnitude of the increment is greater for larger values of $v = 1.75$.

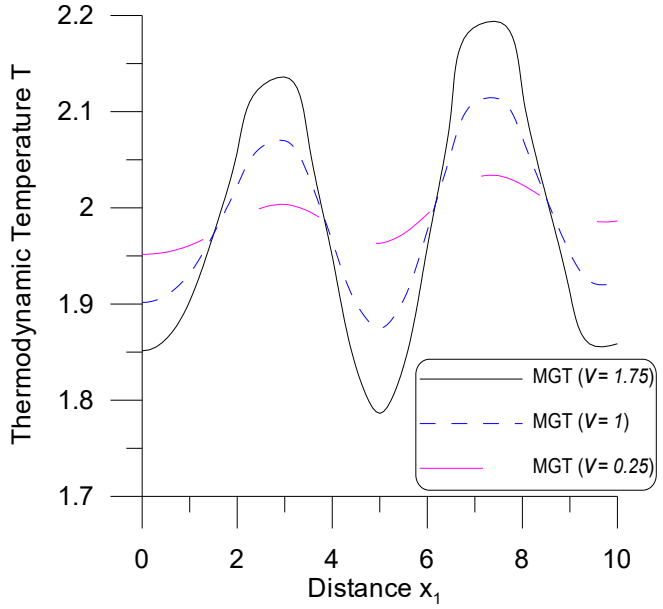

Fig. 3.11: Variation of T vs x_1

Figure 3.11 depicts the trend of T vs x_1. The magnitude of temperature T starts with a large value for velocity, $v = 0.25$ in the range $0 \leq x_1 \leq 2$ .For the left-over interval, T follows oscillatory behaviour. The magnitude of oscillation is higher in the case of $v = 1.75$ than other considered values of v.

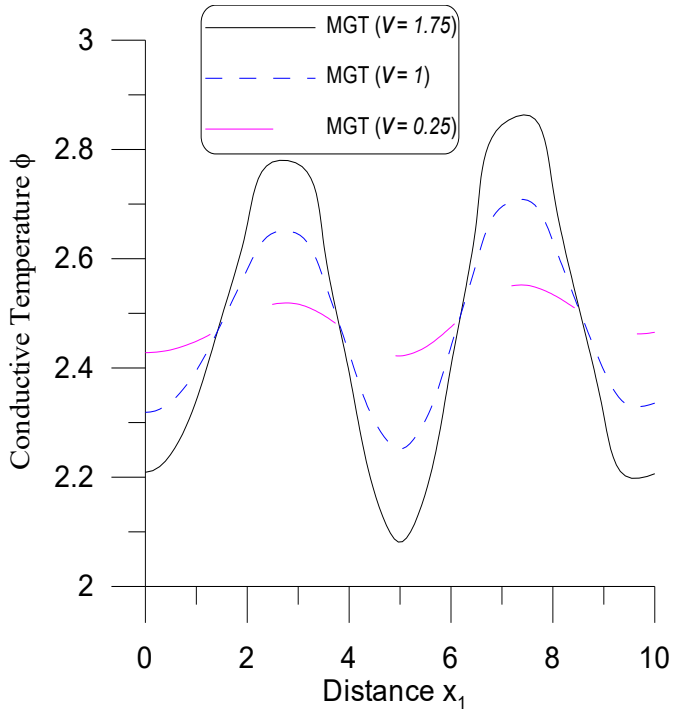

Fig. 3.12: Variation of ϕ vs x_1

Figure 3.12 exhibits ϕ vs x_1 . ϕ follows an oscillatory behavior for all the considered values of v for the entire range, the magnitude of oscillation is greater for higher-values of v.

3.9.2.2 Ramp Type Thermal Source

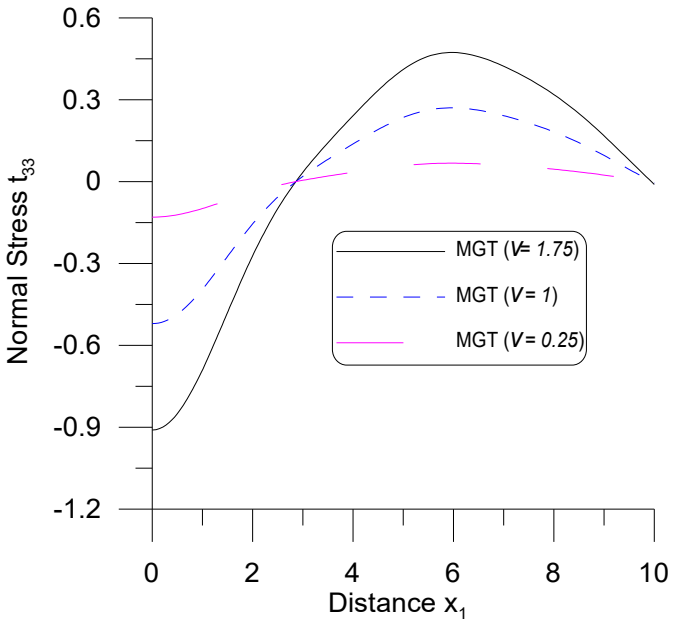

Fig. 3.13: Variation of t_{33} vs x_1

Figure 3.13 depicts the variations of t_{33} vs x_1. The values of t_{33} for $v = 1.75$ and $v = 1$ increases for the range $0 \leq x_1 \leq 6$, magnitude of values for $v = 1.75$ are greater in comparison to those for $v = 1$ and decreases in left over interval, whereas the smaller value of for v ($v = 0.25$), t_{33} shows a steady state about the origin.

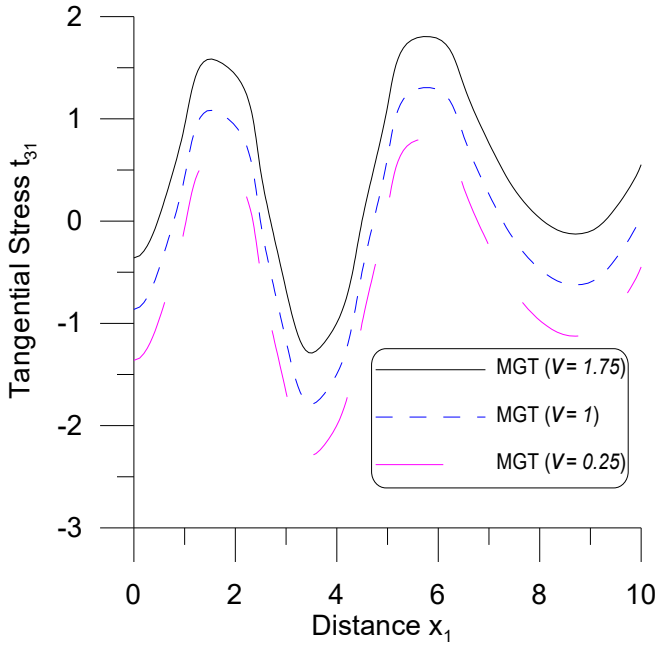

Fig. 3.14: Variation of t_{31} vs x_1

Figure 3.14 is a plot of t_{31} vs x_1. It is evident from the plot that t_{31} follows an oscillatory behavior for all values of v, The magnitude of oscillation is higher for a greater value of v ($v = 1.75$).

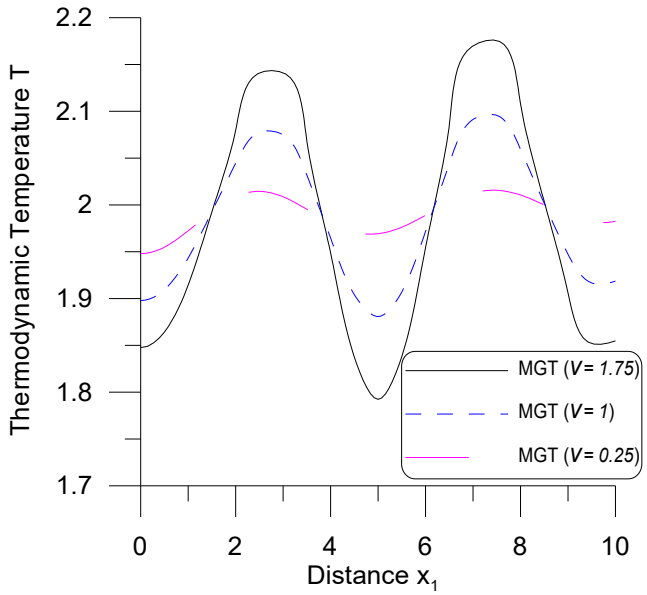

Fig. 3.15: Variation of T vs x_1

Figure 3.15 exhibits the plot for T vs x_1. The value of T for $v = 1.75$ and $v = 1$ decreases for the range $3 \leq x_1 \leq 5$ and $8 \leq x_1 \leq 10$, and increases for the left-over interval, whereas for $v = 0.25$, the values of T exhibit small variations about the value 2.

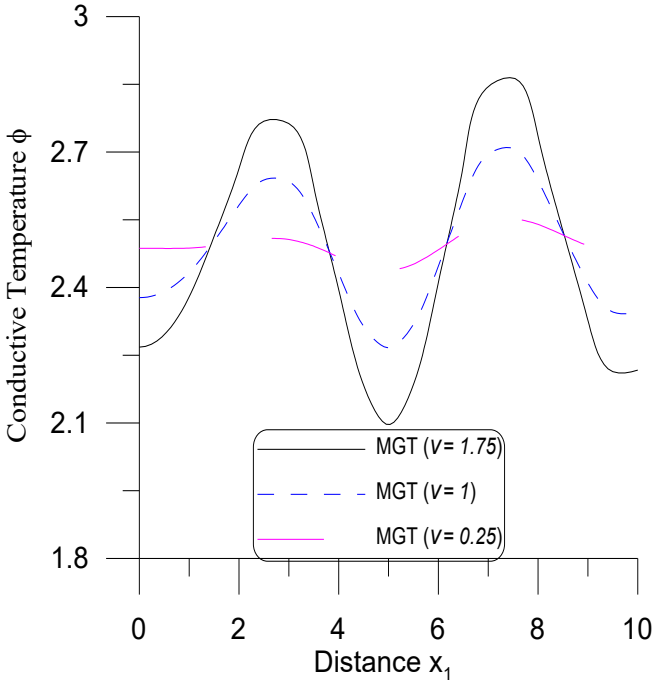

Fig. 3.16: Variation of ϕ vs x_1

Figure 3.16 is plot of ϕ vs x_1. The behavior of ϕ is similar in nature as observed for T with significant difference in their magnitude, which reveals the impact of moving heat source parameter.

3.9.3 Hyperbolic Two Temperature

In this case, we consider HTT parameter $\varsigma = 0.75$, $\varsigma = 0.50$ and TT parameters $a = 0.104$ and $a = 0.0$, N-L parameter $\xi_1 = 0.2$ and moving heat source $v = 1$for the range $0 \leq x_1 \leq 10$.

i. The solid black line (——) corresponds to ($\varsigma = 0.75$).
ii. Small dashed blue line (. . .) corresponds to ($\varsigma = 0.50$).
iii. Solid Magenta line with center symbol ⋄ (——⋄——) corresponds to ($a = 0.104$).
iv. Small dashed red line with center symbol o (-o -) represents the case of ($a = 0.0$).

3.9.3.1 Normal Distributed Force

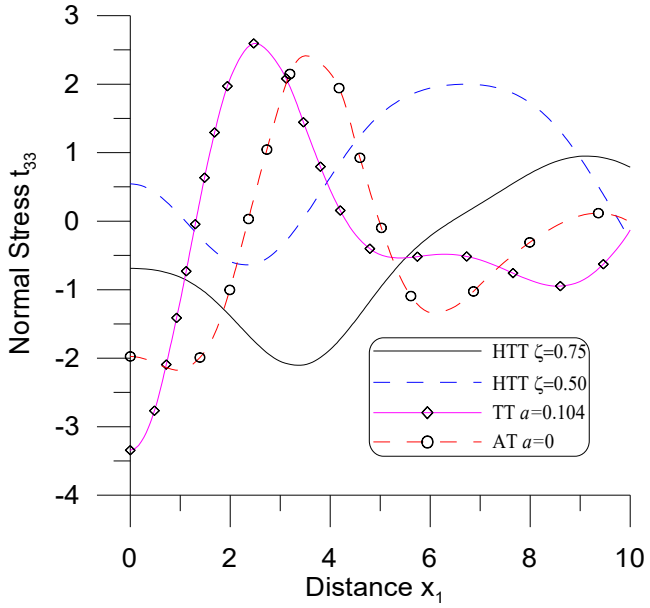

Fig. 3.17: Variation of t_{33} vs x_1

It is evident from the figure 3.17, which is plot of t_{33} vs x_1 that the trend of t_{33} are similar in nature for higher value HTT ($\varsigma = 0.75, \varsigma = 0.50$) in the entire interval except in the range $9 \leq x_1 \leq 10$ with a magnitude of values is higher for higher value of HTT parameter for $\varsigma = 0.50$, whereas in case of TT ($a = 0.104, a = 0.0$) the trend of t_{33} are similar in nature in the first half of the interval, whereas opposite behavior in the rest of the interval.

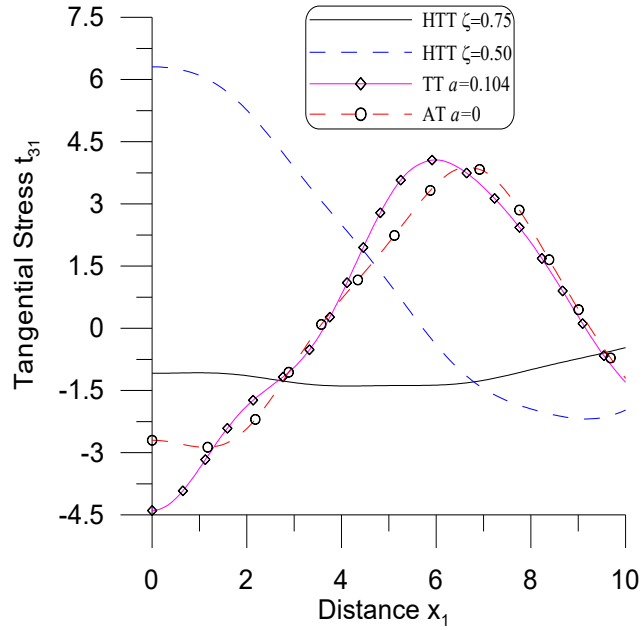

Fig. 3.18: Variation of t_{31} vs x_1

Figure 3.18 is a plot of t_{31} vs x_1. It is noticed that the values of t_{31} for $\varsigma = 0.50$ show a decreasing trend in the entire interval, whereas the values of t_{31} for $a = 0.104$ and $a = 0.0$ increases in the range $0 \leq x_1 \leq 7$ and decreases in the remaining range. It also seen that the value of t_{31} for $\varsigma = 0.75$ shows a small variation about the value '-1' and ultimately approaches to zero.

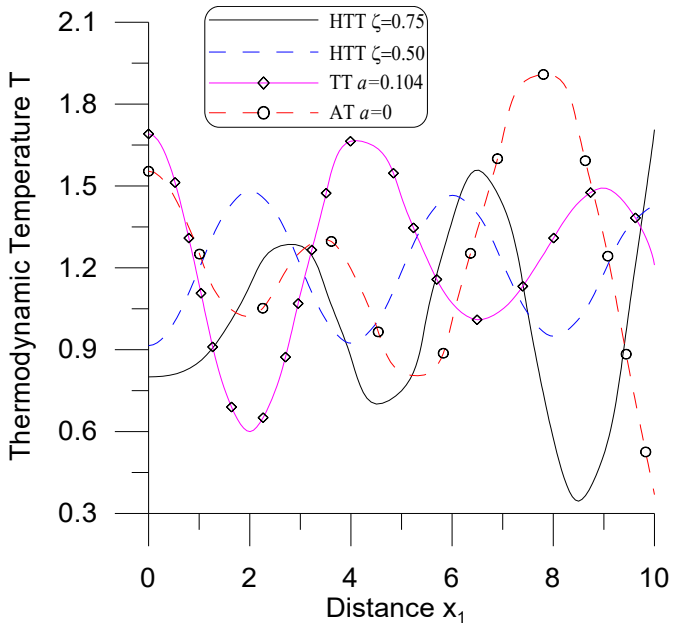

Fig. 3.19: Variation of T vs x_1

Figure 3.19 shows the variations of T vs x_1. It is noticed that the trend of T for HTT i.e. $\varsigma = 0.75$ is opposite in nature as observed for the case of TT ($a = 0.104$) in the entire range, which shows a significant impact of HTT parameter. It is also noticed that the trend of T in the absence of TT parameter are reverse in nature as for the case of HTT ($\varsigma = 0.50$).

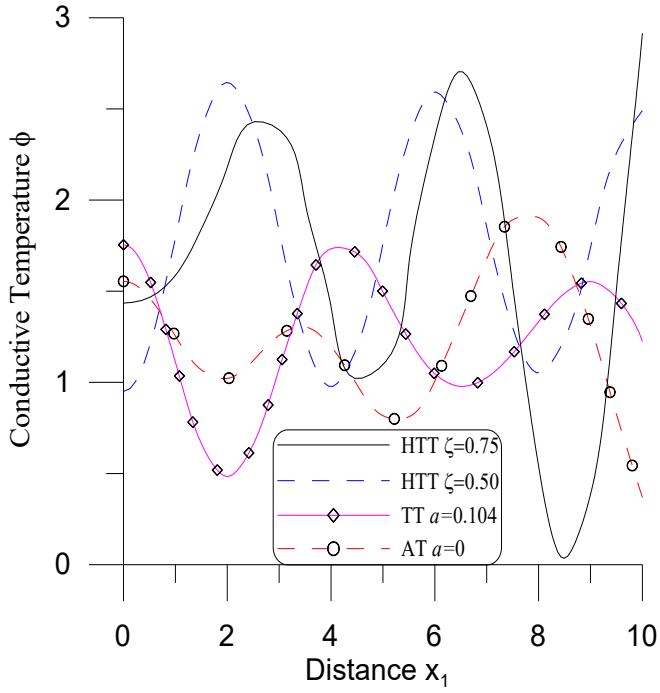

Fig. 3.20: Variation of ϕ vs x_1

Figure 3.20 is plot of ϕ vs x_1. ϕ shows an oscillatory trend in the entire range. It is observed that the magnitude of oscillation is higher for HTT ($\varsigma = 0.75$) as compared to other considered values of HTT parameter.

3.9.3.2 Ramp Type Thermal Source

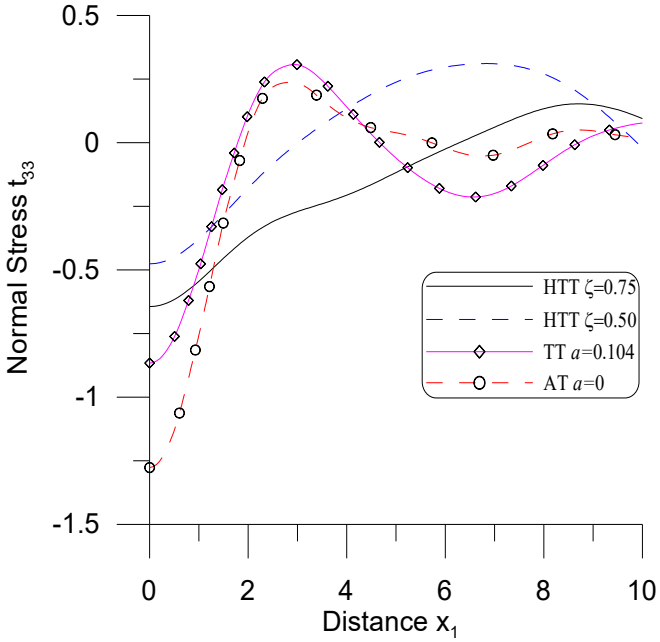

Fig. 3.21: Variation of t_{33} vs x_1

Figure 3.21 is a plot of t_{33} vs x_1. The values of t_{33} increase for the entire range for HTT parameter ($\varsigma = 0.75$ and $\varsigma = 0.50$), magnitude of values for $\varsigma = 0.50$ are greater as compared to those for $\varsigma = 0.75$. Also, the values of t_{33} for $a = 0.104$ and $a = 0.0$ decreases in the range $3 \leq x_1 \leq 7$ and a reverse trend is noticed in the left-over interval.

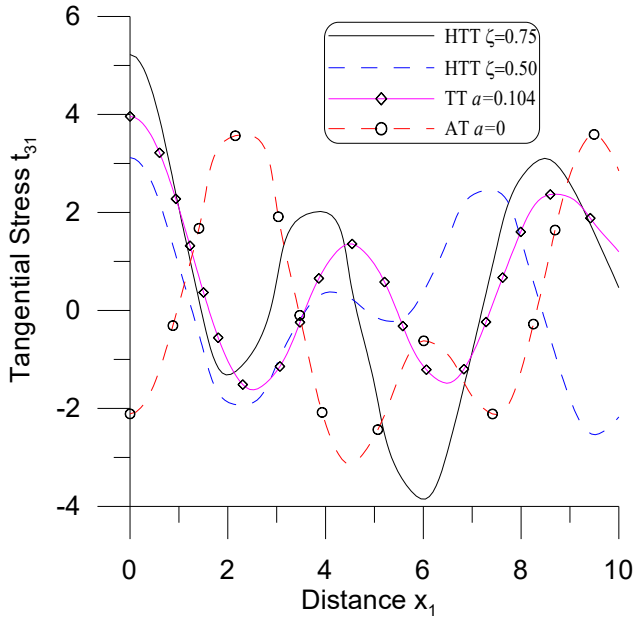

Fig. 3.22: Variation of t_{31} vs x_1

Figure 3.22 is a plot of t_{31} vs x_1. t_{31} for $a = 0.0$ shows the opposite trend as compared to other considered cases for the first half of the interval, which is accounted as significant effect of TT parameters. In the latter half of the interval, the values of t_{31} shows an oscillatory behavior.

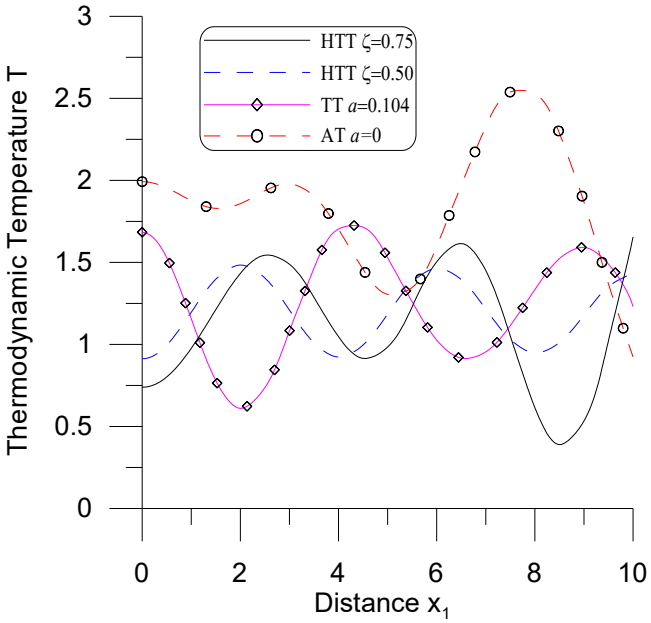

Fig. 3.23: Variation of T vs x_1

Figure 3.23 is the plot of T vs x_1. T shows the opposite behaviour for $a = 0.104$ as compared to other considered values of HTT parameters for the entire range. In the absence of TT parameter T shows a steady state for the interval $0 \leq x_1 \leq 4$ and later, the values of T decrease for the interval $4 \leq x_1 \leq 6$, $8 \leq x_1 \leq 10$ and increases in the left-over interval.

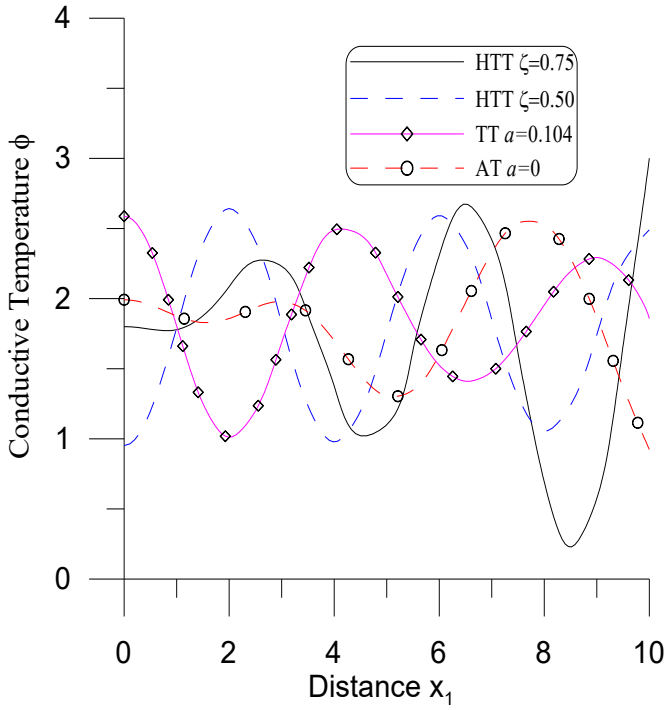

Fig. 3.24: Variation of ϕ vs x_1

Figure 3.24 is plot of ϕ vs x_1. The variation of ϕ shows similar trend as for T with significant difference in their magnitude, which reveals the impact of HTT and TT parameters.

3.10 Conclusions

In this chapter, a two-dimensional problem in thermoelastic half space under MGT heat equation due to thermomechanical source along with heat source is presented. The heat source is considered as a laser pulse decaying with time and moving with constant velocity in one direction. The problem is further examined using a normal distributed force and ramp type thermal source. The LT and FT technique is applied to solve the problem in the transformed domain. The expressions for displacement components, stresses, conductive temperature, and thermodynamic temperature are obtained. The numerically computed inversion technique has been used to obtain the results in the physical domain, and results are displayed graphically to

illustrate the effect of N-L parameter, moving heat source parameter, and HTT. The following observations are obtained from numerical computed result:

Non-Local Parameter

i. **When NDF is applied**, it is observed that increment of N-L parameter increases the magnitude of normal and tangential stresses while thermodynamic temperature and conductive temperature show similar oscillatory behaviour. The magnitude of oscillation is higher for intermediate value of N-L parameter $\xi_1 = 0.50$ as compared to other considered values of N-L parameter.

ii. **When RTTS is applied,** the magnitude of normal stress remains greater for higher value values of ξ_1, tangential stress, thermodynamic temperature, and conductive temperature show oscillatory behaviour in the entire range, although the magnitude of oscillation is higher in the absence of N-L parameter.

iii. **Moving Heat Source**

Higher value of moving heat source parameter enhances the magnitude of normal stress, thermodynamic temperature, and conductive temperature for NDF as well as for RTTS. Furthermore, the behaviour of variations for all physical quantities for different values of velocity is qualitatively similar in nature with the differences in their magnitude of oscillations.

iv. Hyperbolic two temperature

The HTT parameter enhances the magnitude of thermodynamic temperature and conductive temperature in contrast to normal and tangential stresses due to NDF and RTTS. It is also observed that in most of the range, the behaviour of all physical quantities for intermediate value of HTT parameter ($\varsigma = 0.50$) due to NDF and RTTS.

The problem discussed although theoretical but it finds the application in material science The physical applications of the model can be found in the mechanical engineering and geophysics.

Chapter 4

Modelling of Axi-Symmetric thermoelastic behaviour with Moore-Gibson-Thompson heat equation incorporating hyperbolic two temperature, non-local, and fractional order effects

4.1 Introduction

Kumar et al. (2019) [72] used eigen value method to study axisymmetric problem of thermoelastic plate. Sherief and Hussein (2020) [128] investigated two-dimensional axisymmetric problems in solid sphere and semi space with spherical cavity based on FOTT. Sherief et al, (2022) [126] explored two-dimensional axisymmetric problem by virtue of variable heat source using G-L model.

Sherief and Hussein (2023) [129] studied two-dimensional half–space problem whose boundary is rigidly fixed and subjected to an axisymmetric thermal shock within frame work of the generalized micropolar theory of thermoelasticity. Bajpai et al. (2023) [15] used the axisymmetric technique to study the deformation of thermo-diffusive elastic half-space subjected to thermomechanical loading using the integral transform technique under the three-phase lag theory and fractional thermoelastic diffusion model. Khavale and Gaikward (2023) [62] analyzed the effect of axi-symmetric heat supply in the circular plate in the context of fractional-ordered thermoelastic stress analysis. Kumar et al. (2023) [65] presented the axisymmetric deformation problem of a thick circular plate subjected to a ramp-type heat source under modified couple stress thermoelasticity model to analyze the impact of diffusion, phase lags, and voids on studied physical quantities.

Kumar et al. (2024) [68] investigated the axisymmetric problem in micropolar thermoelastic half-space subjected to mechanical loading under the Moore-Gibson-Thompson (MGT) heat equation to study the impact of non-local (N-L) and Hyperbolic two-temperature (HTT) on physical field quantities. Bajpai et al. (2024) [18] explored thermo-diffusive elastic interactions in an axisymmetric half-space under internal heat source by virtue of axisymmetric thermal, mechanical, and mass concentration loads in context of fractional generalized thermoelastic diffusion theory with two temperature (TT) to study the impacts of thermal conductivity and diffusivity on physical field quantities.

The study of thermoelastic materials incorporating fractional order derivatives (FOD), non-local (N-L) effects, and the hyperbolic two-temperature (HTT) model is essential for

advancing heat conduction theories and mechanical response analysis. This chapter is motivated by the need to improve the accuracy of thermoelastic models by integrating FOD and N-L parameters. The study of axisymmetric problems in thermoelasticity is crucial for understanding the behavior of materials and structures under thermal and mechanical loads that exhibit radial symmetry. Many practical engineering and scientific applications involve cylindrical, spherical, or annular geometries, making axisymmetric analysis highly relevant

In this chapter, a two-dimensional axi-symmetric problem in a thermoelastic half-space featuring fractional order derivatives (FOD), with N-L and HTT, in context of the MGT heat equation in response to mechanical loading is presented. The basic field equations and constitutive relations in the absence of body forces and heat sources are formulated. The governing equations are derived in cylindrical coordinates for axisymmetric problems. The resulting two-dimensional equations are normalized using non-dimensional quantities and decomposed using the Helmholtz decomposition theorem. The problem is solved by applying the Laplace transform (L.T) and Hankel transform (H.T). Ring and disc loads are taken as an application. The transformed components of displacement, stresses, conductive temperature, and thermodynamic temperature are computed in physical domain numerically. The graphical representation of numerical findings for displacement components, stresses (normal stress (NS), tangential stress (TS) thermodynamic temperature and conductive temperature reveals the impacts of N-L, HTT and TT parameters. Certain cases of interest are also drawn.

4.2 Constitutive Relations and Basic Equations

The governing equations and the constitutive relations in homogeneous, isotropic, thermoelastic under MGT heat equation with FOD under the influence of N-L and HTT parameters after removing body forces and heat sources are given by [Quintanilla (2019) [105], Ezzat et al. (2018) [45] and Eringen (1974) [42]] as

The equations of motion

$$(\lambda+\mu)\nabla(\nabla\cdot\vec{u})+\mu\Delta\vec{u}-\beta_1\nabla T=\rho\left(1-\xi_1{}^2\Delta\right)\frac{\partial^2\vec{u}}{\partial t^2}, \qquad (4.1)$$

Fractional order heat conduction equation

$$\left(1+\frac{\tau_0{}^\alpha}{\alpha!}\frac{\partial^\alpha}{\partial t^\alpha}\right)\left[\rho C_e\ddot{T}+\beta_1 T_0\ddot{e}\right]=K^*\frac{\partial}{\partial t}\Delta\phi+K_1\Delta\phi, \qquad (4.2)$$

The constitutive equation

$$t_{ij}=\lambda e_{k,k}\delta_{ij}+2\mu\, e_{ij}-\beta_1 T\delta_{ij}, \qquad (4.3)$$

$$\ddot{\phi}-\ddot{T}=\beta^*\Delta\phi, \qquad (4.4)$$

where

$\tau_0{}^{\alpha}$-relaxation time, α-fractional parameter, and other symbols $\lambda, \mu, \beta_1, \rho, \xi_1, C_e, K_1, T_0, T, \phi$ are as specified in section 2.2 [Chapter 2] and K^*, β^* are as defined in Section 3.2 [Chapter 3]. Equations (4.1) - (4.4) in cylindrical polar coordinates (r, θ, z) in components forms can be written as

$$(\lambda+\mu)\frac{\partial e}{\partial r}+\mu\left(\Delta u_r-\frac{u_r}{r^2}-\frac{2}{r^2}\frac{\partial u_\theta}{\partial\theta}\right)-\beta_1\frac{\partial T}{\partial r}=\rho\left(1-\xi_1{}^2\Delta\right)\frac{\partial^2 u_r}{\partial t^2}, \tag{4.5}$$

$$(\lambda+\mu)\frac{1}{r}\frac{\partial e}{\partial\theta}+\mu\left(\Delta u_\theta-\frac{u_\theta}{r^2}+\frac{2}{r^2}\frac{\partial u_r}{\partial\theta}\right)-\beta_1\frac{1}{r}\frac{\partial T}{\partial\theta}=\rho\left(1-\xi_1{}^2\Delta\right)\frac{\partial^2 u_\theta}{\partial t^2}, \tag{4.6}$$

$$(\lambda+\mu)\frac{\partial e}{\partial z}+\mu\Delta u_z-\beta_1\frac{\partial T}{\partial z}=\rho\left(1-\xi_1{}^2\Delta\right)\frac{\partial^2 u_z}{\partial t^2}, \tag{4.7}$$

$$\left(1+\frac{\tau_0{}^{\alpha}}{\alpha!}\frac{\partial^{\alpha}}{\partial t^{\alpha}}\right)\left[\rho C_e\frac{\partial^2 T}{\partial t^2}+\beta_1 T_0\frac{\partial^2 e}{\partial t^2}\right]=\left(K_1+K^*\frac{\partial}{\partial t}\right)\Delta\phi, \tag{4.8}$$

$$t_{zz}=\lambda e+2\mu\frac{\partial u_z}{\partial z}-\beta_1 T, \tag{4.9}$$

$$t_{zr}=\mu\left(\frac{\partial u_r}{\partial z}+\frac{\partial u_z}{\partial r}\right), \tag{4.10}$$

$$t_{rr}=\lambda e+2\mu\frac{\partial u_r}{\partial r}-\beta_1 T, \tag{4.11}$$

$$t_{\theta\theta}=\lambda e+2\mu\left(\frac{u_r}{r}+\frac{\partial u_\theta}{\partial\theta}\right)-\beta_1 T, \tag{4.12}$$

$$t_{r\theta}=\mu\left(\frac{1}{r}\frac{\partial u_r}{\partial\theta}+\frac{\partial u_\theta}{\partial r}-\frac{u_\theta}{r}\right), \tag{4.13}$$

$$t_{z\theta}=\mu\left(\frac{\partial u_\theta}{\partial z}+\frac{1}{r}\frac{\partial u_z}{\partial\theta}\right), \tag{4.14}$$

$$\ddot{\phi}-\ddot{T}=\beta^*\Delta\phi, \tag{4.15}$$

where

$$e=\frac{u_r}{r}+\frac{\partial u_r}{\partial r}+\frac{1}{r}\frac{\partial u_\theta}{\partial\theta}+\frac{\partial u_z}{\partial z},\ \Delta=\frac{\partial^2}{\partial r^2}+\frac{1}{r}\frac{\partial}{\partial r}+\frac{\partial^2}{\partial z^2}+\frac{1}{r^2}\frac{\partial^2}{\partial\theta^2}. \tag{4.16}$$

4.3 Formulation And Solution of The Problem

A homogenous, isotropic thermoelastic solid half-space with HTT and N-L parameters under MGT heat equation with fractional order derivatives is considered. The cylindrical polar coordinates (r, θ, z) are chosen in such a way that z-axis coincide with axis of symmetry. The surface of the half space is taken as the plane z = 0 with z-axis pointing vertically into the medium. A ring or disc load is assumed to be acting at origin of the cylindrical polar coordinate. The geometry of the problem as shown in figure 4.1.

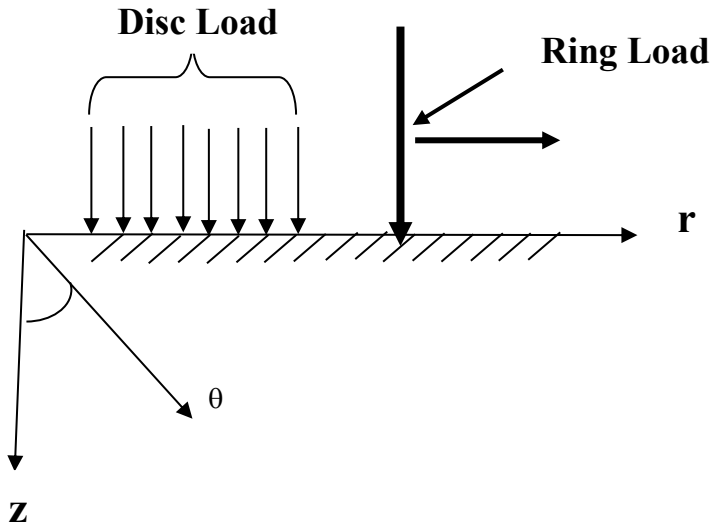

Figure 4.1: Schematic representation of the problem

As due to symmetry about z-axis, all the quantities are independent of θ with condition $\frac{\partial}{\partial\theta}$ = 0, then we take

$\vec{u} = (u_r(r,z,t), 0, u_z(r,z,t)), \quad T = T(r,z,t)$, and $\phi = \phi(r,z,t)$. (4.17)

With these considerations and using (4.17) in equations (4.5)- (4.15), reduce to following

$$(\lambda+\mu)\frac{\partial e}{\partial r} + \mu\left(\Delta - \frac{1}{r^2}\right)u_r - \beta_1\frac{\partial T}{\partial r} = \rho(1-\xi_1^2\Delta)\frac{\partial^2 u_r}{\partial t^2}, \quad (4.18)$$

$$(\lambda+\mu)\frac{\partial e}{\partial z} + \mu\Delta u_z - \beta_1\frac{\partial T}{\partial z} = \rho(1-\xi_1^2\Delta)\frac{\partial^2 u_z}{\partial t^2}, \quad (4.19)$$

$$\left(1+\frac{\tau_0^{\alpha}}{\alpha!}\frac{\partial^{\alpha}}{\partial t^{\alpha}}\right)\left[\rho C_e\frac{\partial^2 T}{\partial t^2} + \beta_1 T_0\frac{\partial^2 e}{\partial t^2}\right] = \left(K_1 + K^*\frac{\partial}{\partial t}\right)\Delta\phi, \quad (4.20)$$

$$t_{zz} = (\lambda+2\mu)\frac{\partial u_z}{\partial z} + \lambda\left(\frac{u_r}{r} + \frac{\partial u_r}{\partial r}\right) - \beta_1 T, \quad (4.21)$$

$$t_{zr} = \mu\left(\frac{\partial u_z}{\partial r} + \frac{\partial u_r}{\partial z}\right), \quad (4.22)$$

$$t_{rr} = \lambda\, e + 2\mu\frac{\partial u_r}{\partial r} - \beta_1 T, \quad (4.23)$$

$$t_{\theta\theta} = \lambda\, e + 2\mu\frac{u_r}{r} - \beta_1 T, \quad (4.24)$$

$$t_{r\theta} = 0, \quad (4.25)$$

$$t_{z\theta} = 0, \quad (4.26)$$

$$\ddot{T} = \ddot{\phi} - \beta^*\Delta\phi, \quad (4.27)$$

where

$$e = \frac{u_r}{r} + \frac{\partial u_r}{\partial r} + \frac{\partial u_z}{\partial z}, \quad \Delta = \frac{\partial^2}{\partial r^2} + \frac{1}{r}\frac{\partial}{\partial r} + \frac{\partial^2}{\partial z^2}. \quad (4.28)$$

For further simplifications, following dimensionless quantities are taken as

$$(r', z', u_r', u_z', \xi_1') = \frac{\omega_1}{c_1}(r, z, u_r, u_z, \xi_1), \qquad (t_{zz}', t_{zr}', F_{10}') = \frac{1}{\beta_1 T_0}(t_{zz}, t_{zr}, F_{10}),$$

$$\left(\phi', T'\right) = \frac{1}{T_0}(\phi, T), \quad \beta^{*'} = \frac{1}{c_1^2}\beta^*, \qquad (t', \tau_0') = \omega_1(t, \tau_0), \tag{4.29}$$

where ω_1, c_1 are same as defined in Section 2.3 [Chapter 2].

Applying equation (4.29) leads to the reduction of equations (4.18) - (4.22) and (4.27) to the following, after removing the primes.

$$a_1 \frac{\partial e}{\partial r} + a_2 \left(\Delta - \frac{1}{r^2}\right) u_r - a_3 \frac{\partial T}{\partial r} = (1 - \xi_1^2 \Delta)\ \frac{\partial^2 u_r}{\partial t^2}, \tag{4.30}$$

$$a_1 \frac{\partial e}{\partial z} + a_2 \Delta u_z - a_3 \frac{\partial T}{\partial z}\ = (1 - \xi_1^2 \Delta) \frac{\partial^2 u_z}{\partial t^2}, \tag{4.31}$$

$$\left(1 + \frac{\tau_0^{\alpha}}{\alpha!} \frac{\partial^{\alpha}}{\partial t^{\alpha}}\right) \left[\frac{\partial^2 T}{\partial t^2} + a_4 \frac{\partial^2 e}{\partial t^2}\right] = \left(k_0 + \frac{\partial}{\partial t}\right) \Delta\phi, \tag{4.32}$$

$$t_{zz} = a_6 \frac{\partial u_z}{\partial z} + a_5 \left(\frac{u_r}{r} + \frac{\partial u_r}{\partial r}\right) - T, \tag{4.33}$$

$$t_{zr} = a_7 \left(\frac{\partial u_z}{\partial r} + \frac{\partial u_r}{\partial z}\right), \tag{4.34}$$

$$\ddot{\phi} - \ddot{T} = \beta^* \Delta\phi\ , \tag{4.35}$$

where

$$a_1 = \frac{\lambda+\mu}{\rho c_1^2}, \qquad a_2 = \frac{\mu}{\rho {c_1}^2}, \qquad a_3 = \frac{\beta_1 T_0}{\rho c_1^2}, \qquad a_4 = \frac{\beta_1 c_1^2}{K^* w_1}\ ,$$

$$a_5 = \frac{\lambda}{\beta_1 T_0}\ , \qquad a_6 = \frac{\lambda+2\,\mu}{\beta_1\, T_0}\ , \qquad a_7 = \frac{\mu}{\beta_1\, T_0}\ , \qquad k_0 = \frac{K_1}{w_1\, K^*}.$$

Applying Helmholtz decomposition, the displacement components u_r, u_z associated to the scalar potential functions are taken as

$$u_r = \frac{\partial q}{\partial r} + \frac{\partial^2 \psi}{\partial r\, \partial z}, \qquad u_z = \frac{\partial q}{\partial z} - \left(\frac{\partial^2}{\partial r^2} + \frac{1}{r}\frac{\partial}{\partial r}\right)\psi. \tag{4.36}$$

With the aid of (4.36) in equations (4.30) - (4.32) yield

$$\Delta q - (1 - \xi_1^2 \Delta)\ \frac{\partial^2 q}{\partial t^2}\ - a_3 T\ = 0, \tag{4.37}$$

$$a_2 \Delta\Psi - (1 - \xi_1^2 \Delta)\ \frac{\partial^2 \Psi}{\partial t^2} = 0, \tag{4.38}$$

$$\left(1 + \frac{\tau_0^{\alpha}}{\alpha!} \frac{\partial^{\alpha}}{\partial t^{\alpha}}\right) \left(\frac{\partial^2 T}{\partial t^2} + a_4 \frac{\partial^2}{\partial t^2} \Delta q\right) = \left(k_0 + \frac{\partial}{\partial t}\right) \Delta\phi. \tag{4.39}$$

We assume the initial conditions of the problem as:

$$u_r(r, z, 0) = \left(\frac{\partial u_r}{\partial t}\right)_{t=0} = 0, \qquad u_z(r, z, 0) = \left(\frac{\partial u_z}{\partial t}\right)_{t=0} = 0,$$

$$\psi(r, z, 0) = \left(\frac{\partial \psi}{\partial t}\right)_{t=0} = 0, \qquad T(r, z, 0) = \left(\frac{\partial T}{\partial t}\right)_{t=0} = 0,$$

$$\phi(r, z, 0) = \left(\frac{\partial \phi}{\partial t}\right)_{t=0} = 0\ . \tag{4.40}$$

Following [Debnath (1995)] [37], Laplace Transform (L.T) of a function $f(x_1, x_3, t)$ w.r.t time variable t and L.T parameter s is defined as:

$$\hat{f}(r, z, s) = L\{f(r, z, t)\} = \int_0^{\infty} f(r, z, t)\, e^{-st} dt, \tag{4.41}$$

With basic properties

i) $\mathrm{L}\left(\frac{\partial \mathrm{f}}{\partial \mathrm{t}}\right) = \mathrm{s}\hat{\mathrm{f}}(\mathrm{r},\mathrm{z},\mathrm{s}) - \mathrm{f}(\mathrm{r},\mathrm{z},0),$ (4.42)

ii) $\mathrm{L}\left(\frac{\partial^2 \mathrm{f}}{\partial \mathrm{t}^2}\right) = \mathrm{s}^2\hat{\mathrm{f}}(\mathrm{r},\mathrm{z},\mathrm{s}) - \mathrm{sf}(\mathrm{r},\mathrm{z},0) - \left(\frac{\partial \mathrm{f}}{\partial \mathrm{t}}\right)_{\mathrm{t}=0}.$ (4.43)

The Hankel transform (H.T) following [Sneddon (1979)] [137], of order n of $\bar{\mathrm{f}}(\mathrm{r},\mathrm{z},\mathrm{s})$ w.r.t variable r, is defined as

$\bar{\mathrm{f}}(\eta,\mathrm{z},\mathrm{s}) = \mathrm{H}_\mathrm{n}\{\hat{\mathrm{f}}(\mathrm{r},\mathrm{z},\mathrm{s})\} = \int_0^\infty \hat{\mathrm{f}}\,(\mathrm{r},\mathrm{z},\mathrm{s})\mathrm{r}\mathrm{J}_\mathrm{n}(\eta\mathrm{r})\mathrm{dr},$ (4.44)

where η denotes the H.T parameter and $\mathrm{J}_\mathrm{n}()$ is Bessel function of first kind of order n, with basic properties:

$\mathrm{H}_0\left(\frac{\partial \hat{f}}{\partial \mathrm{r}} + \frac{1}{r}\,\hat{\mathrm{f}}\right) = \eta\mathrm{H}_1(\bar{\mathrm{f}}), \qquad \mathrm{H}_0\left(\frac{\partial^2 \hat{f}}{\partial \mathrm{r}^2} + \frac{1}{r}\frac{\partial \hat{\mathrm{f}}}{\partial \mathrm{r}}\right) = -\eta^2\mathrm{H}_0(\bar{\mathrm{f}}),$

$\mathrm{H}_1\left(\frac{\partial \hat{\mathrm{f}}}{\partial \mathrm{r}}\right) = -\eta\mathrm{H}_0(\bar{\mathrm{f}}), \qquad \mathrm{H}_1\left(\frac{\partial^2 \hat{\mathrm{f}}}{\partial \mathrm{r}^2} + \frac{1}{r}\frac{\partial \hat{\mathrm{f}}}{\partial \mathrm{r}} - \frac{1}{r^2}\hat{\mathrm{f}}\right) = -\eta^2\mathrm{H}_1(\bar{\mathrm{f}}).$ (4.45)

Applying L.T defined by equation (4.41) and H.T defined by equation (4.44) on equations (4.37) - (4.39) and (4.35) with the aid of (4.42) - (4.43), and (4.45) yield

$[(1 + \xi_1^2\,\mathrm{s}^2)\,D^2 - \,(\eta^2 + \,(1 + \eta^2\,\xi_1^2)s^2)]\bar{q} - a_3\,\bar{T} = 0,$ (4.46)

$[(a_2 + \xi_1^2\,s^2)D^2 - (\mathrm{a}_2\eta^2 + (\,1 + \,\xi_1^2\eta^2)s^2)]\bar{\Psi} = 0,$ (4.47)

$\left(1 + \frac{{\tau_0}^\alpha}{\alpha!}\,\mathrm{s}^\alpha\right)\mathrm{s}^2\bar{T} - (\mathrm{k}_0 + \mathrm{s})(\mathrm{D}^2 - \eta^2)\bar{\phi} + \left(1 + \frac{{\tau_0}^\alpha}{\alpha!}\,\mathrm{s}^\alpha\right)\mathrm{a}_4\mathrm{s}^2(D^2 - \eta^2)\,\bar{q} \;= 0,$ (4.48)

$\bar{\mathrm{T}} = \bar{\phi} - \varsigma(\,D^2 - \eta^2)\bar{\phi},$ (4.49)

where

$$\varsigma = \begin{cases} 0, \text{for one temperature (1T)} \\ a, \text{for two temperature (TT)} \\ \frac{\beta^*}{\mathrm{s}^2}, \text{for hyperbolic two temperature (HTT)} \end{cases}.$$

Using equation (4.49) in equation (4.46) and (4.48), yield

$(R_1\,D^2 - R_2)\bar{q} - (R_4D^2 + R_3)\bar{\phi} = 0\,,$ (4.50)

$(R_6\,D^2 + R_{10})\bar{q} + (R_8 - R_9\,D^2\,)\bar{\phi} = 0\,,$ (4.51)

$\mathrm{R}_1 = 1 + \xi_1^2\mathrm{s}^2, \qquad \mathrm{R}_2 = \eta^2 + (1 + \eta^2\xi_1^2)\mathrm{s}^2, \qquad \mathrm{R}_3 = \mathrm{a}_3(1 + \varsigma\eta^2), \qquad \mathrm{R}_4 = -\mathrm{a}_3\varsigma,$

$\mathrm{R}_5 = \mathrm{s}^2\left(1 + \frac{{\tau_0}^\alpha}{\alpha!}\mathrm{s}^\alpha\right), \qquad \mathrm{R}_6 = \left(1 + \frac{{\tau_0}^\alpha}{\alpha!}\mathrm{s}^\alpha\right)\mathrm{a}_4\mathrm{s}, \qquad \mathrm{R}_7 = \mathrm{a}_5 + \mathrm{s},$

$\mathrm{R}_8 = \mathrm{R}_5(1 + \varsigma\eta^2) + \mathrm{R}_7\eta^2, \quad \mathrm{R}_9 = \mathrm{R}_5\,\varsigma + \mathrm{R}_7, \qquad \mathrm{R}_{10} = \,-\mathrm{R}_6\eta^2, \qquad \mathrm{D} = \frac{\mathrm{d}}{\mathrm{dz}}.$

After some algebraic simplifications, equations (4.50)- (4.51), yield

$(\mathrm{D}^4 + \mathrm{B}_{01}\mathrm{D}^2 + \mathrm{B}_{02})(\bar{\mathrm{q}},\bar{\phi}) = 0,$ (4.52)

where

$B_{01} = \frac{B_2}{B_1}, \qquad B_{02} = \frac{B_3}{B_1}, \qquad \mathrm{B}_1 = \mathrm{R}_4\mathrm{R}_6 - \mathrm{R}_1\mathrm{R}_9\,,$

$B_2 = R_1R_8 + R_2R_9 + R_3R_6 + R_4R_{10}, \qquad B_3 = R_3R_{10} - R_2R_8 .$

Simplification of equation (4.47), yield

$$(D^2 - \lambda_3^2)\,\bar{\Psi} = 0\,, \tag{4.53}$$

where

$$\lambda_3 = \sqrt{\frac{R_{11}}{R_{12}}}, \quad R_{11} = a_2\eta^2 + (1 + \eta^2\xi_1^2)s^2, \qquad R_{12} = \eta^2 s^2.$$

Solution of equations (4.52) and (4.53) satisfying the radiation conditions that $\bar{q}, \bar{\phi}$, and $\bar{\Psi} \to 0$ as $z \to \infty$, can be written as

$$\bar{q} = A_1 e^{-\lambda_1 z} + A_2 e^{-\lambda_2 z}, \tag{4.54}$$

$$\bar{\phi} = d_1 A_1 e^{-\lambda_1 z} + d_2 A_2 e^{-\lambda_2 z}, \tag{4.55}$$

$$\bar{\Psi} = A_3 e^{-\lambda_3 z}, \tag{4.56}$$

where $\pm\lambda_i$ $(i = 1,2)$ and λ_3 are the roots of the characteristic equations $D^4 + B_{01}D^2 + B_{02} = 0$, $D^2 - {\lambda_3}^2 = 0$ respectively and the coupling constant d_i are given by

$$d_i = \frac{{\lambda^2}_i R_1 - R_2}{R_3 + R_4 {\lambda_i}^2}, \qquad i = 1, 2.$$

4.4 Boundary Conditions

As an application of the present problem, we are examining mechanical loads (Disc/Ring load) displayed in figure 4.1, which act perpendicular to the surface. These loads originate from the coordinates' origin and uniformly expand over the surface at a constant rate 'c', while the tangential stress diminishes and the boundary remains isothermal. These boundary restrictions can be expressed mathematically as follows:

$$\text{(i) } t_{zz} = F_1(r,t), \qquad \text{(ii) } t_{zr} = 0, \quad \text{(iii) } \phi = 0 \qquad \text{at } z = 0 \tag{4.57}$$

where

$$F_1(r,t) = F_{10}\begin{cases} \frac{H(ct-r)}{\pi(ct)^2} & \text{for disc load} \\ \frac{\delta(ct-r)}{2\pi r} & \text{for ring load} \end{cases} \tag{4.58}$$

F_{10}- magnitude of the force, H( ) - the Heaviside function, δ( ) - Dirac delta function.

Applying L.T and H.T defined by equation (4.41), (4.44) in equation (4.57) along with (4.58) after using dimensionless quantities given by (4.29) yield

$$\text{(i)}\overline{t_{zz}} = \overline{F_1}(\eta, s) \qquad \text{(ii) } \overline{t_{zr}} = 0 \quad \text{(iii) } \bar{\phi} = 0 \qquad \text{at } z = 0. \tag{4.59}$$

$$\overline{F_1}(\eta, s) = F_{10}\begin{cases} \frac{1}{\pi c \eta}\left(\sqrt{\eta^2 + \frac{s^2}{c^2}} - \frac{s}{c}\right) & \text{for disc load.} \\ \frac{1}{2\pi}\frac{1}{\sqrt{\eta^2 + \frac{s^2}{c^2}}} & \text{for ring load.} \end{cases} \tag{4.60}$$

Using (4.41) and (4.44) in (4.36), (4.33) and (4.34) and with the aid of equations (4.42) and (4.43) and (4.45), along with (4.49), the components of displacement, and stress yield

$$\overline{u_r} = -\eta\left(\bar{q} + \frac{d\bar{\Psi}}{dz}\right), \tag{4.61}$$

$$\overline{u_z} = \frac{d\bar{q}}{dz} + \eta^2\bar{\Psi}\,, \tag{4.62}$$

$$\overline{t_{zz}} = a_6\frac{d\overline{u_z}}{dz} + a_7\,\eta\,\overline{u_z} - \varsigma\left(\frac{d^2}{dz^2} - \eta^2\right)\bar{\phi}\,, \tag{4.63}$$

$$\overline{t_{zr}} = a_8\left(\frac{d\overline{u_r}}{dz} - \eta\,\overline{u_z}\right). \tag{4.64}$$

Substituting the values $\bar{q}, \bar{\phi}, \bar{\Psi}$ from equations (4.54) - (4.56) in the boundary conditions (4.59) and using equations (4.60) - (4.64) we arrive at the matrix formulation as follows

$AX = B$,

where

$$A = \begin{bmatrix} H_1 & H_2 & H_3 \\ H_4 & H_5 & H_6 \\ d_1 & d_2 & 0 \end{bmatrix}, \quad X = \begin{bmatrix} A_1 \\ A_2 \\ A_3 \end{bmatrix}, \qquad B = \begin{bmatrix} F_{10} \\ 0 \\ 0 \end{bmatrix}. \tag{4.65}$$

From equation (4.65) we obtain the value of unknown parameters as

$$A_i = \frac{\Delta_i}{\Delta}, \qquad i = 1, 2, 3. \tag{4.66}$$

Where

$$\Delta = \begin{vmatrix} H_1 & H_2 & H_3 \\ H_4 & H_5 & H_6 \\ d_1 & d_2 & 0 \end{vmatrix},$$

Δ_i, (i = 1 - 3) is obtained by replacing $|F_{10} \quad 0 \quad 0|^T$ with i^{th} column of Δ

$\Delta_{11} = -d_2H_6, \Delta_{21} = d_1H_6, \quad \Delta_{31} = (d_2H_4 - d_1H_5)$,

$H_i = a_6\lambda_i{}^2 - a_5\eta^2 - (1 + \varsigma\eta^2)d_i + \varsigma d_i\lambda_i{}^2$,

$H_3 = \lambda_3\eta^2(a_5 - a_6)$, $\qquad H_{i+3} = 2\lambda_i\eta a_7$, $\qquad H_6 = \eta a_7\left(\lambda_3{}^2 + \eta^2\right)$,

$H_{i+6} = (1 + \varsigma\eta^2)d_i - \varsigma d_i\lambda_i^2$, $\qquad$ (i = 1, 2).

Substituting the values of A_i from (4.66) in equations (4.54) -(4.56) yield

$$\bar{q} = \frac{F_{10}}{\Delta}\sum_{i=1}^{2}\ \Delta_{i1}e^{-\lambda_i z}\,, \tag{4.67}$$

$$\bar{\phi} = \frac{F_{10}}{\Delta}\sum_{i=1}^{2} d_i\ \Delta_{i1}e^{-\lambda_i z}\,, \tag{4.68}$$

$$\bar{\Psi} = \frac{F_{10}}{\Delta}\,\Delta_{31}\ e^{-\lambda_3 z}\,. \tag{4.69}$$

Invoking the value of $\bar{q}, \bar{\phi}, \bar{\Psi}$ from (4.67) - (4.69) in equations (4.61) - (4.64) and (4.49) determine

$$\overline{u_r} = \frac{F_{10}}{\Delta}\left(\eta\left[-\sum_{i=1}^{2}\Delta_{i1}\,e^{-\lambda_i z} + \lambda_3\Delta_{31}e^{-\lambda_3 z}\right]\right), \tag{4.70}$$

$$\overline{u_z} = \frac{F_{10}}{\Delta}\left(\left[-\sum_{i=1}^{2}\lambda_i\Delta_{i1}\,e^{-\lambda_i z} + \eta^2\Delta_{31}e^{-\lambda_3 z}\right]\right), \quad (4.71)$$

$$\overline{t_{zz}} = \frac{F_{10}}{\Delta}\left[\sum_{i=1}^{3} H_i\,\Delta_{i1}e^{-\lambda_i z}\right], \quad (4.72)$$

$$\overline{t_{zr}} = \frac{F_{10}}{\Delta}\left[\sum_{i=1}^{3} H_{i+3}\Delta_{i1}\,e^{-\lambda_i z}\right], \quad (4.73)$$

$$\overline{\phi} = \frac{F_{10}}{\Delta}\left[\sum_{i=1}^{2} d_i\Delta_{i1}e^{-\lambda_i z}\right], \quad (4.74)$$

$$\overline{T} = \frac{F_{10}}{\Delta}\left[H_7\Delta_{11}e^{-\lambda_1 z} + H_8\Delta_{21}e^{-\lambda_2 z}\right]. \quad (4.75)$$

4.5 Validation

i. By substituting $K_1 = \xi_1 = \alpha = \tau_0 = 0$ along with $\varsigma = a$ in equations (4.70) - (4.75), give the expressions in thermoelastic under Lord-Shulman (1967) with TT these results are as obtained by Miglani and Kaushal (2011) [86] (In the absence of NF and TS at boundary) with changed value of constants

$a_8 = 0$, $R_1 = 1$, $R_2 = \eta^2 + s^2$, $R_3 = a_3(1 + a\eta^2)$,

$R_4 = -a_3 a$, $R_5 = s^2$, $R_6 = a_4 s$, $R_7 = as$,

$R_8 = R_5(1 + a\eta^2) + R_7\eta^2$, $R_9 = R_5\, a + R_7$, $R_{10} = -R_6\eta^2$.

ii. The required expressions for thermoelastic GN-II model for FOTT are recovered by taking $K^* = {\tau_0}^{\alpha} = 0, K_1 > 0$ in equations (4.70) - (4.75) and these findings are aligned with those reported by Sharma et al. (2015) [115] as specific case.

iii. Resulting expressions for thermoelastic Green- Naghdi-III (GN-III) model with HTT and FOTT are obtain by taking $K_1^* \neq 0, K^* \neq 0$ and ${\tau_0}^{\alpha} = 0$ in equations (4.70) - (4.75).

iv. Neglecting fractional order parameter and HTT parameter using (4.70) - (4.75) determine the results which are similar as obtained by Lata and Singh (2022) [78] as a unique case.

v. The expressions for axisymmetric problem in thermoelastic without N-L and TT can be obtained if we omit fractional order parameter α appearing in the heat equation. In addition, if we omit TT and N-L parameters in equations (4.70) - (4.75) then the analytical solutions for modified formulation match with those reported by Kumar et al. (2014) [70].

4.6 Special Cases

4.6.1 Taking $\boldsymbol{\varsigma = a}$ in equations (4.70) - (4.75) yields the results for thermoelasticity MGT with FOTT, TT and N-L.

4.6.2 Putting $\boldsymbol{\varsigma = 0}$ in equations (4.70) - (4.75) determine the results for thermoelasticity MGT with FOTT, one temperature along with N-L effect is obtained.

4.7 Inversion of the Transforms

In this section we shall illustrate the method to invert the transformed components to physical dominion. The transformed components of transforms for the equations (4.70) - (4.75) are

components of displacement (CD), normal stress (NS), tangential Stress (TS), conductive temperature and thermodynamic temperature. These terms are functions of z, s and η where s is the parameter of L.T and η is the H.T parameter. To acquire the $f(r, z, t)$ from the $\bar{f}(\eta, z, s)$ in the physical dominion, first we invert the H.T as

$$\hat{f}(r, z, s) = \int_0^{\infty} \eta\, \bar{f}(\eta, z, s)\, J_n(\eta r) d\eta, \qquad (4.76)$$

Compute the integral (4.76) according to the instructions provided by Press et al. (1986) [103].

Thus, the expression (4.76) gives us the L.T $\hat{f}(r, z, s)$ of, $f(r, z, t)$.

For the static values of the variables r and z, $\hat{f}(r, z, s)$ in the equation (4.76) might be assume as the L.T $\hat{g}(s)$ of g(t).

The inverse function g(t) of transformed function $\hat{g}(s)$ can be written [Honig and Hirdes (1984)] [53] as

$$g(t) = \frac{1}{2\pi i} \int_{A-i\infty}^{A+i\infty} \hat{g}(s) \exp(st)\, ds\,. \qquad (4.77)$$

The final stage is to compute the integral given in equation (4.77). The details of approach can be found in section 2.8 of [Chapter 2].

4.8 Numerical Result and Discussion

Following the approach of Dhaliwal and Singh (1980) [38], we focused on a material magnesium crystal. The physical constants used are consistent with those defined in Section 2.9 [Chapter 2]. To analyze the impact of different factors, we conducted numerical simulations computed using a mathematical software Force 2.0 and Grapher for various scenarios. We inspected the impact of (i) HTT (ii) N-L parameters for ring load and disc load in a thermoelastic medium, using the MGT heat equation. To demonstrate the theoretical outcomes discussed in the previous section, we present certain numerical results in form of graphs.

4.8.1 Hyperbolic Two-Temperature

In the figures 4.2 - 4.9, we can observe the influence of HTT parameter, TT parameter and classical one temperature on NS (t_{zz}), TS (t_{zr}), thermodynamic temperature (T) and conductive temperature (ϕ). The computation is performed for dimensionless two temperature a = 0.0, a = 0.0104, a = 0.5, HTT $\varsigma = 0.75$ in the range $0 \leq r \leq 10$.

In all these figures

i. Solid black line (——) represents the curve corresponds a = 0.
ii. Dashed brown line (- - -) stands for TT a = 0.0104.
iii. Solid blue line with center symbol '⋄' (- ⋄-) represent TT a = 0.5.
iv. Dashed red line with center symbol 'o' (- ⋄-) related to HTT ς =0.75.

4.8.1.1 Disc Load

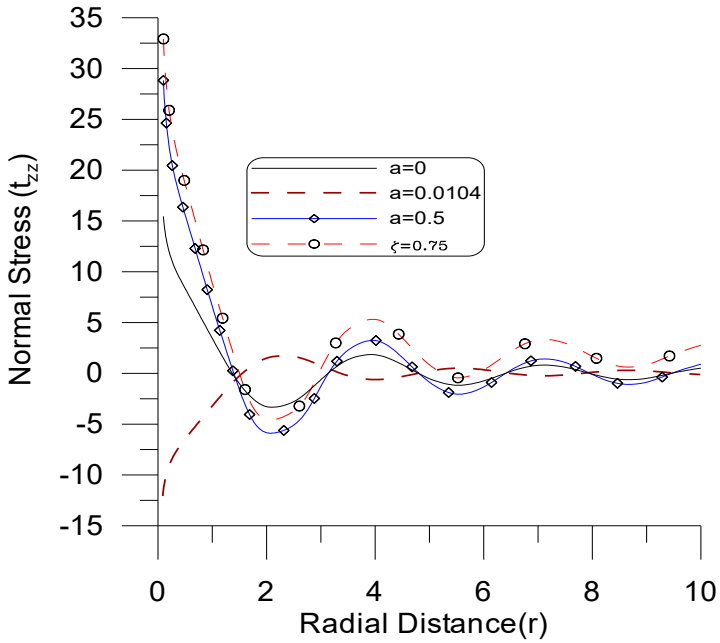

Figure 4.2 Profile of t_{zz} vs r

Figure 4.2 shows the variation of t_{zz} vs r. Near the point of loading, t_{zz} depicts decreasing trend whereas for ς =0.0104 reverse behavior is observed. Away from loading points, t_{zz} follows oscillatory behavior. Also, the values of t_{zz} remains more for $\varsigma = 0.75$ in comparison to all considered cases.

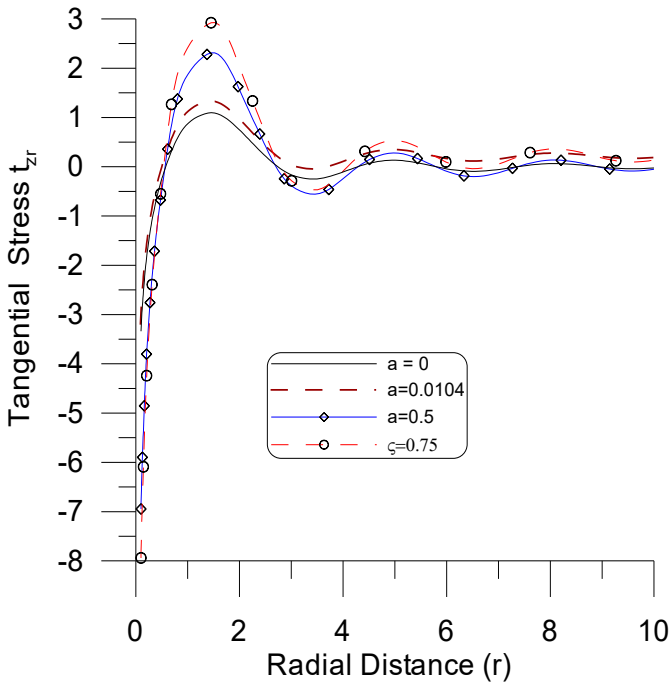

Figure 4.3 Profile of t_{zr} vs r

Figure 4.3 displays variation of t_{zr} vs r. The values of t_{zr} increases with r for all the assumed scenario for $0 \leq r \leq 2$, after that oscillatory behavior with a small amplitude

about the origin is noticed. Moreover, the immensity of t_{zr} is more for $\varsigma = 0.75$ in comparison to other cases throughout the range, which reveals that HTT parameter impact the immensity of t_{zr}.

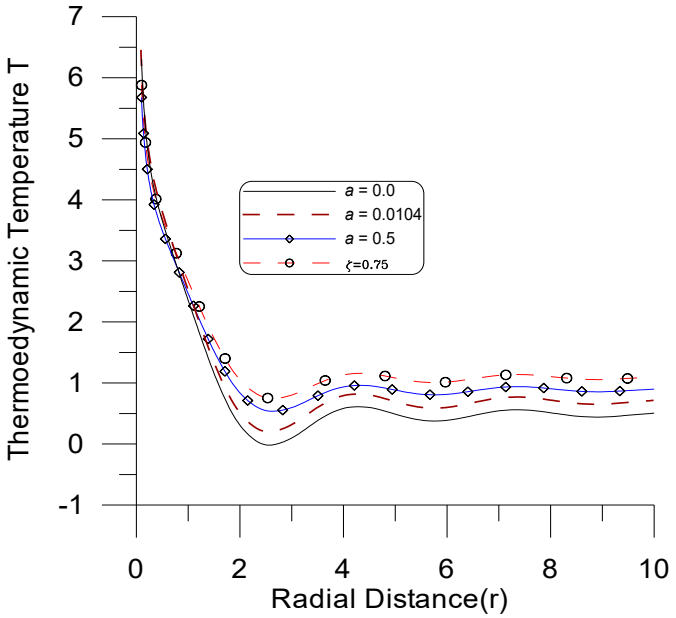

Figure 4.4 Profile of T vs r

Figure 4.4 depicts the decreasing trend of T for $0 \leq r \leq 2$, afterwards the immensity of T follows oscillatory behavior with a small amplitude and finally become stationary about zero value.

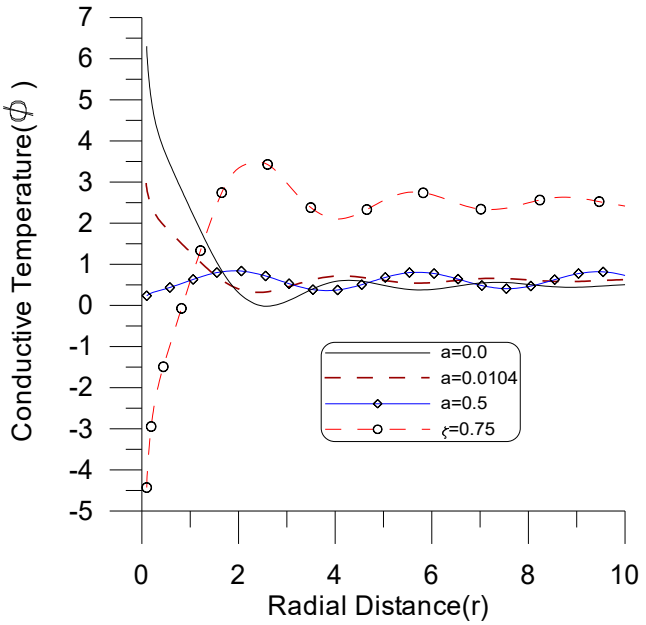

Figure 4.5 Profile of ϕ vs r

Figure 4.5 shows ϕ vs r. It is noticed that ϕ behave in opposite manner for curve corresponds to $\varsigma = 0.75$ and $a = (0.0,\ 0.0104)$ in the first half of the interval and follows similar

behavior for remaining region, whereas for intermediate value of 'ς' slight variations are observed about origin.

4.8.1.2 Ring Load

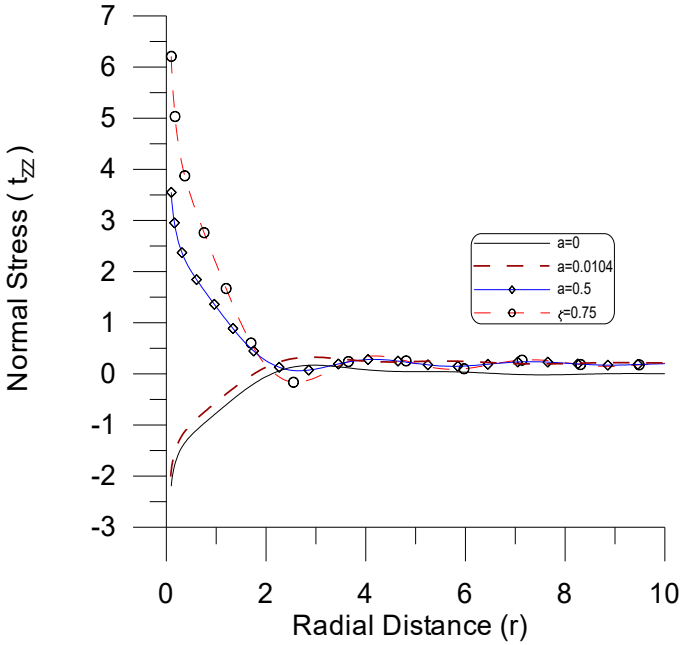

Figure 4.6 Profile of t_{zz}vs.r

Figure 4.6, depicts trend of t_{zz} vs r. The curve corresponding to t_{zz} for $a = 0.5$ and $\varsigma = 0.75$ are opposite in nature as observed for (a = 0.0, a = 0.0104) in the range $0 \leq r \leq 2$, afterwards, stationary behavior about the '0' value is noted for all the curves.

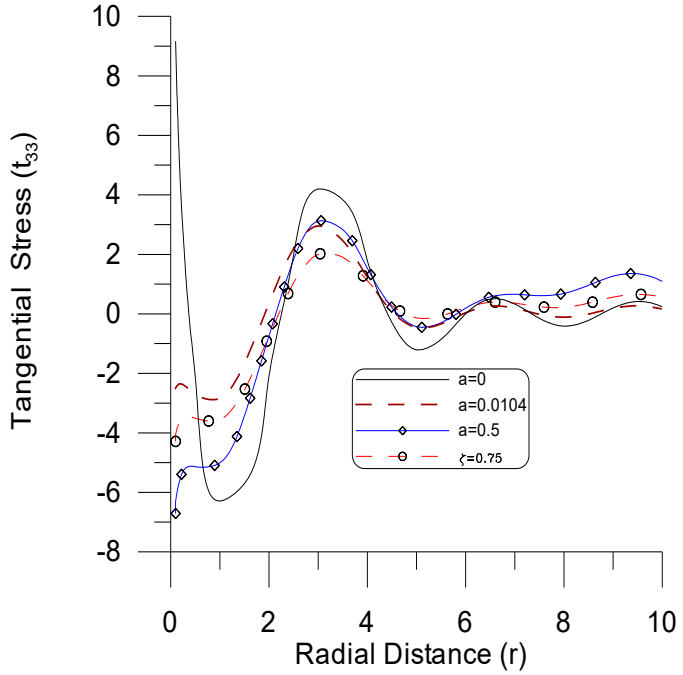

Figure 4.7 Profile of t_{zr}vs. r

Figure 4.7 expresses that the trends and variation of t_{zr} for all the curves are alike for all the considered cases in the entire range except for $0 \leq r \leq 1$, where opposite behaviour is

observed for $a = 0.0$. Moreover, the magnitude of oscillation remains on higher side for $a = 0.0$ than other cases.

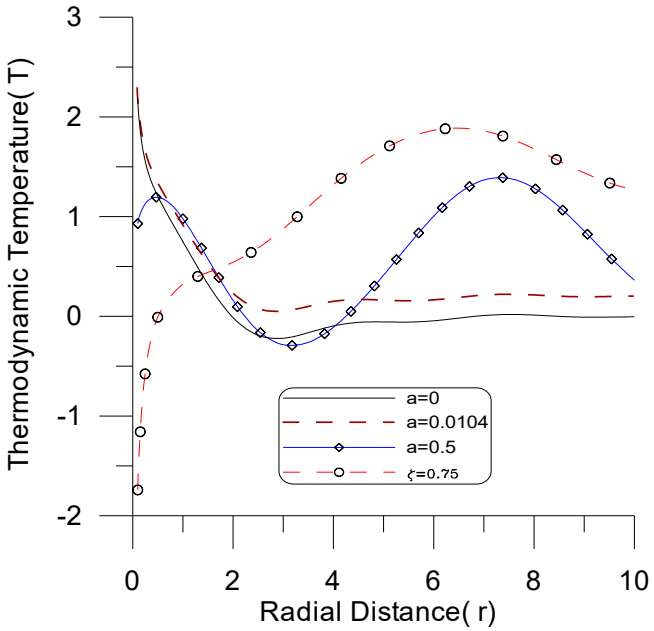

Figure 4.8 Profile of T vs. r

Figure 4.8 demonstrate trends of T vs r. For $0 \leq r \leq 1$, the response and variation of T is mirror image for the value $\varsigma = 0.75$ as compared with $a = 0.0$ and $a = 0.0104$. Moreover, the values of T remain more for $\varsigma = 0.75$ than that for the other considered cases. Also, the value of T for $a = 0.5$ increase for $0 \leq r \leq 1$, $3 \leq r \leq 7$ and follows decreasing trend for remaining region.

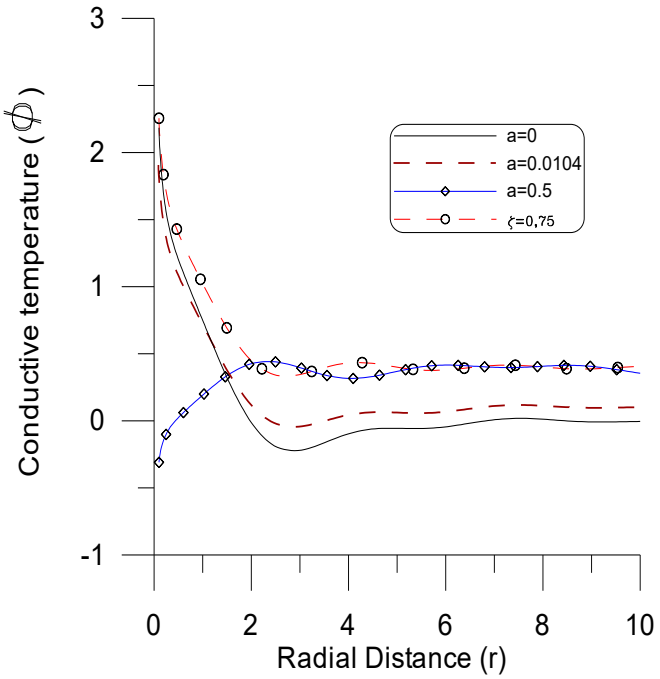

Figure 4.9 Profile of ϕ vs. r

Figure 4.9 depicts variation of ϕ vs r . Near the loading surface, for intermediate value of TT parameter the values of ϕ, decreases and afterwards oscillatory behaviour is noticed while reverse behaviour is observed for $a = 0.5$ than other cases. Moreover, the immensity of ϕ increases for $\varsigma = 0.75$ than other considered cases hence HTT effect enhances the immensity of ϕ .

4.8.2 Different Theories of Thermoelastic

Figures 4.10 – 4.17 depicts the impact of various thermoelasticity theories (MGT, GN-III, and L-S) for dimensionless two-temperature parameter $\varsigma = 0.75$ and $\xi_1 = 0.5$ for $0 \leq r \leq 10$.

i. The solid black line (——) relates to MGT model.
ii. The big dashed Magenta line (– –) corresponds to GN-III theory of thermoelasticity.
iii. The small dashed blue line (- - -) corresponds to L-S theory of thermoelasticity.

4.8.2.1 Disc Load

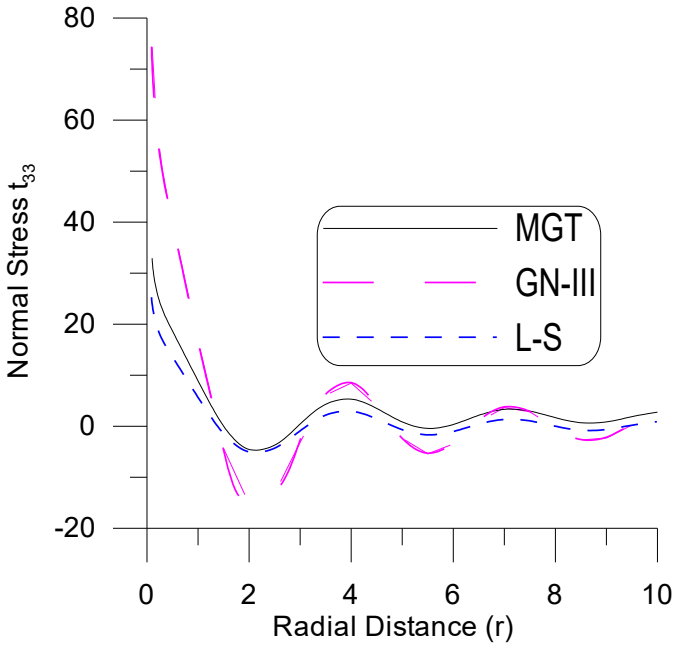

Figure 4.10 Profile of t_{zz} vs r

Figure 4.10 shows t_{zz} vs r. For $0 \leq r \leq 2$, near the loading points, the values of t_{zz} decreases sharply and oscillatory behaviour is observed for left over interval. Also, values of t_{zz} corresponding to GN-III theory of thermoelasticity remains on higher side when compared to other scenarios.

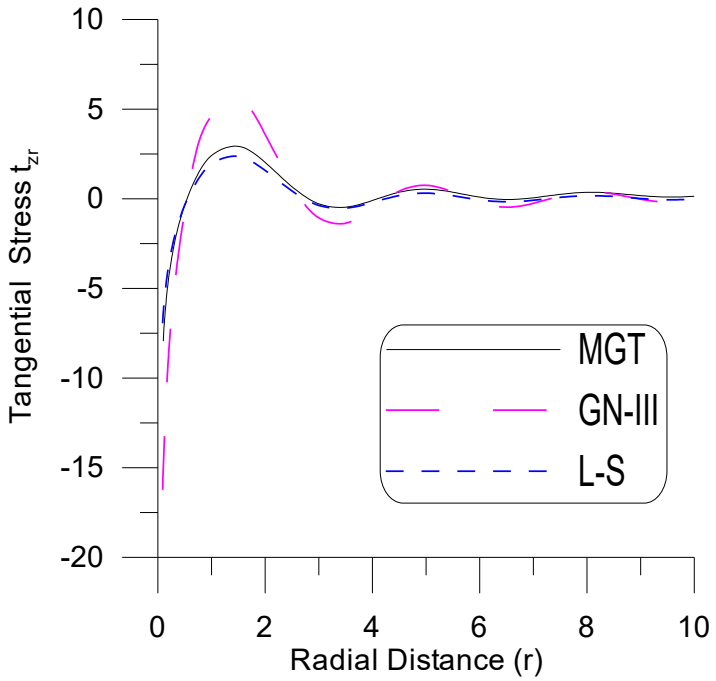

Figure 4.11 Profile of t_{zr}vs r

Figure 4.11 depicts trend of t_{zr} vs r. The values of t_{zr} exhibit abrupt increase, owing to the disc load for $0 \leq r \leq 1$ for all curves. Afterwards negligible variations are observed for all the considered models of thermoelasticity. However, the immensity of t_{zr} remains on higher side for GN-III model for the interval $2 \leq r \leq 5$.

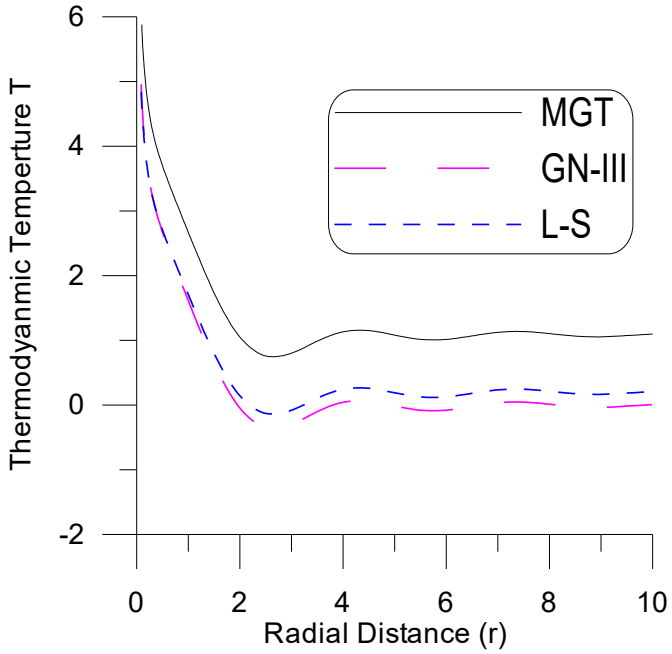

Figure 4.12 Profile of Tvs r

Figure 4.12 depicts the trend of T vs r. For $1 \leq r \leq 3$, the magnitude of T sharply decreases for all considered model, afterwards, it become stationary. Also, the immensity of T is on higher side for the MGT model as compared to other considered models.

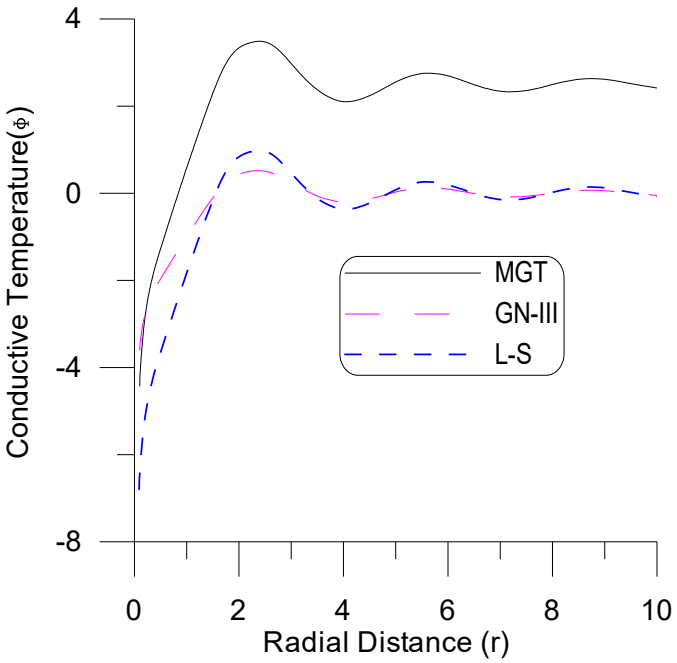

Figure 4.13 Profile of ϕ vs r

Figure 4.13 views the variation of ϕ vs r. The values of ϕ increases for $1 \leq r \leq 3$ and for the remaining range, trends are oscillatory with small amplitude. Also, MGT model enhance the immensity ϕ in comparison to other considered theories.

4.8.2.2 Ring Load

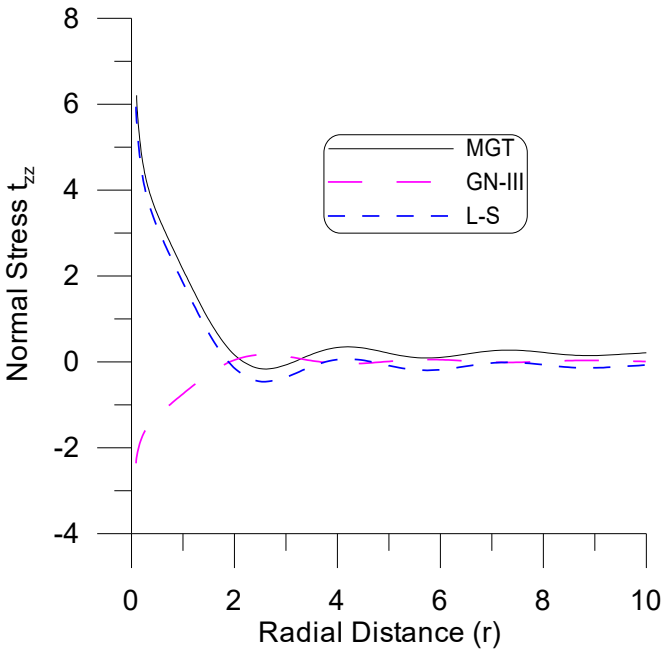

Figure 4.14 Profile of t_{zz} vs. r

Figure 4.14 displays that in the vicinity of loading surface, the values of t_{zz} exhibits strict decreasing behaviour for MGT and LS models, whereas it shows increasing trend for GN-

III model in the interval $1 \leq r \leq 2$ and for the remaining region, t_{zz} shows small variations about zero value for all the cases.

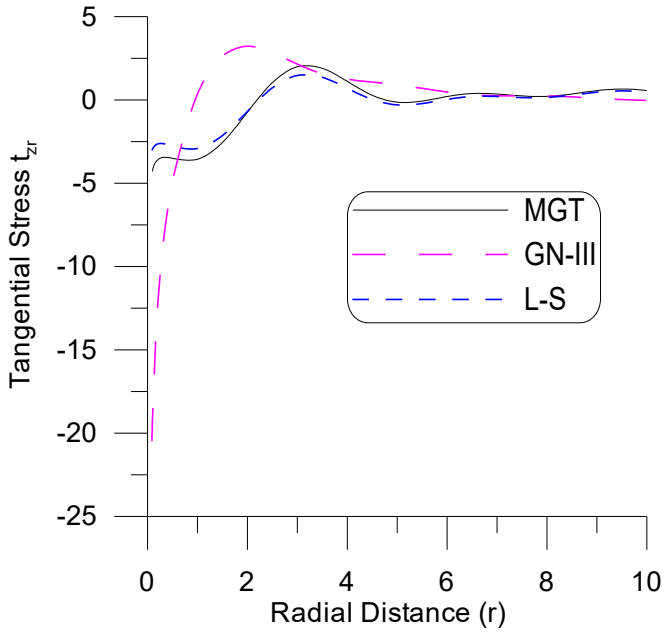

Figure 4.15 Profile of t_{zr} vs. r

Figure 4.15 depicts t_{zr} vs r. For $1 \leq r \leq 3$, the curve corresponding to t_{zr} increases for GN- III model, whereas gradual increase is observed for LS and MGT models after that, t_{zr} shows similar variations for all the assumed cases.

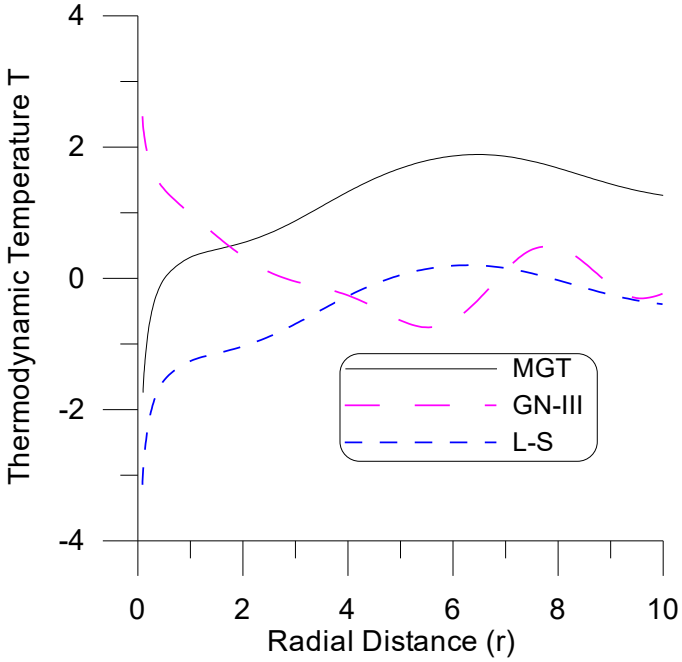

Figure 4.16 Profile of T vs r

Figure 4.16 demonstrate trend of T vs r. The curve corresponding to T follows increasing trend for MGT and LS models while decreasing trends is noticed for GN-III model for most of the range.

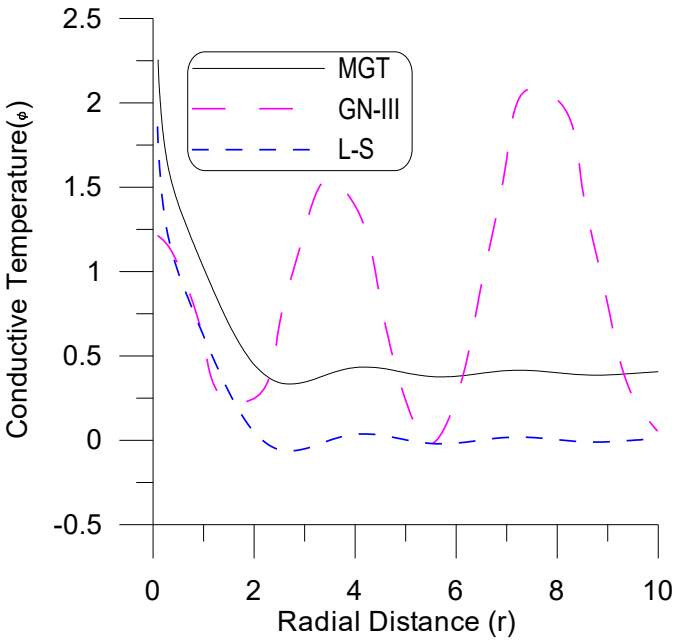

Figure 4.17 Profile of ϕ vs. r

Figure 4.17 depicts trend of ϕ vs r. in the initial range, ϕ decrease for $0 \leq r \leq 2$ for all considered model afterwards oscillatory behaviour is observed corresponding to GN-III model while all the curve corresponding to ϕ follows stationary behaviour corresponding to MGT and LS models. However, the magnitude of variations is more pronounced for MGT model in comparison to other considered theories.

4.8.3 Non-Local

Figures 4.18 - 4.26 are depicted to display the impact of N-L effect carried out for dimensionless N-L parameter ξ_1=0, 0.25, 0.50 and 0.75.

i. The solid black line (——) corresponds to N-L ξ_1= 0.
ii. The dashed brown line (- - -) corresponds to N-L ξ_1 = 0.25.
iii. The solid blue line with centre symbol '◊' (—◊—) relates to N-L ξ_1 = 0.50.
iv. The dashed red line with centre symbol 'o' (...o…) corresponds to N-L ξ_1= 0.75.

4.8.3.1 Disc Load

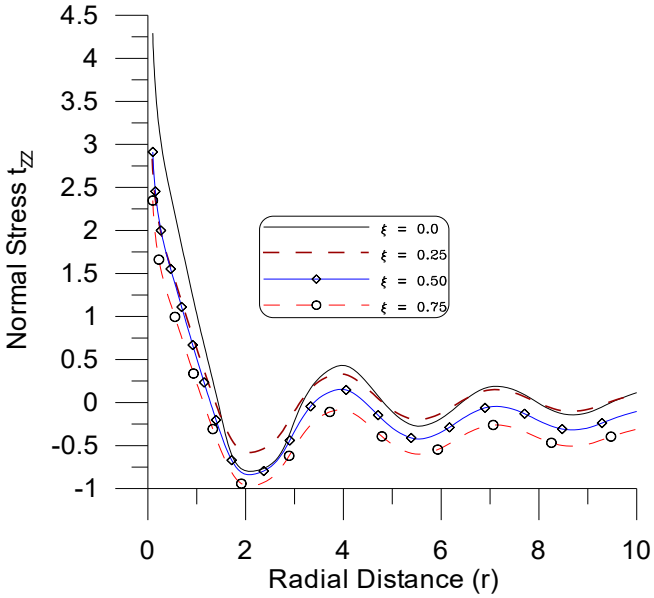

Figure 4.18 Profile of t_{zz} vs. r

Figure 4.18 displays the trend of t_{zz} vs r. Near the loading surface, all the curve corresponding to t_{zz} decreases for all the considered case. The magnitude of t_{zz} is higher for absence of N-L parameter and then t_{zz} follows an oscillating behaviour.

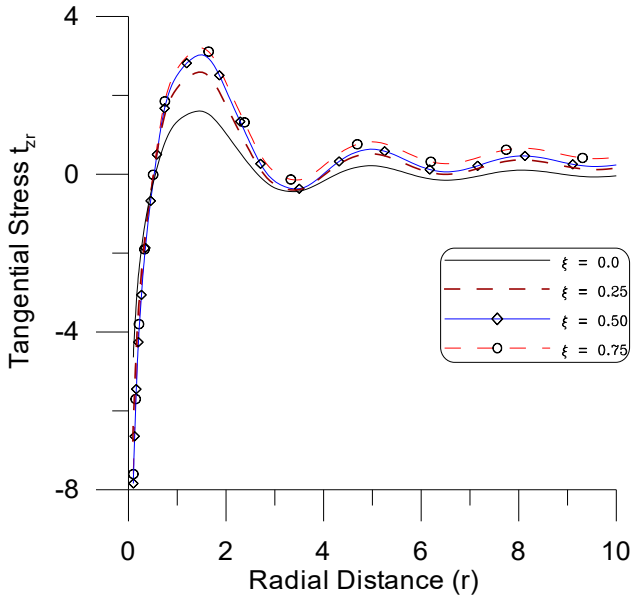

Figure 4.19 Profile of t_{zr} vs. r

Figure 4.19 represents t_{zr} vs r. The observed pattern is consistent across all the models examined, although there are notable variations in their magnitude. Also, the magnitude of t_{zr} remains on higher side for $\xi_1 = 0.75$, and on lower side in case of absence of N-L parameters in comparison to all assumed cases.

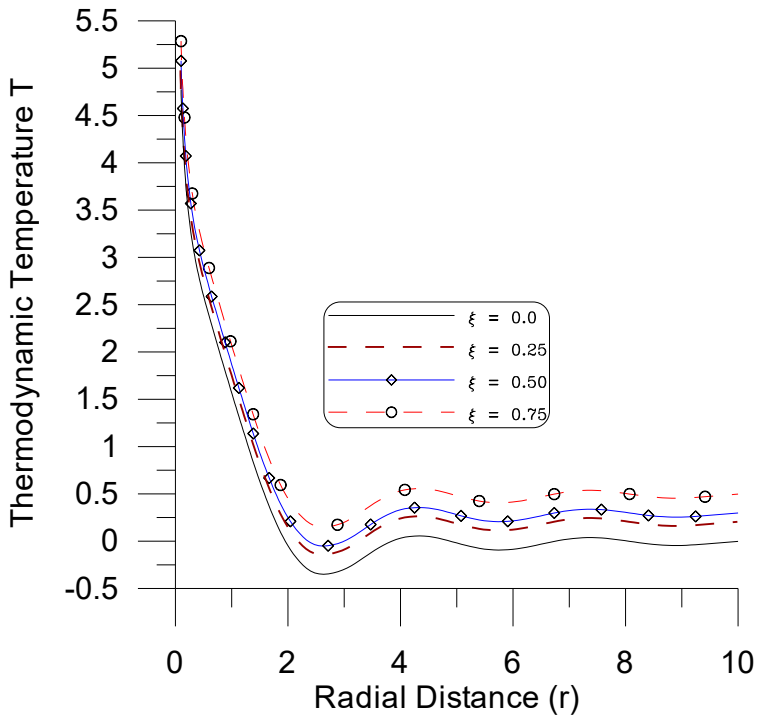

Figure 4.20 Profile of T vs. r

Figure 4.20 displays variation of T vs r. The curve corresponds to T show strictly decreasing behaviour in the range $0 \leq r \leq 2$, after that all the curve corresponds to T behave almost similar for all assumed scenario. Moreover, the value of T is more for $\xi_1 = 0.75$ in comparison to other considered values, which reveals that N-L parameter enhance T.

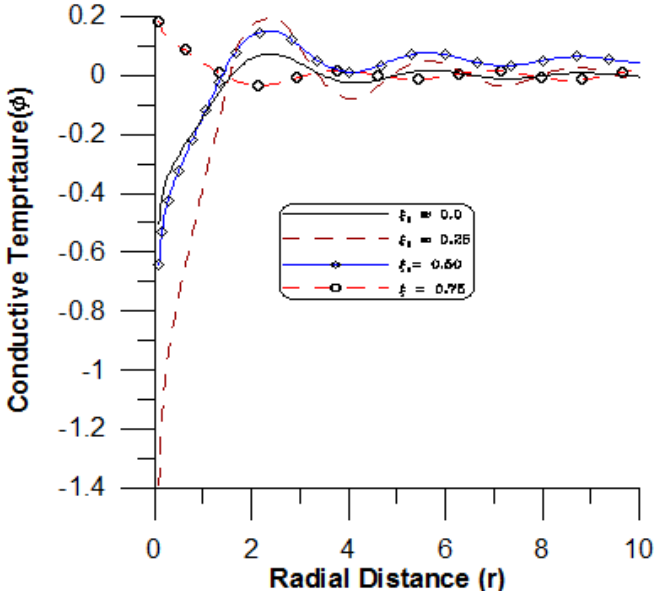

Figure 4.21 Profile of ϕ vs. r

Figure 4.21 displays the trend of ϕ vs r. The value ϕ exhibits strictly increasing trend and followed by oscillatory behaviour. Moreover, higher value of ϕ is observed for $\xi_1 = 0.50$ as compared to other cases.

4.8.3.2 Ring Load

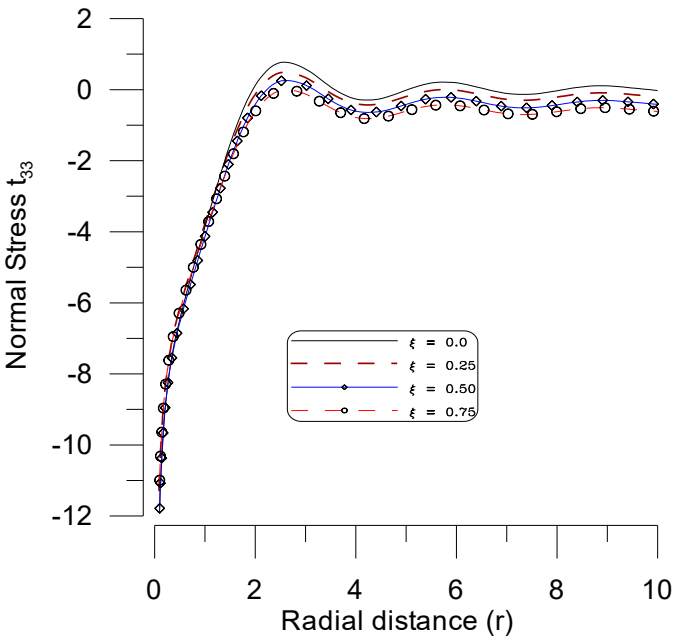

Figure 4.22 Profile of t_{zz} vs. r

Figure 4.22 show trend of t_{zz} vs r. Near the loading points, the values of t_{zz} shows an increasing trend for all the considered models and, after that, a steady behaviour is noted for all the curves. Also, the value of normal stress remains on higher side for the absence of N-L parameter in comparison to all other scenario.

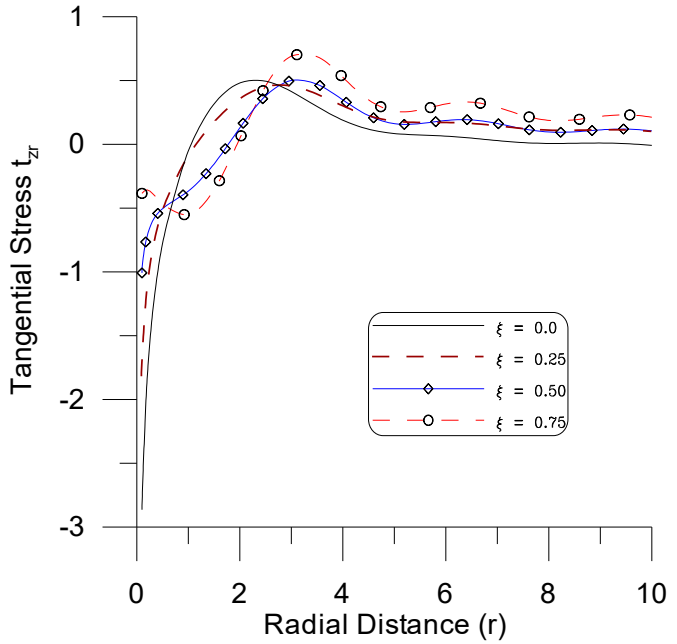

Figure 4.23 Profile of t_{zr} vs. r

Figure 4.23 depicts trend of t_{zr} vs r. The values of t_{zr} exhibit increasing trends for $0 \leq r \leq 2$ and with increase in r, it shows stationary variations about origin. Also, higher variations

are seen for greater value of ξ_1, ($\xi_1 = 0.75$ than other cases, which reveals impact of N-L parameter on tangential stress.

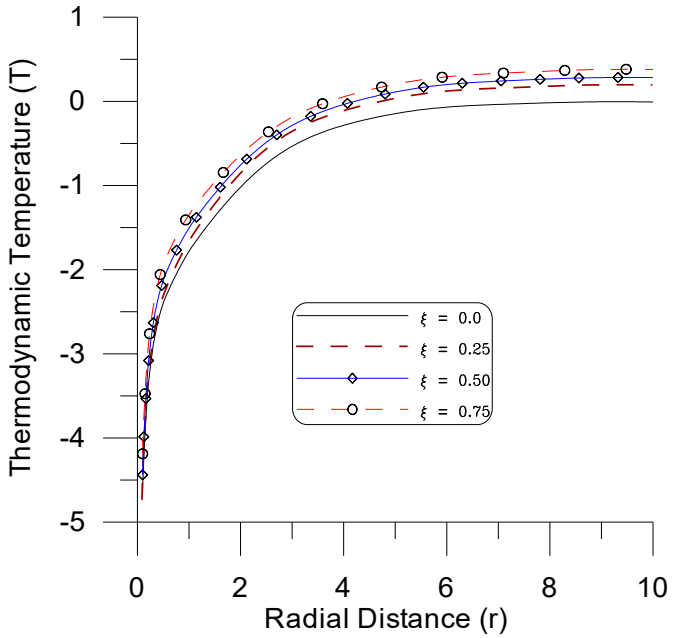

Figure 4.24 Profile of T vs. r

Figure 4.24 depicts that the magnitude of T follows a sharp uptrend near the loading surface, and for the moderate values of r, there is a gradual increment, and with further increase in r, T follows a steady behaviour. However, immensity of T is enhanced for higher value of N-L parameter $\xi_1 = 0.75$.

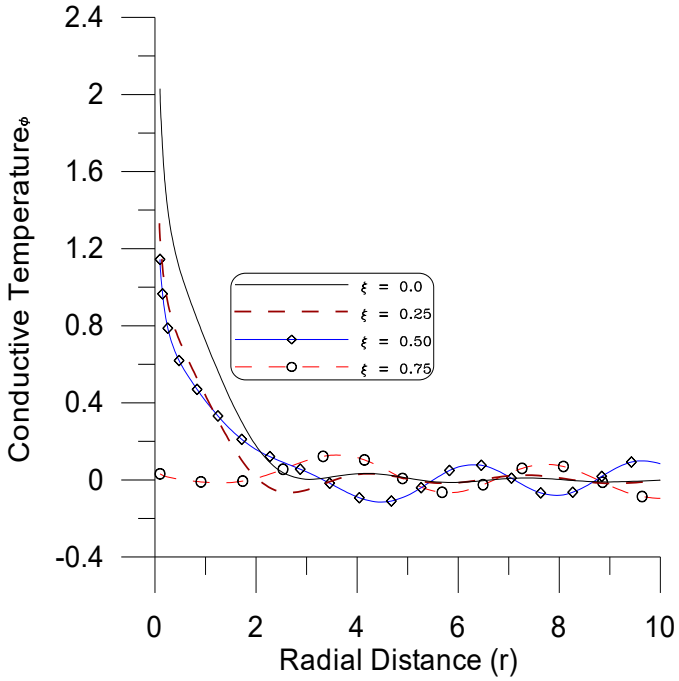

Figure 4.25 Profile of ϕ vs. r

Figure 4.25 displays variation of ϕ vs r. the curve corresponding to ϕ strictly decreases for $0 \leq r \leq 2$, and afterwards it shows small variations about origin. Also, the curve corresponding to $\xi_1 = 0.50$ is mirror image of curve for $\xi_1 = 0.25$.

4.9 Conclusions

In this chapter, a two-dimensional axisymmetric problem within a thermoelastic medium featuring fractional order derivatives, focusing on the MGT heat equation in response to N-L and mechanical loading, is investigated. The governing equations are rendered dimensionless, simplified by introducing potential functions, and solved using Laplace and Hankel transforms. The applicability of the problem is assessed under specific loads (ring and disc loads). Analytical expressions for component of displacement, stresses, thermodynamic temperature, and conductive temperature are derived in the transformed domain. Numerical inversion techniques are employed to obtain solutions in the physical domain. The manuscript aims to analyse the effects of N-L, HTT parameters and various theories of thermoelasticity on resulting physical quantities. From the empirical study, following observations are made:

i) Impact of HTT Parameter

Disc load

It is observed that the due to disc load, HTT parameter effects increase the value of normal stress (NS), tangential stress (TS), and thermodynamic temperature while opposite behaviour is observed for conductive temperature near the application of loading surface. On the other hand, away from loading surface, oscillatory behaviour is observed for all physical field quantities.

Ring load

Near the loading surface, normal stress and conductive temperature shows opposite behaviour for ς= 0.75 and *a*= 0.5, and away from loading surface follow oscillatory behaviour. On other hand, tangential stress and thermodynamic temperature exhibit oscillatory behaviour due to ring load.

ii) **Impact of Different Thermoelasticity Theories**

Disc load

It is observed that absolute value of NS and TS remains on higher side for GN- III model whereas magnitude of thermodynamic temperature and conductive temperature get enhanced under MGT model due to disc load. Energy dissipation enhances the magnitude

of stresses for GN-III model whereas immensity of thermodynamic and conductive temperatures gets enhanced under MGT thermoelastic model.

Ring Load

Due to ring load, the behaviour of all the curve corresponding to thermodynamic and conductive temperature is quite similar for MGT and L-S model while oscillatory behaviour is observed for GN-III model.

iii) Impact of Non-local Parameter

Disc load

Near the loading surface, the decreasing impact of N-L parameter is observed on NS and thermodynamic temperature and away from the loading surface oscillatory behaviour is observed. Meanwhile, tangential stress and conductive temperature decreases near the loading point and away from loading point it follows oscillatory behaviour for all considered cases due to a disc load.

Ring load

When subjected to a ring load, both NS and TS increases near loading points, while the stress component values are notably higher in the absence of the N-L parameter, while moderate value of N-L parameter enhance the immensity of thermodynamic temperature and conductive temperature. Additionally, then N-L parameter considerably increases the values of T and ϕ. While the absence of the N-L parameter amplifies the stress component. The HTT parameter exerts a more pronounced influence on both temperature fields and NS as opposed to the classical TT parameter. The HTT parameter augments the immensity of the T and NS as compared with the effect of the classical TT parameter.

It is observed that the behavior of composite materials under mechanical loading is affected by N-L and HTT. It will provide information about the different constituents of a composite material respond to temperature changes and mechanical stresses, which is crucial for designing and optimizing composite structures.

Chapter 5

Plane-wave vibrations in thermoelastic non-local medium utilizing Moore-Gibson-Thompson heat equation with hyperbolic two temperature model

5.1 Introduction

Sharma (2013) [120] used coupled thermoelasticity theory to explore the impact of two-temperature (TT) on reflection coefficients of plane waves propagating micropolar thermoelastic medium. Kaushal et al. (2021) [61] used reflection technique for plane wave propagation in thermoelastic medium under G-L theory to explore the impact of relaxation time on amplitude ratios (AR) of reflected wave due to impedance boundary. Jangid et al. (2021) [57] used Moore-Gibson-Thompson (MGT) theory to explore impact of material parameter (phase velocity, specific loss and penetration depth on propagation of plane wave in thermoelastic medium by employing harmonic wave technique.

Singh and Mukhopadhyay (2023) [133] obtained fundamental solution for steady vibration using MGT heat equation. Singh and Mukhopadhyay (2023) [134] utilized MGT model to predict the thermoelastic vibration of the microstructure model for a Timoshenko beam. Askar et al. (2023) [11] examined the photothermal effect semiconducting medium to study the impact of various parameter laser pulse ramp time, viscosity, and thermal parameter on physical quantities under MGT theory. Bajpai et al. (2023) [16] explored wave propagation due to thermomechanical loading under TT theory. Abouelregal et al. (2023) [7] explored the thermoelastic behaviour of elastic medium due to laser in the context of the MGT model with memory-dependent derivative.

Das et al. (2024) [36] used MGT theory to examine the phenomenon of reflection at impedance boundary of thermoelastic half- space and investigated the impression of non-local (N-L) parameter on reflection coefficients and energy ratios due to impedance boundary conditions. Yadav et al. (2024) [146] investigated the impacts of fractional order derivative and diffusion parameters on waves in a micro stretch thermoelastic material subjected to magnetic field and impedance boundary. Singh (2024) [130] examined the wave propagation problem in thermoelastic medium to investigate the effect of N-L, conductivity rate, and angular frequency parameter on the wave.

Understanding wave propagation in thermoelastic media is essential for various scientific and engineering applications, including geophysics, materials science, and non-

destructive testing. Motivated by the need to enhance theoretical models, this study explores the behavior of plane waves in complex thermoelastic systems and contributes to the development of more accurate predictive models

This chapter presents study of the plane wave in a homogeneous, isotropic, thermoelastic medium with the MGT heat equation, along with the effects of N-L, Hyperbolic two temperature (HTT) and impedance parameter. For two-dimensional problem, the governing equations are made dimensionless, and potential functions are used for further simplification. The plane wave solution of these equations determines the effectiveness of longitudinal (P-wave), thermal (T-wave), and transverse (SV-wave). For the assumed model when a wave (P-wave, or T-wave or SV-wave) is incident on the surface $x_3 = 0$, three varieties of reflected waves are produced: P-wave, T-wave and SV-wave. The AR for these reflected waves is obtained numerically and displayed graphically to investigate the influence of specific parameters (N-L, HTT, and impedance). Additionally, special cases are inferred from the current investigation.

5.2 Basic Equations

Following [Quintanilla (2019) [105], Eringen (1974) [42], Youseff and El-Bary (2018) [149]] the basic equations and constitutive relations in isotropic, thermoelastic homogeneous semi-space under MGT heat equation with the influence of N-L, HTT parameters, without body forces and heat sources, are presented as follows

$$(\lambda+\mu)\nabla(\nabla\cdot\vec{u})+\mu\Delta\vec{u}-\beta_1\nabla T=\rho\left(1-{\xi_1}^2\Delta\right)\frac{\partial^2\vec{u}}{\partial t^2}, \tag{5.1}$$

$$\left(1+\tau_0\frac{\partial}{\partial t}\right)\left[\rho C_e\ddot{T}+\beta_1 T_0\ddot{e}\right]=K^*\frac{\partial}{\partial \mathrm{t}}\Delta\phi+K_1\Delta\phi, \tag{5.2}$$

$$\ddot{\phi}-\ddot{T}=\beta^*\Delta\phi, \tag{5.3}$$

$$t_{ij}=\lambda e_{k,k}\delta_{ij}+2\mu\ \mathrm{e_{ij}}-\beta_1 T\delta_{ij}. \tag{5.4}$$

where symbols are same as defined in section 2.2 [Chapter 2] and Section 3.2 of [Chapter 3]. Equations (5.1) -(5.4) in component form for Cartesian coordinates (x_1, x_2, x_3) are written as

$$\left[(\lambda+\mu)\frac{\partial e}{\partial x_1}+\mu\,\Delta u_1\right]-\beta_1\frac{\partial T}{\partial x_1}=\rho(1-\xi_1^2\Delta)\frac{\partial^2 u_1}{\partial t^2}, \tag{5.5}$$

$$\left[(\lambda+\mu)\frac{\partial e}{\partial x_2}+\mu\,\Delta u_2\right]-\beta_1\frac{\partial T}{\partial x_2}=\rho(1-\xi_1^2\Delta)\frac{\partial^2 u_2}{\partial t^2}, \tag{5.6}$$

$$\left[(\lambda+\mu)\frac{\partial e}{\partial x_3}+\mu\,\Delta u_3\right]-\beta_1\frac{\partial T}{\partial x_3}=\rho(1-\xi_1^2\Delta)\frac{\partial^2 u_3}{\partial t^2}, \tag{5.7}$$

$$\frac{\partial^2 T}{\partial\, t^2}=\left(\frac{\partial^2}{\partial\, t^2}-\beta^*\Delta\right)\phi, \tag{5.8}$$

$$\left(1+\tau_0\frac{\partial}{\partial t}\right)\left[\rho C_e\frac{\partial^2 T}{\partial t^2}+\beta_1 T_0\frac{\partial^2 e}{\partial t^2}\right]=K^*\Delta\dot{\phi}+K_1\Delta\phi, \tag{5.9}$$

$$t_{11} = \lambda\, e + 2\,\mu\, e_{11} - \beta_1 T, \tag{5.10}$$

$$t_{22} = \lambda\, e + 2\,\mu\, e_{22} - \beta_1 T, \tag{5.11}$$

$$t_{33} = \lambda\, e + 2\,\mu\, e_{33} - \beta_1 T, \tag{5.12}$$

$$t_{31} = 2\mu\, e_{31}, \tag{5.13}$$

$$t_{32} = 2\mu\, e_{32}, \tag{5.14}$$

$$t_{21} = 2\mu\, e_{21}, \tag{5.15}$$

where Δ, e are same as defined in Section 2.2 [Chapter 2].

5.3 Problem Statement

An isotropic thermoelastic and homogeneous semi-space is considered to examine MGT heat equation with N-L and HTT, initially at the uniform temperature. The coordinate system (x_1, x_2, x_3) with the origin is positioned at the plane boundary at the x_3 = 0. The x_3-axis directing vertically downward into the medium, as signified through $x_3 \geq 0$ and depicted in figure 5.1. The wave propagation direction is considered in such a way so that every particle on a line parallel to the x_2 -axis are correspondingly displaced. As a result, the x_2-coordinate will not affect any of the field quantities.

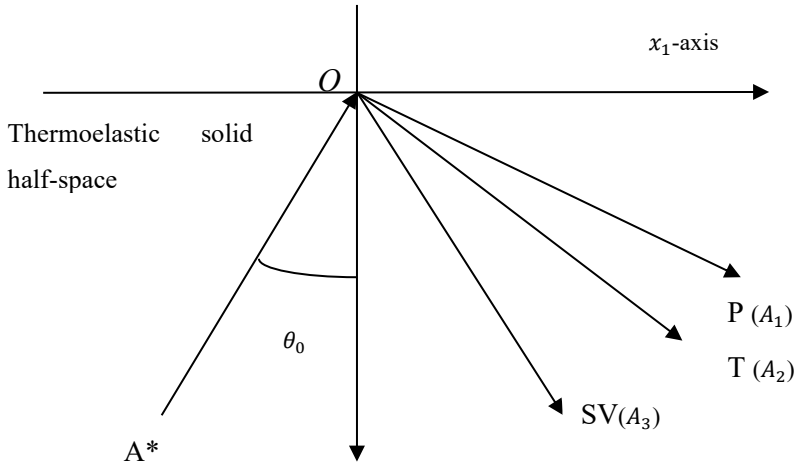

Figure 5.1 diagrammatic presentation of the problem

For the assumed model, we take

$$\vec{u} = (\, u_1(x_1, x_3, t), 0, u_3(x_1, x_3, t)),\ \ T = T(x_1, x_3, t), \qquad \phi = \phi(x_1, x_3, t). \tag{5.16}$$

Using equation (5.16) in (5.5) - (5.9) and (5.12) - (5.13), we get

$$(\lambda + \mu)\frac{\partial e}{\partial x_1} + \mu \Delta u_1 - \beta_1 \frac{\partial T}{\partial x_1} = \rho\left(1 - {\xi_1}^2 \Delta\right)\frac{\partial^2 u_1}{\partial t^2}, \tag{5.17}$$

$$(\lambda + \mu)\frac{\partial e}{\partial x_3} + \mu \Delta u_3 - \beta_1 \frac{\partial T}{\partial x_3} = \rho\left(1 - {\xi_1}^2 \Delta\right)\frac{\partial^2 u_3}{\partial t^2}, \tag{5.18}$$

$$\left(1+\tau_0\frac{\partial}{\partial t}\right)\left[\rho C_e\frac{\partial^2 \mathrm{T}}{\partial t^2}+\beta_1 T_0\frac{\partial^2 \mathrm{e}}{\partial t^2}\right]=K^*\Delta\dot{\phi}+K_1\Delta\phi, \qquad (5.19)$$

$$\frac{\partial^2 T}{\partial\, t^2}=\left(\frac{\partial^2}{\partial\, t^2}-\beta^*\Delta\right)\phi, \qquad (5.20)$$

$$t_{33}=\lambda\,\mathrm{e}+2\,\mu\,e_{33}-\beta_1 T\,, \qquad (5.21)$$

$$t_{31}=2\mu e_{31}\,, \qquad (5.22)$$

where

e and Δ are same as defined in equation (2.16) [Chapter 2].

The following dimensionless quantities are taken in addition to dimensionless quantities defined by equation (3.23) [Chapter 3]:

$$(z'_1, z'_2)=\frac{c_1}{\beta_1 T_0}(z_1, z_2), \qquad z'_3=\frac{c_1}{\mathrm{K}^*}z_3, \qquad \omega'=\frac{\omega}{\omega_1}\,. \qquad (5.23)$$

where c_1^2 and ω_1 are same as defined in equation (2.34) [Chapter 2].

Equations (5.17) - (5.22), with the aid of equations (5.23) and (3.23) [Chapter 3] reduce to the following equations after suppressing the primes,

$$a_1\frac{\partial e}{\partial x_1}+a_2\Delta u_1-a_3\frac{\partial T}{\partial x_1}=\left(1-{\xi_1}^2\Delta\right)\frac{\partial^2 u_1}{\partial t^2}, \qquad (5.24)$$

$$a_1\frac{\partial e}{\partial x_3}+a_2\Delta u_3-a_3\frac{\partial T}{\partial x_3}=\left(1-{\xi_1}^2\Delta\right)\frac{\partial^2 u_3}{\partial t^2}, \qquad (5.25)$$

$$\left(1+\tau_0\frac{\partial}{\partial t}\right)\left(\frac{\partial^2 T}{\partial t^2}+a_4\frac{\partial e}{\partial t^2}\right)=\left(\frac{\partial}{\partial t}+k'_0\right)\Delta\phi, \qquad (5.26)$$

$$\ddot{\phi}-\ddot{T}=\beta^*\Delta\phi\,, \qquad (5.27)$$

$$t_{33}=a_5\frac{\partial u_1}{\partial x_1}+a_6\frac{\partial u_3}{\partial x_3}-T, \qquad (5.28)$$

$$t_{31}=a_7\left(\frac{\partial u_3}{\partial x_1}+\frac{\partial u_1}{\partial x_3}\right), \qquad (5.29)$$

where $\mathrm{k}'_0=\frac{K_1}{K^*\omega_1}$.

5.4 Solution Procedure

The relation between displacement and scalar potentials is same as given by equation (2.32) [Chapter 2].

The dimensionless form specified by (2.32) is used to decompose equations (5.24) - (5.29) by utilizing potential functions q and Ψ defined by equation (2.32) [Chapter 2].

$$\Delta q-a_3 T=\left(1-{\xi_1}^2\Delta\right)\frac{\partial^2 q}{\partial t^2}\,, \qquad (5.30)$$

$$\left[a_2\Delta-(1-\xi_1^2\Delta)\frac{\partial^2}{\partial\, t^2}\right]\Psi=0\,, \qquad (5.31)$$

$$\left(1+\tau_0\frac{\partial}{\partial t}\right)\left(\frac{\partial^2 T}{\partial t^2}+a_4\frac{\partial}{\partial t^2}\Delta q\right)=\left(\frac{\partial}{\partial t}+\mathrm{k}'_0\right)\Delta\phi\,, \qquad (5.32)$$

$$\ddot{\mathrm{T}} = \ddot{\phi} - \beta^{*}\Delta\phi, \qquad (5.33)$$

$$t_{33} = a_5 \frac{\partial u_1}{\partial x_1} + a_6 \frac{\partial u_3}{\partial x_3} - T, \qquad (5.34)$$

$$t_{31} = a_7 \left(\frac{\partial u_1}{\partial x_3} + \frac{\partial u_3}{\partial x_1}\right), \qquad (5.35)$$

where

$a_1 = \frac{\lambda+\mu}{\rho c_1^2}$, $a_2 = \frac{\mu}{\rho {c_1}^2}$, $a_3 = \frac{\beta_1 T_0}{\rho c_1^2}$, $a_4 = \frac{\beta_1 c_1^2}{K^{*} w_1}$,

$a_5 = \frac{\lambda}{\beta_1 T_0}$, $a_6 = \frac{\lambda+2\,\mu}{\beta_1\, T_0}$, $a_7 = \frac{\mu}{\beta_1\, T_0}$.

In order to solve the equations (5.30) - (5.32), we adopt the solution of the type

$$(\mathrm{q}, \mathrm{T}, \Psi, \phi) = (\mathrm{q}^0, \mathrm{T}^0, \Psi^0, \phi^0)\mathrm{e}^{\iota\kappa(\mathrm{x}_1 \sin\theta_0 - \mathrm{x}_3 \cos\theta_0 + \nu \mathrm{t})}, \qquad (5.36)$$

where ι is known as iota, κ is the wave number, ν is the phase speed, ω is the angular frequency with the relation ω = k ν, $(\sin\theta_0, \cos\theta_0)$ represents the wave normal's projection onto the x_1-x_3 plane and $\mathrm{q}^0, \mathrm{T}^0, \Psi^0$, and ϕ^0 are random constants representing the wave amplitudes.

Substituting the value of T from equation (5.36) in (5.33), (after removing the bars) yield

$$\mathrm{T} = \phi + \varsigma\Delta\phi, \qquad (5.37)$$

where $\varsigma = \begin{cases} \frac{\beta^{*}}{\omega^2}, \text{for (HTT)}, \\ \mathrm{a}, \text{for two temperature (TT)}, \\ 0, \text{for one temperature (1T)}. \end{cases}$

Using the equation (5.37) in equations (5.30) and (5.32), yield

$$\left(\Delta q - \left(1 - {\xi_1}^2\Delta\right)\frac{\partial^2 \boldsymbol{q}}{\partial t^2}\right) = a_3(\phi + \varsigma\Delta\phi), \qquad (5.38)$$

$$\left(1 + \tau_0 \frac{\partial}{\partial t}\right)\left(\frac{\partial^2}{\partial t^2}(\phi + \varsigma\Delta\phi) + a_4 \frac{\partial}{\partial t^2}\Delta q\right) = \left(\frac{\partial}{\partial t} + \mathrm{k'}_0\right)\Delta\phi. \qquad (5.39)$$

Substituting the values of q and ϕ from the equation (5.36) in equations (5.38), and (5.39), after simplification, we get the following equation

$$(\upsilon^4 + \mathrm{A}\upsilon^2 + \mathrm{B})(\mathrm{q}, \phi) = 0, \qquad (5.40)$$

where

$\mathrm{A} = \frac{\iota\omega + a_5 + \iota\,\omega\,\tau_0^{*}\left(1-\xi_1^2\omega^2 + a_3 a_4\right) + \iota\omega\tau_0^{*}\beta^{*}}{\iota\omega\tau_0^{*}}$, $B = \frac{(\iota\omega + a_5)\left(1-\xi_1^2\omega^2\right) + \iota\,\omega\,\tau_0^{*}\left(1-\xi_1^2\omega^2 + a_3 a_4\right)}{\iota\omega\tau_0^{*}}$, $\tau_0^{*} = \tau_0 - \frac{\iota}{\omega}$.

Inserting the value of Ψ from (5.36) in (5.31), after simplification yield

$$(\upsilon^2 - A_1)\Psi = 0, \qquad (5.41)$$

where

$A_1 = \sqrt{\frac{a_2}{1+\xi_1^2\, k^2}}$.

Let υ_i (i = 1,2) are roots of biquadratic characteristic equation $(\upsilon^4 + \mathrm{A}\upsilon^2 + \mathrm{B}) = 0$ and υ_3 is

roots of characteristic equation $(\upsilon^2 - A_1) = 0$. υ_1, υ_2, correspond to velocities of the P-wave and T-wave in order of decreasing, whereas υ_3 correspond to velocity of SV- wave .

5.5 Reflection Phenomenon of Waves

A thermoelastic half-space is being analysed using MGT heat equation which includes N-L and HTT parameters. The phenomenon involves the incidence of either a P-wave, T-wave, SV-wave at a plane, with its propagation angle θ_0 makes with perpendicular to the surface. In the half-space $x_3 \geq 0$, we obtain a reflected (P, T, and SV) -wave for each incident wave. Assume that the reflected P, T and SV waves make angles $\theta_1,\ \theta_2,$ and θ_3 respectively, with the x_3−axis. The incident and reflected waves are illustrated in figure 5.1, providing a complete representation of the geometry.

The potential functions and conductive temperature can be expressed as:

$$q = \sum_{i=0}^{2} A_{0i} e^{\iota\kappa_l(x_1 \sin\theta_0 - x_3 \cos\theta_0)+\iota\omega t} + A_i e^{\iota\kappa_l(x_1 \sin\theta_l - x_3 \cos\theta_l)+\iota\omega t}, \qquad (5.42)$$

$$\phi = \sum_{i=0}^{2} d_i \left(A_{0i} e^{\iota\kappa_l(x_1 \sin\theta_0 - x_3 \cos\theta_0)+\iota\omega t} + A_i e^{\iota\kappa_l(x_1 \sin\theta_1 + x_3 \cos\theta_l)+\iota\omega t}\right), \qquad (5.43)$$

$$\Psi = \sum A_{03}\, e^{\iota\kappa_0(x_1 \sin\theta_0 - x_3 \cos\theta_0)+\iota\omega t} + A_3 e^{\iota\kappa_3(x_1 \sin\theta_3 - \cos\theta_3)+\iota\omega t},\ i=1,2 \qquad (5.44)$$

where

$$d_i = \frac{\omega^2[(1+\xi_1{}^2 k_i{}^2)\omega^2 - k_i{}^2]}{a_8\left(\omega^2 - k_i{}^2\beta^*\right)}, (i = 1,2). \qquad (5.45)$$

The amplitudes of the P- wave and T-wave are denoted by A_{0i} (i = 1, 2) and while the amplitude of the incident SV-wave is denoted by A_{03}. $A_i (i = 1, 2, 3)$ are the amplitudes of the reflected P-wave, T-wave and SV-wave respectively.

5.6 Boundary Conditions

The impedance boundary is determined by a combination of unspecified functions and their corresponding derivative which are defined along the boundary. Typically, a contact surface that is ideally welded is presumed in the context of seismic wave interactions with discontinuities, ensuring the continuity of appropriate displacement and stress components. Therefore, following [Tiersten (1969) [141] and Malischewsky (1987) [84]], the appropriate impedance boundary restrictions at $x_3 = 0$ are

$$\text{(i) } t_{33} + \omega z_1 u_3 = 0, \qquad \text{(ii) } t_{31} + \omega z_2 u_1 = 0, \quad \text{(iii) } K^* \frac{\partial\phi}{\partial x_3} + \omega z_3 \phi = 0, \qquad (5.46.)$$

where z_1, z_2 signifies impedance parameter with dimensions Nsm^{-3}, and z_3 is impedance parameter with dimensions Nsm^{-1} respectively. The stress-free boundary conditions are implemented by setting $z_1 = z_2 = z_3 = 0$.

Using non-dimensional quantities given by (5.23) on equation (5.46), yield

$$\text{(i) } t_{33} + \omega z_1 u_3 = 0, \quad \text{(ii) } t_{31} + \omega z_2 u_1 = 0, \quad \text{(iii) } \frac{\partial \phi}{\partial x_3} + \omega z_3 \phi = 0\,. \qquad (5.47)$$

Using equation (2.32) [Chapter 2] in equations (5.34), (5.35) and with the aid of equation (5.37), yield

$$t_{33} = a_5\left(\frac{\partial^2 q}{\partial x_3^2} - \frac{\partial^2 \Psi}{\partial x_3 \partial x_1}\right) + a_6\left(\frac{\partial^2 q}{\partial x_3^2} + \frac{\partial^2 \Psi}{\partial x_3 \partial x_1}\right) - \phi + \varsigma \Delta\phi, \qquad (5.48)$$

$$t_{31} = a_7\left(\frac{\partial^2 \Psi}{\partial x_1^2} + \frac{\partial^2 q}{\partial x_1 \partial x_3} + \frac{\partial^2 q}{\partial x_1 \partial x_3} - \frac{\partial^2 \Psi}{\partial x_3^2}\right). \qquad (5.49)$$

To satisfy the boundary conditions (5.47) at $x_3 = 0$, the angle of reflected waves needs to be linked to the angle of incident (P-, T-, SV-) wave by using Snell's Law is specified as

$$\frac{\sin\theta_0}{v_0} = \frac{\sin\theta_1}{v_1} = \frac{\sin\theta_2}{v_2} = \frac{\sin\theta_3}{v_3}, \qquad (5.50)$$

where

$k_1 v_1 = k_2 v_2 = k_3 v_3 = \omega$ at $x_3 = 0$.

$$v_0 = \begin{cases} v_1, \text{incident P} - \text{wave} \\ v_2, \text{incident T} - \text{wave} \\ v_3, \text{incident SV} - \text{wave} \end{cases}. \qquad (5.51)$$

After simplification, a system of three non-homogeneous equations is obtained by substituting the values of potential functions q, ϕ, and ψ in the boundary condition (5.47) and utilizing equations (5.48) - (5.49) and (5.50) - (5.51) as

$$\sum_{i,j=1}^{3} a_{ij} R_j = Y_j, \qquad (5.52)$$

where

$$a_{1i} = -\left(a_5 {k_i}^2 \cos\theta_i^2 + a_6 {k_i}^2 \sin^2\theta_i + d_i(1 - \zeta k_1^2) - \iota k_i w z_i \cos\theta_i\right),$$

$$a_{13} = \quad (a_5 + a_6){k_3}^2 \cos\theta_3 \sin\theta_3 + \iota k_3 w z_1 \sin\theta_3,$$

$$a_{2i} = -2a_7 k_i^2 \cos\theta_i \sin\theta_i + \iota k_i w z_i \sin\theta_i, \qquad a_{23} = -\left(\iota k_3 w z_3 \cos\theta_3 + {k_3}^2\right),$$

$$a_{3i} = (\iota k_i K^* \cos\theta_i + w z_3) d_i, \qquad a_{33} = 0, \qquad (i = 1,2). \qquad (5.53)$$

Also, $R_j (j = 1,2,3)$ are AR of reflected P-wave, reflected T-wave, and SV-wave as given by

$$R_1 = \frac{A_1}{B^*}, R_2 = \frac{A_2}{B^*}, R_3 = \frac{A_3}{B^*}. \qquad (5.54)$$

For incident P-wave $B^* = A_{01}$, and $A_{02} = A_{03} = 0$.

$$Y_1 = a_5 k_0^2 \cos^2\theta_0 + a_6 k_0 \sin^2\theta_0 + d_1\,(1 - \zeta k_0^2) + w\, z_1 \iota\, k_0 \cos\theta_0,$$

$$Y_2 = -(2a_7 k_0^2 \cos\theta_0 \sin\theta_0 + w\, z_2 \iota\, k_0 \sin\theta_0),$$

$$Y_3 = \ (K^* \iota\, k_0 \cos\theta_0 - w\, z_3\,) d_1\,. \qquad (5.55)$$

For incident T-wave $B^* = A_{02}$, and $A_{01} = A_{03} = 0$.

$$Y_1 = a_5 k_0^2 \cos^2\theta_0 + a_6 k_0 \sin^2\theta_0 + d_2\,(1 - \zeta k_0^2) + w\, z_1 \iota\, k_0 \cos\theta_0\,,$$

$$Y_2 = -(2k_0^2\, a_7 \sin\theta_0 \cos\theta_0 + w z_2 \sin\theta_0 \iota\, k_0),$$

$$Y_3 = (K^* \iota\, k_0 \cos\theta_0 - w\, z_3)d_2 . \qquad (5.56)$$

For incident SV-wave $B^* = A_{03}$, and $A_{01} = A_{02} = 0$.

$$Y_1 = -(a_5 k_0^2 \cos\theta_0 \sin\theta_0 - a_6 k_0^2 \cos\theta_0 \sin\theta_0 + w\, z_1 \iota\, k_0 \sin\theta_0),$$

$$Y_2 = -[a_7 k_0^2 (\cos^2\theta_0 - \sin^2\theta_0) + w\, z_2 \iota\, k_0 \cos\theta_0],$$

$$Y_3 = 0. \qquad (5.57)$$

5.7 Validation

i) By letting $K^* = 0$, and $\varsigma = 0$, in (5.52), the corressponding expressions for AR are obtain for coupled thermoelasticity theory under impedance boundary. The findings of this study align with those of Kaushal et al. (2021) [61] for the specific case, excluding diffusion.

ii) Letting $\xi_1 = \varsigma = K^* = 0$ in equation (5.52), we can derive similar results for the L-S model, which are consistent with those obtained by Yadav (2021) [144] in a specific scenario without considering diffusion and void parameters as a particular case.

iii) By setting $\varsigma = K^* = 0$, in (5.52), we derive the compatible outcomes for generalised thermoelasticity (L-S model) with N-L and these results are the consistent with those obtained by Singh and Bijarnia (2021) [131] (in the absence of impedance) as a particular case with stress free boundary .

iv) By setting $K_1 = 0, \tau_0 = 0$ and $\varsigma = a$, the matching expressions for AR can be obtained by equation (5.52) for the GN-II model alongwith N-L and TT effects under the impedance boundary.

v) The results reduce to thermoelastic with energy dissipation (GN-III model (1993)) without TT effects by considering $\xi_1 = 0$, $\tau_0 = 0$ and $\varsigma = 0$ along with $z_1 = z_2 = z_3 = 0$ in equation (5.52).

5.8 Special Cases

i) If $z_2 = z_3 = 0$, in (5.52), then the corresponding relation for AR can be derived for a generalized thermoelastic semi-space with a normal impedance parameter.

ii) The findings are obtained for a generalized thermoelastic semi-space with a tangential impedance parameter by taking $z_1 = z_3 = 0$, in (5.52).

5.9 Numerical result and discussion

Some numerical results are presented to exemplify the theoretical results derived in the previous section. The influence of N-L , HTT and impedance parameters $(z_1 = 1, z_2 = 5, z_3 = 2)$ and without impedance parameters $(z_1 = z_2 = z_3 = 0)$ on AR with angle of

incidence θ_0 under MGT heat equation is illustrated in figures 5.2 - 5.19. We consider the case of magnesium crystal-like material in accordance with Dhaliwal and Singh (1980) [38]. The physical constants employed are as same as appeared in section 2.9 [Chapter 2].

5.9.1 Non-Local Effect

The computation for the following cases is as:

i. A solid black line (——) is used to represent MGT model with N-L parameter ($\xi_1 = 0.5$) and with impedance parameters (NI).
ii. A dashed red line (----) corresponds MGT model without N-L parameter ($\xi_1 = 0$) and with impedance parameters (ANI).
iii. A solid blue line with a triangle symbol ($-\Delta-$) denotes MGT model with N-L parameter ($\xi_1 = 0.5$) and without impedance parameter (NWI).
iv. A dashed green line with the symbol ($-\circ-$) corresponds to the MGT model in absence of N-L parameter and without impedance parameters (ANWI).

5.9.1.1 P- wave

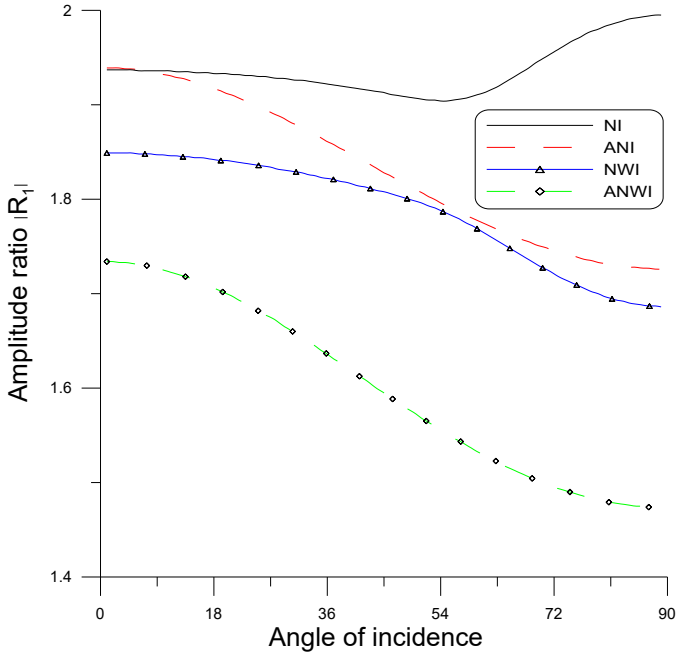

Fig.5.2 Profile of $|R_1|$ for P- wave

Figure 5.2 represents the trend of $|R_1|$ vs θ_0. The values of $|R_1|$ decreases for all curves in whole domain except for $0 \leq \theta \leq 60^0$, $|R_1|$ exhibit increasing trend for NI. It is seen that the amplitude of $|R_1|$ remains on higher side for NI as compared to other cases which can be accounted as the effect of N-L and impedance parameter.

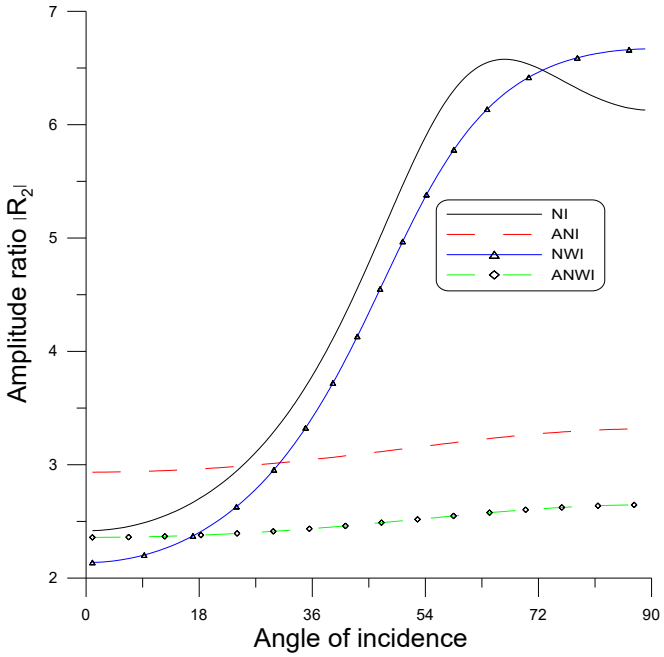

Fig.5.3 Profile of $|R_2|$ for P- wave

Figure 5.3 shows that the values of $|R_2|$ follows the uptrend for NI and NWI for whole range except for $72^{\circ} \leq \theta \leq 90^{\circ}$,where the reversed behaviour is observed. However, the values of $|R_2|$ remains higher for NWI than that for NI. Also, the values of $|R_2|$ remains stationary for ANWI and ANI for all θ_0.

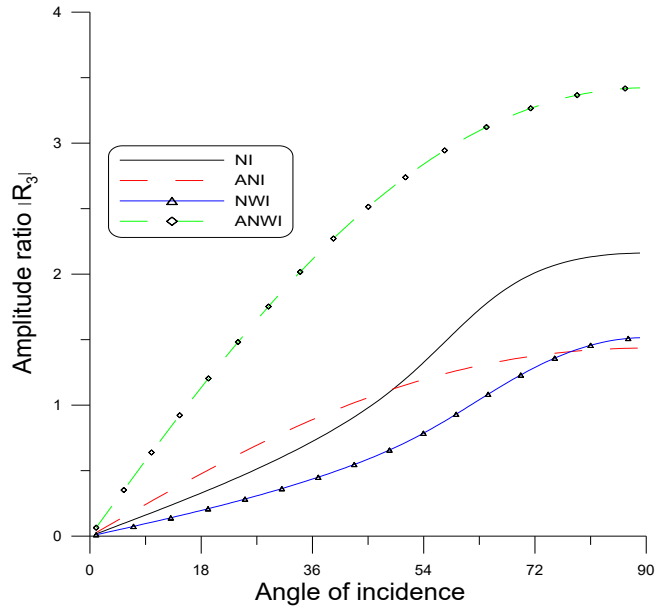

Fig.5.4 Profile of $|R_3|$ for P- wave

Figure 5.4, depicts that the immensity of $|R_3|$ follows increasing trend for all the considered cases for all θ_0, but the values of $|R_3|$ remains higher for ANWI in comparison to all considered cases.

5.9.1.2 T- Wave

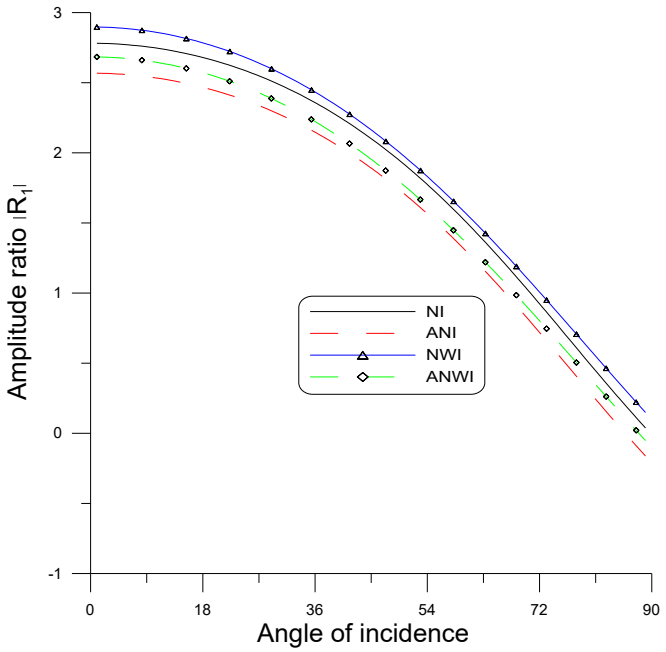

Fig 5.5. Profile of $|R_1|$ for T- wave

Figure 5.5 depicts variations of $|R_1|$ with θ_0. All the curve corresponding to $|R_1|$ decrease throughout range, while due to N-L effect, the curve corresponding to NWI remain higher than other curves.

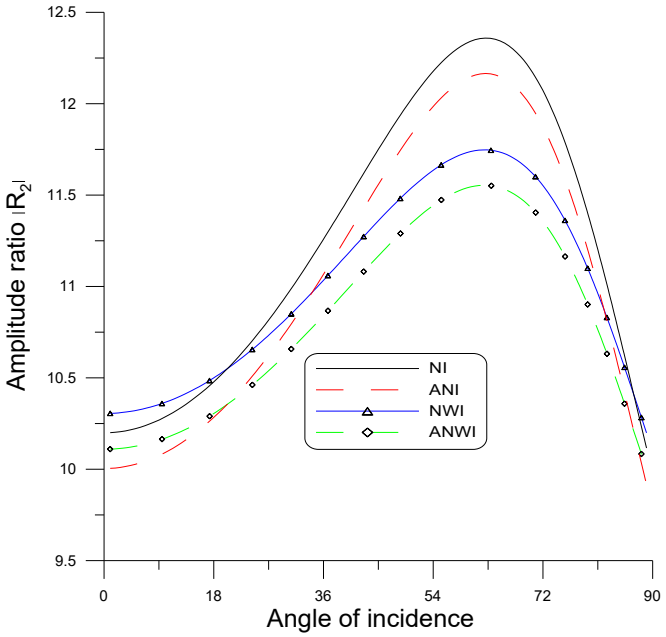

Fig.5.6 Profile of | R_2 | for T-Wave

Figure 5.6 depicts the variations of $|R_2|$ with θ_0. The values of $|R_2|$ shows increasing trend for $0 \leq \theta \leq 60^0$and follows a decreasing trend in the left-over interval. Also, the magnitude of variations is relatively higher for NI than other considered curves.

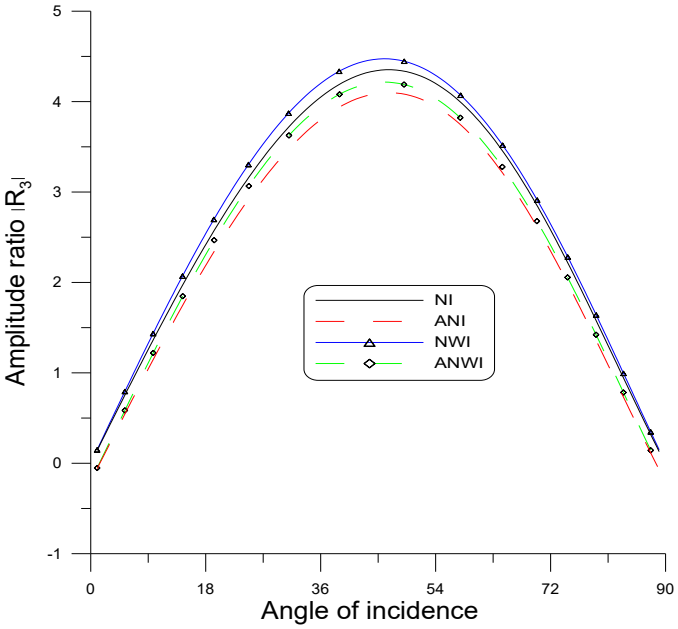

Fig. 5.7 Profile of $|R_3|$ for T-Wave

Figure 5.7 depicts that the values of $|R_3|$ shows a positive uptrend in the first half of the interval, whereas reverse behaviour is observed for remaining region. Moreover, the values of $|R_3|$ is highest for NWI, while lowest for ANI.

5.9.1.3 SV-Wave

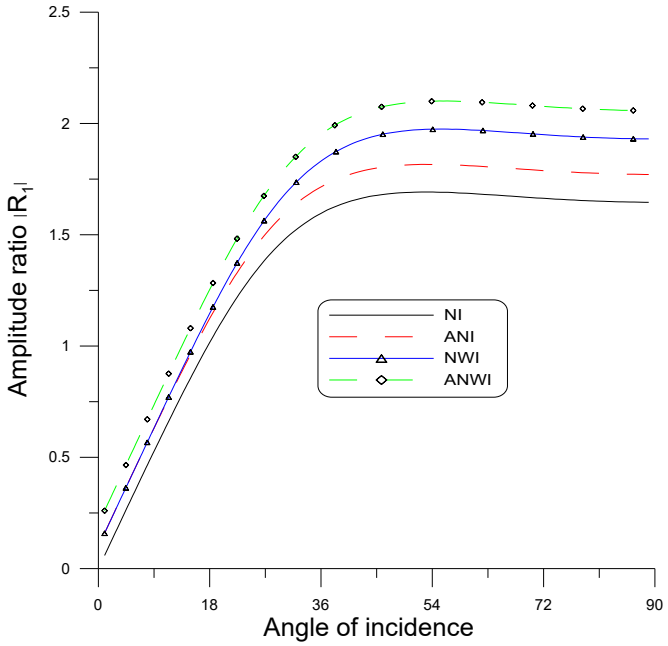

Fig.5.8 Profile of $|R_1|$ for SV-Wave

It is depicted in figure 5.8 that values of $|R_1|$ shows rising trend in the range $0 \leq \theta \leq 36^0$, and magnitude of variations remains higher for the case of ANWI in comparison to other cases. For the remaining range, $|R_1|$ shows a steady trend for all the cases.

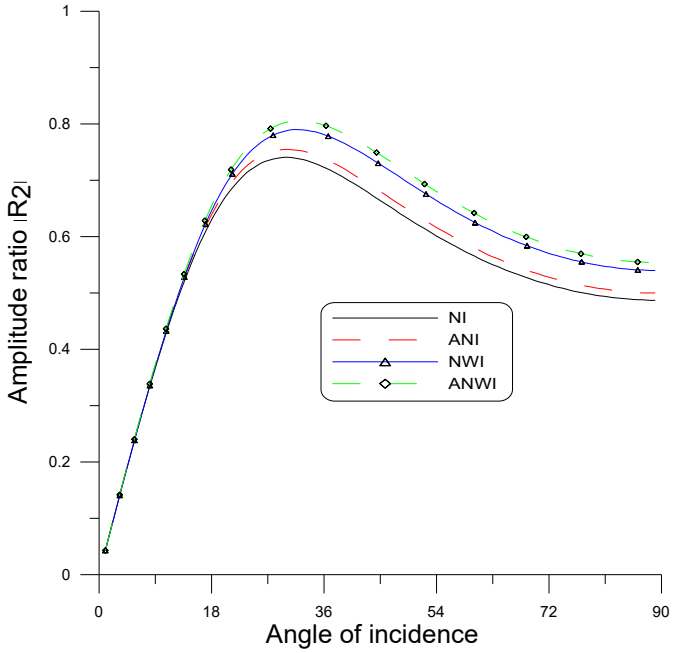

Fig.5.9 Profile of $|R_2|$ for SV-Wave

Figure 5.9 displays that the values of $|R_2|$ increases for $0 \leq \theta \leq 25^{\circ}$and then decreases monotonically for all the cases, although the magnitude of the decrement is relatively small.

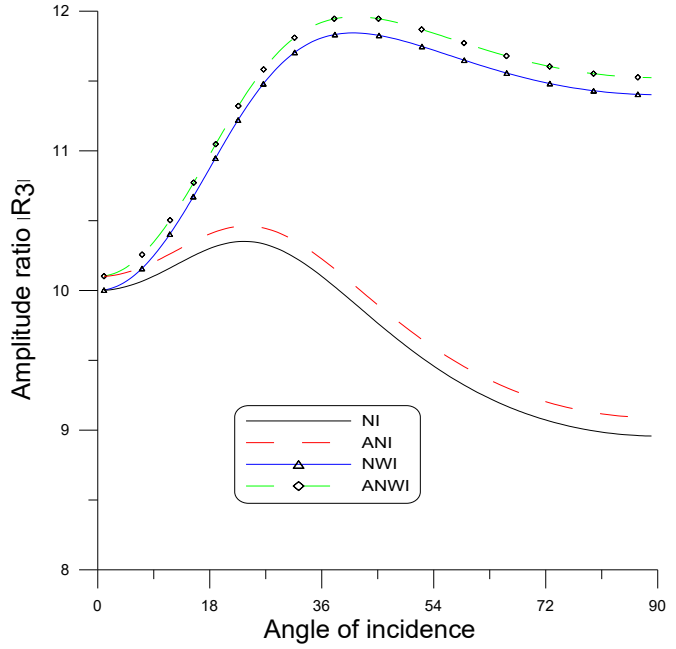

Fig.5.10 Profile of $|R_3|$ for SV-Wave

From figure 5.10, it is seen that for both NWI and ANWI the values of $|R_3|$ increases for $0 \leq \theta \leq 45^{\circ}$, and it remains almost stationary for remaining range and the immensity $|R_3|$ remains on higher side for ANWI. Also, the values of $|R_3|$ exhibit a decreasing pattern for ANI and NI for the entire range except for $0 \leq \theta \leq 25^{\circ}$.

5.9.2 Hyperbolic Two Temperature effect

The computation for the following cases is as:

i. A solid black line (——) represents the MGT model with HTT ($\varsigma = 0.75$) with impedance parameter **(HI)**.

ii. A dotted red line (----) corresponds to the MGT model with HTT ($\varsigma = 0.0$) and with impedance parameter (**WHI**).

iii. A blue line with a triangle symbol ($-\Delta-$) denotes the MGT model with HTT ($\varsigma = 0.75$) and without impedance parameter (**HWI**).

iv. A green line with a symbol ($-\circ-$) represents the MGT model with ($\varsigma = 0.0$) and without impedance parameter (**AHWI**).

5.9.2.1 P- wave

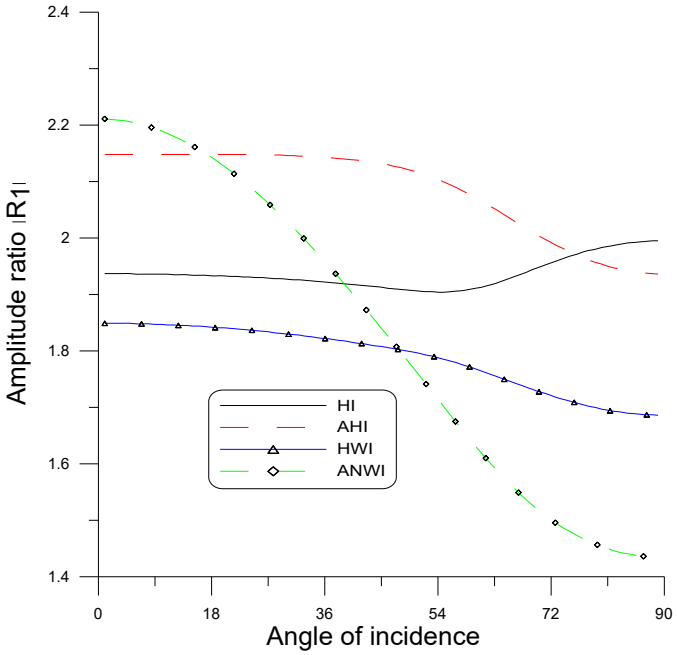

Fig. 5.11 Profile of $|R_1|$ for P- wave

Figure 5.11, represents the trend of $|R_1|$ with θ_0. The values of $|R_1|$ shows a decreasing trend for the case ANWI in the whole region, while for AHI, it displays a steady state in initial half of the range and decreases in the remaining region. Also, for HI and HWI, behaviour and variations are similar for $0 \leq \theta \leq 54^0$, while reverse trend is observed for the left-over range.

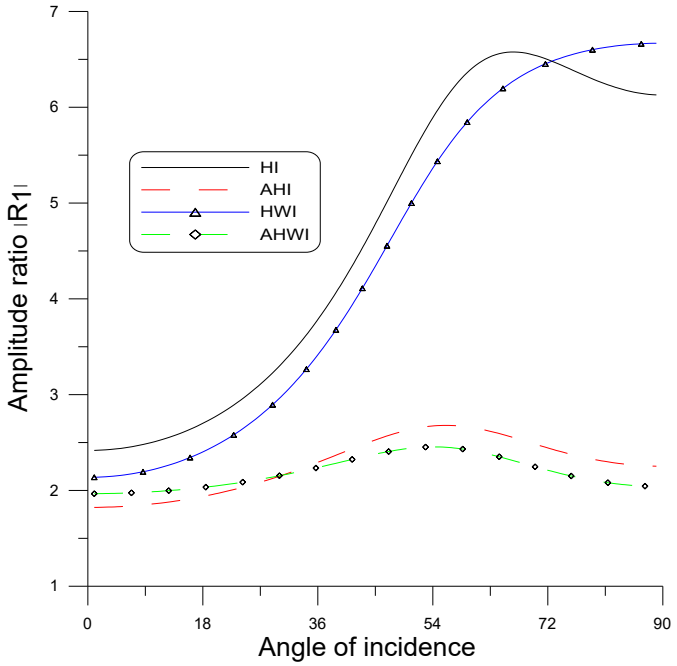

Fig. 5.12 Profile of $|R_2|$ for P- Wave

Figure 5.12 represents that the values of $|R_2|$shows incremental behaviour for HWI and HI in almost the entire range. Also, it is evident that the pattern of variation of $|R_2|$ for both AHI and AHWI is similar, with substantial differences in their absolute values.

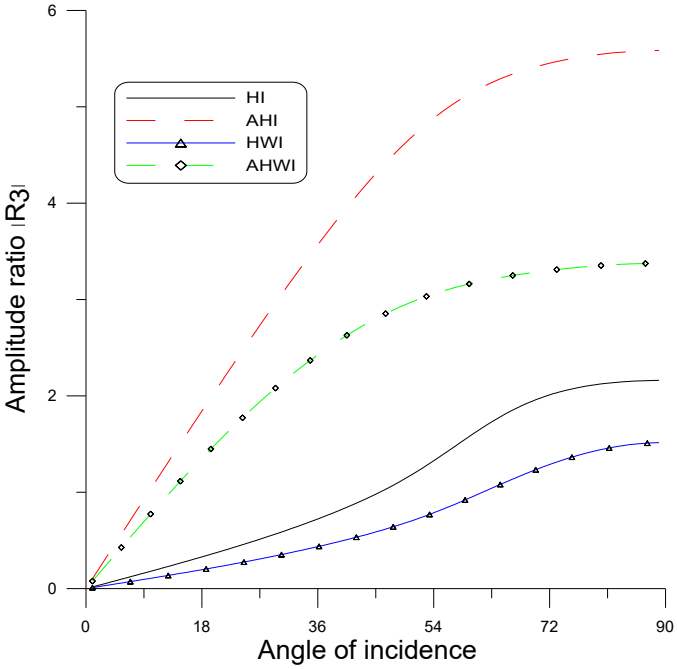

Fig.5.13 Profile of $|R_3|$ for P- wave

Figure 5.13 represents the trend of $|R_3|$ vs θ_0. The immensity of all the curve corresponding to $|R_3|$ remains on higher side. Further, the immensity of $|R_3|$ is on higher side for AHI, while on lower side for HWI in comparison to other cases.

5.9.2.2 T- Wave

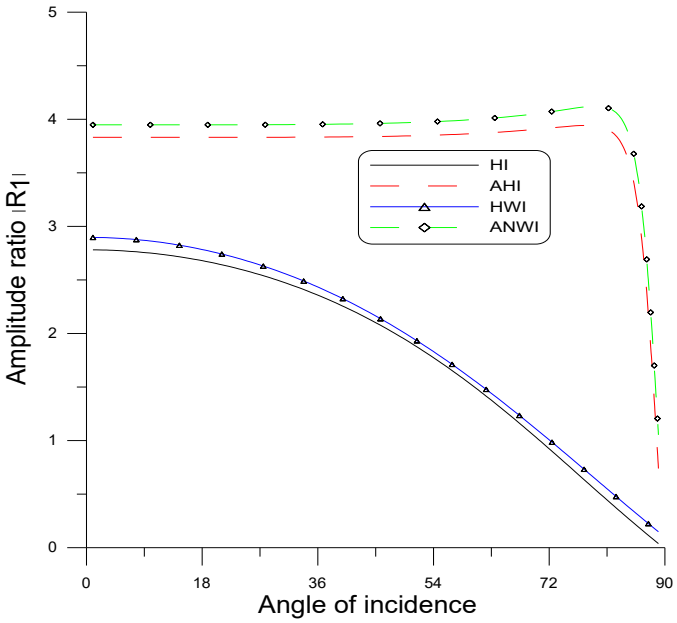

Fig.5.14 Profile of $|R_1|$ for T -Wave

It is depicted from figure 5.14, that for HI and HWI, a decreasing trend is noticed throughout the region, whereas for both AHI and AHWI, the magnitude of $|R_1|$ remains stationary in almost for all θ_0 except near $\theta_0 = 90^{\circ}$where the values decrease sharply.

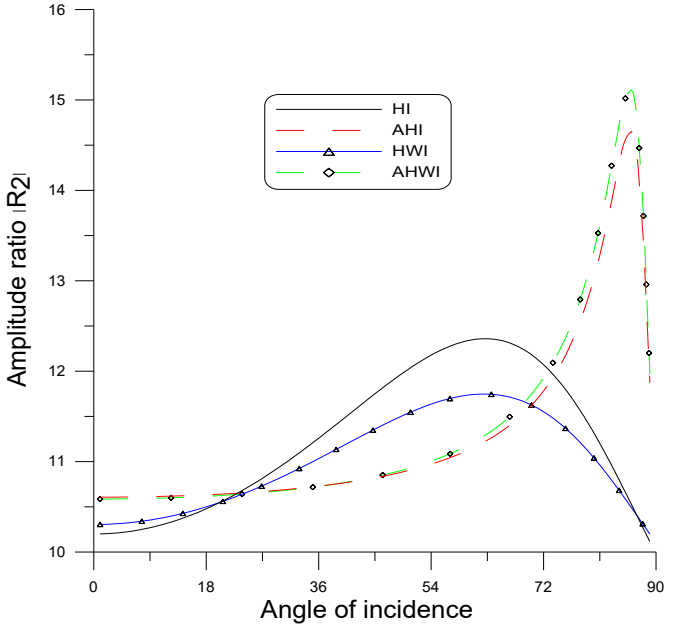

Fig.5.15 Profile of $|R_2|$ for T-wave

Figure 5.15 displays that for AHI and AHWI the values of $|R_2|$ show similar trends in the entire range with significant differences in the magnitude and attain maximum value at $\theta_0 = 80^{\circ}$and then, it decreases sharply. It is further found that the magnitude of $|R_2|$ follows increasing behaviour for HI and HWI for $0 \leq \theta \leq 65^{0}$and decreases in the left-over interval,

magnitude of value for $|R_2|$ remains higher for HI than HWI.

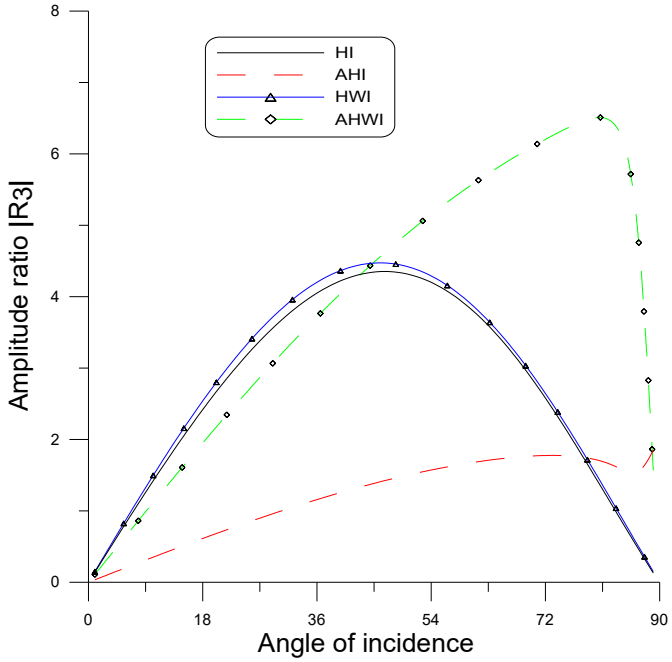

Fig.5.16 Profile of $|R_3|$for T-Wave

From figure 5.16, the immensity of $|R_3|$ for HI and HWI rise in the first half of the interval, whereas reverse trend is observed in the remaining range. Also, for AHWI and AHI, the trend of variation is increasing in the entire range except at grazing angle where the values decrease sharply for the case AHWI.

5.9.2.3 SV- Wave

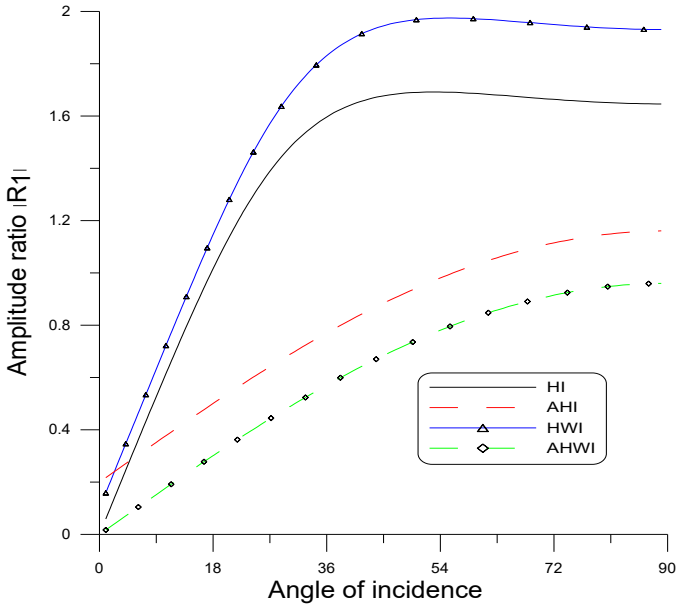

Fig.5.17 Profile of $|R_1|$ for SV-wave

It is depicted from figure 5.17, that the values of $|R_1|$ shows rising trends for the case of HI and HWI in the range $0 \leq \theta \leq 36^{\circ}$ and as θ_0 increases, $|R_1|$ shows a steady behaviour.

Initially, $|R_1|$ shows an upward trend for AHI and AHWI, with a magnitude of values greater for AHI than AHWI, which reveals the impact of the impedance parameter.

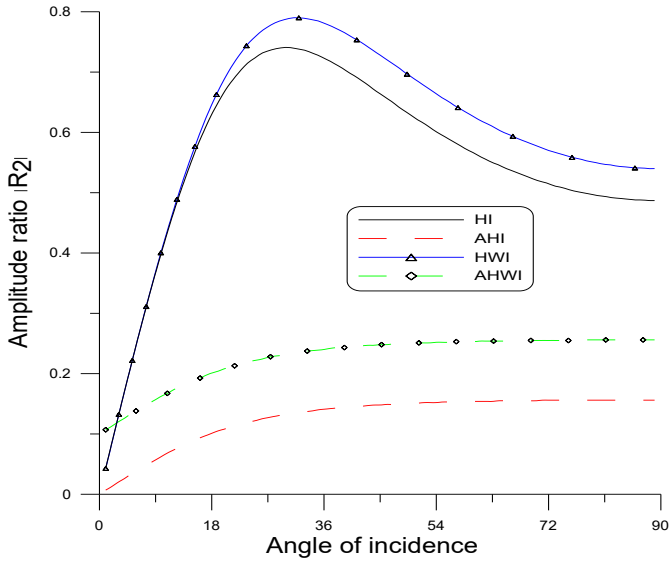

Fig.5.18 Profile of $|R_2|$ for SV- wave

Figure 5.18 indicates an increasing trend of variation for HI and HWI in the range $0 \leq \theta \leq 18^{\circ}$ followed by a decreasing trend, whereas it shows a steady state for AHWI and AHI in the whole range, except when $0 \leq \theta \leq 18^{\circ}$, where the values of $|R_2|$ shows an increasing behaviour for AHIWI and AHI due to absence of HTT parameter.

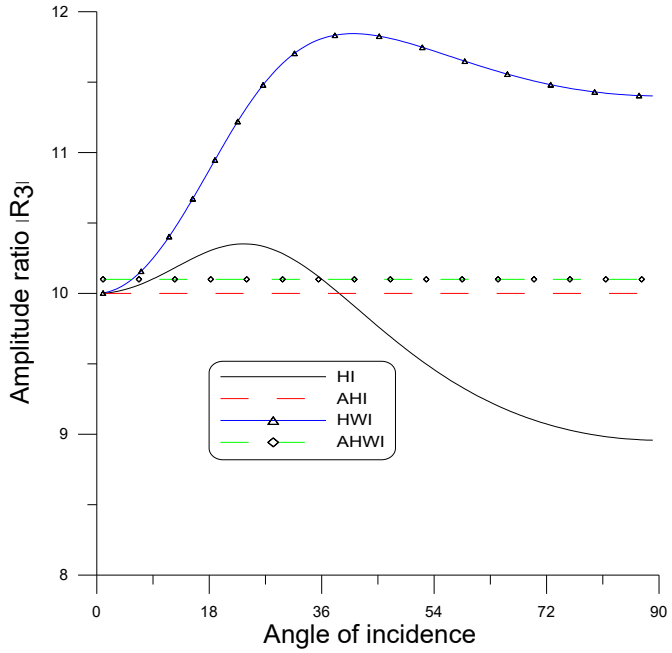

Fig.5.19 Profile of $|R_3|$ for SV-wave

Figure 5.19 demonstrates that $|R_3|$ for HI shows an increasing trend in the interval $0 \leq \theta \leq 27^{\circ}$, decreases in the left-over interval, whereas for HWI, $|R_3|$ rises in the interval $0 \leq \theta \leq 40^{\circ}$ and thereafter decreases. while for AHI and AHWI, stationary behaviour is observed.

5.10 Conclusion

In this chapter, a plane wave reflection problem for thermoelastic half-space under MGT heat equation with N-L and HTT parameters due to impedance boundary is investigated. The problem is simplified by using dimensionless quantities and potential functions. The effects of N-L, HTT, TT and impedance parameters on the AR corresponding to various reflected wave namely, P-wave, T-wave, SV-wave are computed numerically and shown graphically. The results concluded from above analysis can be summarized as

(i) It is observed that for P-wave, the N-L parameter and impedance parameter enhance the values of the AR corresponding to reflected P and T waves, whereas opposite behaviour is observed for AR of reflected SV-wave.

(ii) For T-wave, the AR relating to reflected P and SV waves increase with presence of N-L and absence of impedance parameter. Also, AR for reflected SV-wave remain higher as compared to other cases in entire domain. whereas the values of AR for reflected T-wave increases with N-L and impedance parameter which shows that N-L and impedance significantly affect the AR of reflected waves.

(iii) For SV - wave, it is observed that the AR corresponding to reflected P, T and SV waves increase and remain higher in comparison to other cases for absence of N-L and impedance parameters.

(iv) For longitudinal (P) wave, the AR relating to reflected P and SV waves exhibit increasing trend due to impedance parameter and absence of HTT parameter whereas the values of AR of reflected T wave get enhanced with HTT and impedance parameter.

(v) For T-wave, the AR corresponding to reflected P and SV waves show increasing trend due to absence of impedance and HTT parameters whereas the AR corresponding to reflected T get enhanced with HTT and impedance parameters.

(vi) For SV -wave is incident, the AR corresponding to reflected (P, T and SV) waves get enhanced and remain greater than other cases with HTT and absence of impedance parameters.

This study's findings highlight the significant impact of N-L, HTT, and impedance parameters on AR of reflected waves. The current research will be beneficial for scientists studying thermoelasticity using non-Fourier heat conduction models in solid materials within the Earth. This study is particularly relevant to geophysical investigations, especially those related to earthquakes, seismology, and engineering phenomena.

Conclusion and Future Scope

In Chapter 2, a mathematical model of thermoelasticity incorporating non-local (N-L) effects and two temperatures is developed to address the deformation problem in a homogeneous, isotropic, thermoelastic semi-space. The governing equations are simplified using dimensionless variables and potential functions. Integral transform techniques, specifically Laplace Transform and Fourier Transform ((L.T and F.T) are employed to solve the problem. The effects of non-local and two-temperature phenomena are investigated through an exponentially decaying normal force and a concentrated ramp-type heat source. The results indicate that the non-local parameter substantially increases the normal stress, tangential stress, and both thermodynamic and conductive temperatures. The study shows that while normal stress, tangential stress, thermodynamic temperature, and conductive temperature exhibit comparable behavior across varying heat source parameter values, their oscillation amplitudes differ. Furthermore, for smaller values of the heat source parameter lead to an increase in normal stress, thermodynamic temperature, and conductive temperature. The Two-Temperature (TT) parameter boosts the conductive temperature, whereas the values of normal and tangential stress remain unchanged. The Green and Lindsay (G-L) model forecasts greater values for stress and conductive temperature compared to the modified Green-Lindsay (M G-L) and Lord-Shulman (L-S) models

In chapter 3, the deformation problem of a thermoelastic half-space is explored using the Moore-Gibson-Thompson (MGT) heat equation with non-local and hyperbolic two-temperature. The equations are simplified with dimensionless quantities, and potential functions along with integral transforms (L.T and F.T) are applied. The study focuses on a heat source modeled as a laser pulse that decays over time and moves with a constant velocity, along with thermomechanical loading. Normal distributed force and ramp-type thermal source are used to demonstrate the problem's effectiveness. The introduction of Normal Distributed Force (NDF) leads to increased normal and tangential stresses, with more noticeable effects, especially at intermediate values of the N-L parameter. In contrast, when a ramp-type thermal source (RTTS) is present, normal stress remains elevated across

all intervals, while tangential stress and temperature display oscillatory patterns, with more significant fluctuations occurring in the absence of the N-L parameter. A higher value of the moving heat source parameter significantly raises normal stress, thermodynamic temperature, and conductive temperature for both NDF and RTTS. Furthermore, the Hyperbolic Two-Temperature (HTT) parameter substantially amplifies the effects of thermodynamic and conductive temperatures compared to the normal and tangential stresses produced by NDF and RTTS.

In Chapter 4, a two-dimensional axi-symmetric problem is examined within a thermoelastic half-space, which incorporates fractional order derivatives (FOD) along with N-L and hyperbolic two-temperature (HTT) in relation to the MGT heat equation as a response to mechanical loading. The field equations and the constitutive relations are established, assuming there are no body forces or heat sources present. The governing equations are formulated using cylindrical coordinates specifically for axisymmetric scenarios. The resulting two-dimensional equations are adjusted with non-dimensional terms and analyzed through the Helmholtz decomposition theorem. The solution to the problem is obtained by employing the Laplace transform (L.T) and the Hankel transform (H.T). Applications include considerations of ring and disc loads.

It has been noticed that when subjected to the disc load, the effects of the HTT parameter lead to an increase in the normal stress, tangential stress, and thermodynamic temperature, whereas a contrasting effect is seen for the conductive temperature close to the loading surface. Whereas when subjected to ring load, the tangential stress and thermodynamic temperature show oscillatory behavior. It has been noted that the absolute values of normal stress , tangential stress are higher in the GN (Green and Naghdi)-III model, whereas the levels of thermodynamic temperature and conductive temperature increase in the MGT model due to the disc load. Energy dissipation elevates the stress levels in the GN-III model, while the magnitude of thermodynamic and conductive temperatures rises in the MGT thermoelastic model. As a result of ring load, the patterns of the curves related to thermodynamic and conductive temperature are quite alike for both the MGT and L-S models, whereas an oscillatory behavior is noted in the GN-III model.

The tangential stress and conductive temperature decrease near the loading point, and beyond that point, they exhibit oscillatory behavior in all examined scenarios because of a disc load. Under a ring load, both normal stress, tangential stress rise near the loading surface, while the stress component values are significantly greater without the N-L parameter. However, a moderate non-local parameter enhances the intensity of thermodynamic and conductive temperatures..

Chapter 5 explores the behavior of plane waves in a homogeneous, isotropic, thermoelastic medium using the MGT heat equation, and examines the impacts of non-local effects, hyperbolic two-temperature (HTT) , and impedance parameters. For the two-dimensional scenario, the governing equations are normalized, and potential functions are employed for further clarification. A reflection problem involving a plane wave in a thermoelastic half-space governed by the MGT heat equation with non-local N-L and HTT parameters due to an impedance boundary is addressed. It is noticed that for P-wave, the non-local parameter and impedance parameter enhance the values of the Amplitude ratios (AR) corresponding to reflected P and T waves, whereas opposite behaviour is observed for AR of reflected SV-wave. For T-wave, the AR relating to reflected P and SV waves increase with presence of non-local and absence of impedance parameter. Also, AR for reflected SV-wave remain higher as compared to other cases in entire domain. whereas the values of AR for reflected T-wave increases with N-L and impedance parameter which shows that N-L and impedance significantly affect the AR of reflected waves. For SV - wave, it is observed that the AR corresponding to reflected P, T and SV waves increase and remain higher in comparison to other cases for absence of N-L and impedance parameters.

The thesis may be extended to consider material anisotropy and higher-order symmetries over time. The research presented in this thesis can be applied to visco-thermoelastic media, micropolar thermoelastic media, orthotropic thermoelastic materials, fibre-reinforced thermoelastic materials, composite materials, non-local thermoelastic materials, thermoelastic materials with cubic symmetry, piezo-electric thermoelastic, and piezo-thermoelastic materials. These challenges may also be examined by considering the effects of magnetic, rotation, etc.

Mathematical modeling can be described using finite element, homotopy perturbation, and other numerical techniques. The governing equations of these models can be solved analytically as well as numerically to obtain expressions for displacement components, stress components, temperature change and various other components considered in the studies by using various other methods like Normal mode analysis, complex analysis (integral using residue at poles etc.), State space approach, fractional calculus and Eigen value approach. The fundamental models listed above can be extended to spherical coordinates. As a result, the research presented in this thesis is available to a wide range of researchers interested in thermoelasticity. There is a scope for investigating waves and vibration difficulties in the considered models

Bibliography

[1] Abbas, I. Hobiny, A., and El-Bary, A.: The effects of fractional time derivatives in bioheat conduction technique on tumor thermal therapy, *Journal of Non-Equilibrium Thermodynamics*, 49(1), 61-72, (2024), https://doi.org/10.1515/jnet-2023-006.

[2] Abbas, I., Hobiny, A., Vlase, S. and Marin, M.: Generalized Thermoelastic Interaction in a Half-Space under a Nonlocal Thermoelastic Model, *Mathematics*, 10(13), 2168, (2022),https://doi.org/10.3390/math10132168.

[3] Abouelregal, A.E., Akgöz,B., and Civalek,O.: Magneto-thermoelastic interactions in an unbounded orthotropic viscoelastic solid under the Hall current effect by the fourth-order Moore-Gibson-Thompson equation, *Computers and Mathematics with Applications*, 141, 102-115, (2023), https://doi: 10.1016/j.camwa.2023.04.001.

[4] Abouelregal, A.E., and Alesemi, M.: Evaluation of the thermal and mechanical waves in anisotropic fiber-reinforced magnetic viscoelastic solid with temperature-dependent properties using the MGT thermoelastic model, *Case Studies in Thermal Engineering*, 36, 102187, (2022), https://doi.org/10.1016/j.csite.2022.102187.

[5] Abouelregal, A.E., Mohammad-Sedighi, H., and Shirazi, A.H.:Computational analysis of an infinite magneto-thermoelastic solid periodically dispersed with varying heat flow based on non-local Moore–Gibson–Thompson approach.Continuum, *Mechanics and Thermodynamics*, 34, 1067–1085, (2022), https://doi.org/10.1007/s00161-021-00998-1.

[6] Abouelregal, A.E., Marin, M., Alharbi, H.A., and Alrouili, K.J.A.: Modeling the thermal behavior of functionally graded media with a spherical gap: rectified sine wave heating via fourth-order Moore–Gibson–Thompson model, *Mechanics of Time-Dependent Materials*, 28, 681–707, (2024), https://doi.org/10.1007/s11043-024-09688-2.

[7] Abouelregal, A.E., Marin, M., and Öchsner, A.: The influence of a non-local Moore–Gibson–Thompson heat transfer model on an underlying thermoelastic material under the model of memory-dependent derivatives, *Continuum Mechanics and Thermodynamics*, 35, 545-562, (2023), https://doi.org/10.1007/s00161-023-01195-y.

[8] Al-Lehaibi, E A.N.: The vibration analysis of a nanobeam due to a ramp-type heating under Moore-Gibson-Thompson theory of thermoelasticity, *Journal of Vibration engineering*, 24(3), 394-404, (2022).

[9] Ailawalia, P., and Gupta, P.: Effect of thermal conductivity in a semiconducting medium under modified Green-Lindsay theory, *International Journal of Computing Science and Mathematics*, 19, 167-179, (2024), https://doi.org/10.1504/IJCSM.2024.137263.

[10] Amin, M.M., El-Bary, A.A., and Youssef, H.M.: Two-dimensional problem of generalized thermoelastic half-space subjected to moving heat source, *Microsystem Technologies*, 23, 4611–4617, (2017), https://doi.org/10.1007/s00542-017-3281-4.

[11] Askar, S.S., Abouelregal, A.E., Foul, A., and Sedighi, H.M.: Pulsed excitation heating of semiconductor material and its thermomagnetic response on the basis of fourth-order MGT photothermal model, *Acta Mechanica*,234, 4977–4995, (2023), https://doi.org/10.1007/s00707-023-03639-7 .

[12] Bachher, M., and Sarkar, N.: Nonlocal theory of thermoelastic materials with voids and fractional derivative heat transfer, *Waves in Random and Complex Media*, 29(4), 595–613, (2018), https://doi.org/10.1080/17455030.2018.1457230 .

[13] Bagley R.L., and Torvik, P.J.: A theoretical basis for the application of fractional calculus to viscoelasticity, *Journal of Rheology*, 27, 201–210, (1983).

[14] Bajpai, A., Kumar, R., and Sharma, P.K.: Modeling of hyperbolic two temperature fractional thermodiffusive elastic circular plate, *Mechanics of Solids*, 58, 297–314, (2023), https://doi.org/10.3103/S0025654422601136 .

[15] Bajpai, A., Kumar, R., and Sharma, P.K.: Axisymmetric half-space problem in thermoelastic diffusion under phase lags and hyperbolic two temperature, *Journal of Thermal Stresses,* 46, 535-551, (2023), https://doi.org/10.1080/01495739.2023.2191661.

[16] Bajpai, A., Kumar, R. and Sharma, P.K.: Analysis of wave motion and deformation in elastic plate based on two temperature theory of thermoelasticity, *Waves in Random and Complex Media*, 33(3), 680-701, (2023).

[17] Bajpai, A., Sharma, P.K., and Kumar, R.: Modeling of thermoelastic diffusion plate under two temperature, fractional-order and temperature-dependent material properties, *Journal of Applied Mathematics and Mechanics*, 101(10), (2021), https://doi.org/10.1002/zamm.202000321.

[18] Bajpai, A., Sharma, P.K., and Mishra, K.C.: Transient response of two-temperature axisymmetric fractional thermo-diffusive elastic half-space with variable thermal conductivity and diffusivity, *Waves in Random and Complex Media*, (2024), https://doi.org/10.1080/17455030.2024.2307452.

[19] Balta, F., and Suhubi, E. S.: Theory of nonlocal generalised thermoelasticity, *The International Journal of Engineering Science*, 15, 579–588, (1977).

[20] Bayones, F.S.: An internal heat source in temperature rate dependent thermoelastic medium subjected to the effect of rotation and gravity field, *African Journal of Mathematics and Computer Science Research*, 13(1), 24–38, (2020), https://doi: 10.5897/ajmcsr2019.0805.

[21] Bazarra, N., Fernández, J.R., Liverani, L., and Quintanilla, R.: Analysis of a thermoelastic problem with the Moore–Gibson–Thompson micro temperatures, *Journal of Computational and Applied Mathematics*, 438, (2024), https://doi.org/10.1016/j.cam.2023.115571

[22] Bazarra, N., Fernández, J.R., and Quintanilla, R.: On the decay of the energy for radial solutions in Moore–Gibson–Thompson thermoelasticity, *Mathematics and Mechanics of Solids*, 26, (2021), https://doi.org/10.1177/1081286521994258.

[23] Bazarra, N., Fernández, J.R., and Quintanilla, R.: Numerical analysis of a thermoelastic dielectric problem arising in the Moore–Gibson–Thompson theory, *Journal of Computational and Applied Mathematics*, 414, (2022), https://doi.org/10.1016/j.cam.2022.114454.

[24] Biot, M.A.: Thermoelasticity and irreversible thermodynamics, *Journal of Applied Physics*, 27, (1956), https://doi.org/10.1063/1.1722351.

[25] Caputo, M.: Vibrations of an infinite viscoelastic layer with a dissipative memory, *The Journal of the Acoustical Society of America*, 56(3), 897-904, (1974).

[26] Caputo, M., and Mainardi,F.: A new dissipation model based on memory mechanism, *Pure and applied Geophysics*, 91, 134-147, (1971).

[27] Caputo, M. and Mainardi,F.: Linear models of dissipation in anelastic solids, *La Rivista del Nuovo Cimento*, 1(2) , 161-198, (1971).

[28] Cattaneo, C.: A form of heat-conduction equations which eliminates the paradox of instantaneous propagation, *Comptes rendus,* 247, 431-433, (1958).

[29] Chandrasekharaiah D.S.; Hyperbolic thermoelasticity: *a review of recent literature. Applied Mechanics Reviews*, 51(12), 705-72, (1998).

[30] Chen, P.J., and Gurtin, M E.: On a theory of heat conduction involving two-temperatures, *Journal of Applied Mathematics and Physics*,19, 614–627, (1968).

[31] Chen, P.J., Gurtin, M.E., and Williams, W.O.: On the thermodynamics of non-simple elastic materials with two temperatures, *Journal of Applied Mathematics and Physics*, 107–112, (1969).

[32] Conti, M., Dell'Oro, F., Liverani, L. and Pata, V.: Spectral analysis and stability of the Moore-Gibson-Thompson-Fourier model, *Journal of Dynamics and Differential Equations*, 36(1), 775-795, (2024).

[33] Conti, M., Pata, V., Pellicer, M., and Quintanilla, R.: A new approach to MGT-thermoviscoelasticity, *Discrete and Continuous Dynamical Systems*, 41, 4645–4666, (2021), https://doi.org/10.3934/dcds.2021052.

[34] Conti, M., Pata, V.: and Quintanilla, R.: Thermoelasticity of Moore–Gibson–Thompson type with history dependence in the temperature, *Asymptotic analysis*, 27,1-21, (2019), doi:10.3233/ASY-191576.

[35] Conti, M., Pata, V., and Quintanilla, R.: Thermoelasticity of Moore-Gibson-Thompson type with history dependence in the temperature, *Asymptotic Analysis*, 120,1–21 (2020), https://doi.org/10.3233/ASY-191576.

[36] Das, N., De, S., and Sarkar, N.: Plane waves in Moore–Gibson–Thompson thermoelasticity considering nonlocal elasticity effect, *Mathematics and Mechanics of Solids*, 28, (2023), https://doi.org/10.1177/10812865221145737.

[37] Debnath, L.: *Integral transforms and their applications*. CRC Press, (1995).

[38] Dhaliwal, R.S. and Singh, A.: *Dynamical coupled thermoelasticity*, Delhi, Hindustan Publishing Corporation, (1980).

[39] Dhaliwal, R. S. and Rokne, J. G.: One-dimensional thermal shock problem with two relaxation times, *Journal of Thermal Stresses*, 12(2),259–279, (1989).

[40] Duhamel, J.: Une memoire sur les phenomenes thermo-mechaniques, *Journal De I'Ecole Polytechnique,* 15, 1-57, (1837).

[41] Eringen, A.C.: Nonlocal polar elastic continua, *International Journal of Engineering Science,* 10, 1–16, (1972).

[42] Eringen, A.C.: Theory of nonlocal thermoelasticity, *International Journal of Engineering Science,* 12, (1974), https://doi.org/10.1016/0020-7225(74)90033-0.

[43] Eringen, A.C.: *Nonlocal continuum field theories*, Springer, (2002).

[44] Ezzat, M.A., and El-Karamany, A.S.: Fractional order theory of a perfect conducting thermoelastic medium, *Canadian Journal of Physics*, 89, 311–318 (2011), https://doi.org/10.1016/j.aml.2020.106628.

[45] Ezzat, M.A., El-Karamany, A.S., and El-Bary, A.A.: Two-temperature theory in Green–Naghdi thermoelasticity with fractional phase-lag heat transfer, *Microsystem Technologies,* 24, 951–961, (2018), https://doi.org/10.1007/s00542-017-3425-6.

[46] Geetanjali, G., Bajpai, A. and Sharma, P.K.: Memory response of hyperbolic two-temperature thermoelastic diffusive half-space with variable material properties, *Archive of Applied Mechanics*, 93, 467–485, (2023), https://doi.org/10.1007/s0419-022-02276-1.

[47] Green, A.E., and Lindsay, K.A.: Thermoelasticity, *Journal of Elasticity*, 2, 1–7, (1972).

[48] Green, A. E., and Naghdi, P.M.: A re-examination of the basic postulates of thermomechanics, *Proceedings of The Royal Society*, 432, 171–194, (1991).

[49] Green, A.E., and Naghdi, P.M.: On undamped heat waves in an elastic solid, *Journal of Thermal Stresses*, 15, 253–264, (1992).

[50] Green, A.E., and Naghdi, P.M.: Thermoelasticity without energy dissipation, *Journal of Elasticity*, 31, 189–208, (1993).

[51] Gupta, S., Dutta, R., and Das, S.: Memory response in a nonlocal micropolar double porous thermoelastic medium with variable conductivity under Moore-Gibson-Thompson thermoelasticity theory, *Journal of Ocean Engineering and Science*, 8, 263–277, (2023), https://doi.org/10.1016/j.joes.2022.01.010.

[52] Hilfer, R.: *Applications of fractional calculus in physics*. World scientific, Germany (2000).

[53] Honig, G., and Hirdes, U.: A method for the numerial inversion of the Laplace transform, *Journal of Computational and Applied Mathematics*, 10, 113-132, (1984).

[54] Ignaczak, J., and Mr´owka-Matejewska, E.: One-dimensional green's function in temperature-rate dependent thermoelasticity, *Journal of Thermal Stresses*, 13, (1990), https://doi.org/10.1080/01495739008927038.

[55] Jangid, K., and Mukhopadhyay, S.: A domain of influence theorem under MGT thermoelasticity theory, *Mathematics and Mechanics of Solids*, 26, 285–295, (2021), https://doi.org/10.1177/1081286520946820.

[56] Jangid, K., and Mukhopadhyay, S.: Thermoelastic interactions on temperature-rate-dependent two-temperature thermoelasticity in an infinite medium subjected to a line heat source, *Journal of Applied Mathematics and Physics*, 73(5),196, (2022).

[57] Jangid, K., Gupta, M., and Mukhopadhyay, S.: On propagation of harmonic plane waves under the Moore–Gibson–Thompson thermoelasticity theory, *Waves in Random and Complex Media*. (2021), https://doi.org/10.1080/17455030.2021.1949071.

[58] Jeffreys, H.: The thermodynamics of an elastic solid. *Mathematical Proceedings of the Cambridge Philosophical Society*, 26, 101–106, (1930), Cambridge University Press.

[59] Kaur, I., Singh, K., and Craciun, E. M.: New modified couple stress theory of thermoelasticity with hyperbolic two temperature, *Mathematics,* 11(2), 432, (2023).

[60] Kaushal, S., Kumar, R., Lofty, K., and Bala, I.: Response of frequency domain in generalized thermoelastic medium under modified Green-Lindsay with non-local and two temperature, *Journal of Applied Mathematics and Mechanics*, 104, (2024), https://doi.org/10.1002/zamm.202301012.

[61] Kaushal, S., Kumar, R., and Parmar, K.: Influence of Diffusion and Impedence Parameters on Wave Propagation in Thermoelastic Medium, *International Journal of Applied Mechanics and Engineering*, 26, 99–112, (2021), https://doi.org/10.2478/ijame-2021-0052.

[62] Khavale, S.G., and Gaikwad, K.R.: Fractional ordered thermoelastic stress analysis of a thin circular plate under axi-symmetric heat supply, *International Journal of Nonlinear Analysis and Applications*, 4, 207-219, (2023), doi: 10.22075/ijnaa.2023.29131.4067.

[63] Kumar, R., and Devi, S.: Thermoelastic beam in modified couple stress thermoelasticity induced by laser pulse, *Computers and Concrete*, 19(6), 701-710, (2017).

[64] Kumar, R., Ghangas, S., and Vashishth, A. K.: Fundamental and plane wave solution in non-local bio-thermoelasticity diffusion theory, *Coupled Systems Mechanics*, 10(1), 521–538, (2021), doi: 10.12989/csm.2021.10.1.021.

[65] Kumar, R., Kaushal, S., and Dahiya, V.: Axisymmetric problem in modified couple stress thermoelastic with void, diffusion and phase lags, *Journal of Thermal Stresses*, 46, 351–368, (2023), https://doi.org/10.1080/01495739.2023.2174230.

[66] Kumar, R., Kaushal, S., and Kochar A.: Response of impedance parameters on waves in the micropolar thermoelastic medium under modified Green-Lindsay theory, *Journal of Applied Mathematics and Mechanics*, 102, 9 (2022).

[67] Kumar, R., Kaushal, S., and Kochar, A.: Analysis of wave motion in micropolar thermoelastic medium based on Moore–Gibson–Thompson heat equation under non-local and hyperbolic two-temperature, *International Journal of Applied and Computational Mathematics*, 10, (2024), https://doi.org/10.1007/s40819-023-01667-4.

[68] Kumar, R., Kaushal, S., and Kochar, A.: Analysis of axisymmetric deformation in generalized micropolar thermoelasticity within the framework of Moore-Gibson-Thompson heat equation incorporating non-local and hyperbolic two-temperature effect, *Journal of Strain Analysis for Engineering Design*, 59, (2024), https://doi.org/10.1177/03093247241232180.

[69] Kumar, R., Kaushal, S., and Kochar, A.: Mathematical modelling of micropolar thermoelastic problem with nonlocal and hyperbolic two-temperature based on Moore–Gibson–Thompson heat equation, *Canadian Journal of Physics*, 101, 663–672 (2024), https://doi.org/10.1139/cjp-2022-0339.

[70] Kumar, R., Kumar, S., and Gourla, M.G.: Axisymmetric Problem in Thermoporoelastic Medium, *American Journal of Engineering Research*,5(4),1-4, (2014).

[71] Kumar, R., Sharma, N. and Lata P.: Thermomechanical interactions due to hall current in transversely isotropic thermoelastic with and without energy dissipation with two temperatures and rotation, *Journal of Solid Mechanics*, 8(4), 840-858, (2016).

[72] Kumar, R., Rani, R., and Miglani, A.: A problem of axisymmetric vibration of nonlocal microstretch thermoelastic circular plate with thermomechanical sources, *Journal of Solid Mechanics,* 11, 1–13, (2019), https://doi.org/10.22034/JSM.2019.664213

[73] Kumar, R., Sharma, N., and Chopra, S.: Photothermoelastic interactions under Moore-Gibson-Thompson thermoelasticity, *Coupled Systems Mechanics*, 11, (2022), https://doi.org/10.12989/csm.2022.11.5.459.

[74] Kumar, R., Vashishth, A.K. and Ghangas, S.: Nonlocal heat conduction approach in a bi-layer tissue during magnetic fluid hyperthermia with dual phase lag model, *Bio-Medical Material Engineering*, 30, 387-402, (2019), https://doi.org/10.3233/BME-191061.

[75] Kumar, S., Partap, G. and Kumar, R.: Impact of temperature-dependent parameters on wave motion in a micropolar thermoelastic plate involving memory-dependent derivatives, *Acta Mechanica*, 235, 429–439, (2024), https://doi.org/10.1007/s00707-023-03737-6 .

[76] Kumar, S., Partap, G. and Kumar, R.: Memory-dependent derivatives effect on waves in a micropolar generalized thermoelastic plate including three-phase-lag model, *Indian Journal of Physics*, 97, 3589–3600, (2023), https://doi.org/10.1007/s12648-023-02705-z

[77] Kumar, R., Sharma, N. and Chopra, S.: deformation analysis in photo-viscothermoelastic plate with fractional order derivative, *Journal of hunan university*, 49(12), (2023).

[78] Lata, P., and Singh, S.: Axisymmetric deformations in a nonlocal isotropic thermoelastic solid with two temperature, *Forces in Mechanics*, 6, (2022), https://doi.org/10.1016/j.finmec.2021.100068.

[79] Lata, P., and Singh, S.: Effects of nonlocality and two temperature in a nonlocal thermoelastic solid due to ramp type heat source, *Arab Journal of Basic and Applied Sciences*, 27, 357–363, (2020), doi: 10.1080/25765299.2020.1825157.

[80] Liang, H., Lan, M., and Zhang, J.: Influences of Relaxation Times and Interface Effect on the Reflection and Transmission of Thermoelastic Waves under the MGL Model, *Mechanics of Solids*, 58, (2023), https://doi.org/10.3103/S0025654422601203 .

[81] Lord, H.W., and Shulman, Y.: A generalized dynamical theory of thermoelasticity, *Journal of Mechanics and Physics of Solids*, 15(5), 299–309, (1967).

[82] Lotfy, K., Seddeek, M., and Hassanin, W.S.: Analytical Solutions of Photo-Generated Moore–Gibson–Thompson Model with Stability in Thermoelastic Semiconductor Excited Material, *Silicon*, 14, 12447–12457, (2022).

[83] Malik, S., Gupta, D., Kumar, K. and Sharma, R.K.: Plane wave propagation and fundamental solution in functionally graded couple stress micropolar thermoelastic solid with diffusion and voids, *Waves in Random and Complex Media*, 1-27, (2022).

[84] Malischewsky P.G.: Surface Waves and Discontinuities. *Elsevier,* Amsterdam (1987).

[85] Marin, M., Öchsner, A., and Bhatti, M.M.: Some results in Moore-Gibson-Thompson thermoelasticity of dipolar bodies, *Journal of Applied Mathematics and Mechanics*, 100, (2020), https://doi.org/10.1002/zamm.202000090.

[86] Miglani, A., and Kaushal, S.: Axi-Symmetric Deformation in Generalized Thermoelasticity with Two Temperatures, *Arabian Journal for Science and Engineering*, 36, 1581–1595, (2011), https://doi.org/10.1007/s13369-011-0139-4 .

[87] Mirparizi, M., and Razavinasab, M, S.: Modified Green–Lindsay analysis of an electro-magneto elastic functionally graded medium with temperature dependency of materials, *Mechanics of Time-Dependent Materials*, 26, (2022), https://doi.org/10.1007/s11043-021-09517-w.

[88] Mohamed, M.S., Lotfy, K., El-Bary, and Mahdy, M.S.: Absorption illumination of a 2D rotator semi-infinite thermoelastic medium using a modified Green and Lindsay model, *Case Studies in Thermal Engineering*, 26, (2021), https://doi.org/10.1016/j.csite.2021.101165.

[89] Neumann, F.:Vorlesungen uber die theorie der elasticitat, Breslau, Meyer, (1885).

[90] Oldham, K. and Spanier, J.: *The Fractional Calculus Theory and Applications of Differentiation and Integration to Arbitrary Order*, Elsevier, ISBN: 9780080956206 (1974).

[91] Othman, M.I.A., Said, S.M., and Gamal, E.M.: influence of gravity and hall current on a two-temperature fiber-reinforced magneto-visco-thermoelastic medium using a Modified Green-Lindsay model, *Mechanics of Solids*, 58, 3428–3447, (2023), https://doi.org/10.3103/S0025654423601763.

[92] Podlubny, I.: *Fractional differential equations: an introduction to fractional derivatives, fractional differential equations, to methods of their solution and some of their applications*, 198, Elsevier, San Diego (1998).

[93] Povstenko, Y.: Fractional heat conduction equation and associated thermal stress, *Journal of Thermal Stresses,* 28, (2005), https://doi.org/10.1080/014957390523741.

[94] Povstenko, Y.: Thermoelasticity which uses fractional heat conduction equation, *mathematical physics Fields*, 51(2), 239–246, (2008).

[95] Povstenko, Y.: Space-time-fractional heat conduction equation and the theory of thermoelasticity. In: 3rd IFAC Workshop on Fractional Differentiation and its Applications, Ankara, Turkey, 5–7, (2008).

[96] Povstenko, Y.: Thermoelasticity which uses fractional heat conduction equation, *Journal of Mathematical Sciences*, 162, 296–305, (2009).

[97] Povstenko, Y.: Theory of thermoelasticity based on the space-time-fractional heat conduction equation, *Physica Scripta*, 136,1–6, (2009).

[98] Povstenko, Y.: Theories of thermoelasticity based on space-time-fractional Cattaneo-type equation. Proceedings of the 4th IFAC Workshop on Fractional Differentiation and Its Applications, Badajoz, Spain, 18–20, (2010).

[99] Povstenko, Y.: Fractional Cattaneo-type equations and generalized thermoelasticity, *Journal of Thermal Stresses*, 34, 97–114, (2011).

[100] Povstenko, Y.: Non-axisymmetric solutions to time-fractional diffusion-wave equation in an infinite cylinder, *Fractional Calculus Applied Analysis*, 14, 418–435, (2011).

[101] Povstenko, Y.: Different kinds of boundary condition for time-fractional heat conduction equation. In: Proceedings of the 2012 13th International Carpathian Control Conference, ICCC 2012, 588–591, (2012).

[102] Prasad, R., and Kumar, R.: Some qualitative results in hyperbolic two-temperature generalized thermoelasticity, *Mathematics and Mechanics of Solids*, 29(10), 2081-2091, (2024), doi:10.1177/10812865241253208 .

[103] Press, W.H., Teukolsky, S.A., Vellerling, W.T., and Flannery, B.P.: *Numerical recipes*, Cambridge University Press, (1986).

[104] Quintanilla, R.: Some qualitative results for a modification of the Green–Lindsay thermoelasticity, *Meccanica*, 53, 3607–3613, (2018), https://doi.org/10.1007/s11012-018-0889-0.

[105] Quintanilla, R.: Moore–Gibson–Thompson thermoelasticity, *Mathematics and Mechanics of Solids,* 24(12), 4020-4031, (2019).

[106] Quintanilla, R.: Moore-Gibson-Thompson thermoelasticity with two temperatures, *Applications in Engineering Science*, 1, 100006, (2020).

[107] Roychoudhuri, S.K.: On a thermoelastic three-phase-lag model, *Journal of Thermal Stresses*, 30, (2007), https://doi.org/10.1080/01495730601130919.

[108] Sarkar, N., Abo-Dahab, S.M., and Mondal, S.: Reflection of magneto-thermoelastic waves at a solid half-space under modified Green–Lindsay model with two temperatures, *Journal of Thermal Stresses,* 43, (2020), https://doi.org/10.1080/01495739.2020.1768991.

[109] Sarkar, N., and De, S.: Waves in magneto-thermoelastic solids under modified Green–Lindsay model, *Journal of Thermal Stresses*, 43(5), 594-611(2020).

[110] Sarkar, N., De, S., and Sarkar, N.: Modified Green–Lindsay model on the reflection and propagation of thermoelastic plane waves at an isothermal stress-free surface, *Indian Journal of Physics*, 94, 1215–1225 (2020), https://doi.org/10.1007/s12648-019-01566-9.

[111] Sarkar, N., and Lahiri, A.: Effect of fractional parameter on plane waves in a rotating elastic medium under fractional order generalized thermoelasticity, *International Journal of Applied Mechanics*, *4*(03), 1250030, (2012).

[112] Sarkar, N., and Mondal, S.: Thermoelastic plane waves under the modified Green–Lindsay model with two-temperature formulation, *Journal of Applied Mathematics and Mechanics,*100, (2020), https://doi.org/10.1002/zamm.201900267.

[113] Shakeriaski, F., and Ghodrat, M.: The nonlinear response of Cattaneo-type thermal loading of a laser pulse on a medium using the generalized thermoelastic model, *Theoretical and Applied Mechanics Letters*, 10, (2020), https://doi.org/10.1016/j.taml.2020.01.030

[114] Shakeriaski, F., Salehi, F., and Ghodrat, M.: Modified G-L thermoelasticity theory for nonlinear longitudinal wave in a porous thermoelastic medium. *Physica Scripta*, 96, (2021), https://doi.org/10.1088/1402-4896/ac1aff

[115] Sharma N., Kumar R., and Lata P.: Effect of two temperature and anisotropy in an axisymmetric problem in transversely isotropic thermoelastic solid without energy dissipation and with two temperature, *American Journal of Engineering Research*,4(7),176-187, (2015).

[116] Sharma, S., and Kumari, S.: Reflection of Plane Waves in Nonlocal Fractional-Order Thermoelastic Half Space,*International Journal of Mathematics and Mathematical Sciences*, 1223847, (2022).

[117] Sharma, K.: Boundary value problems in generalised thermodiffusive elastic medium, *Journal of Solid Mechanics*, 2(4), 348-362, (2010).

[118] Sharma, K.: Analysis of deformation due to inclined load in generalised thermodiffusive elastic medium, *International Journal of Engineering Science and Technology*, 3(2), 117-129, (2011).

[119] Sharma, K.: Reflection of plane waves in thermodiffusive elastic half-space with voids, *Multidiscipline Modeling in Materials and Structures*, 8(3), 269-296, (2012).

[120] Sharma, K.: Reflection at free surface in micropolar thermoelastic solid with two temperatures, *International Journal of Applied Mechanics and Engineering*, 18(1), 217-234, (2013).

[121] Sharma, K., Sharma, S., and Bhargava, R.R.: Propagation of waves in micropolar thermoelastic solid with two temperatures bounded with layers or half-space of inviscid liquid, *Mathematical Physics and Mechanics*, 16, 66-81, (2013).

[122] Sharma, N., and Kumar, R.: Photo-thermoelastic investigation of semiconductor material due to distributed loads, *Journal of Solid Mechanics*, 13(2), 202-212, (2021).

[123] Sharma, S., and Sharma, K.; Influence of heat sources and relaxation time on temperature distribution in tissues, *International Journal of Applied Mechanics and Engineering*, 19(2), 427-433, (2014).

[124] Sharma, S.,and Khator, S.: Power generation planning with reserve dispatch and weather uncertainties including penetration of renewable sources, *International Journal of Smart Grid and Clean Energy*, 292–303, (2021), https://doi.org/10.12720/sgce.10.4.292-303.

[125] Sharma, S., and Khator, S.: Micro-Grid Planning with Aggregator's Role in the Renewable Inclusive Prosumer Market,*Journal of Power and Energy Engineering*, 10, 47-62, (2022), doi: 10.4236/jpee.2022.104004.

[126] Sherief, H.H., El-Maghraby, N.M., and Abbas, M.F.: Two-dimensional axisymmetric thermoelastic problem for an infinite-space with a cylindrical heat source of a different material under Green–Lindsay theory, *Mechanics Based Design of Structures and Machines*, 50, 3404–3416, (2022), https://doi.org/10.1080/15397734.2020.1807361.

[127] Sherief, H.H., El-Sayed, A.M.A., and Abd El-Latief, A.M.: Fractional order theory of thermoelasticity, *International Journal of Solids and Structures*,47, 269–275, (2010), https://doi.org/10.1016/j.ijsolstr.2009.09.034.

[128] Sherief, H. H., and Hussein, E. M.: The effect of fractional thermoelasticity on two-dimensional problems in spherical regions under axisymmetric distributions, *Journal of Thermal Stresses*, 43(4), 440-455, (2020).

[129] Sherief, H.H., and Hussein, E.M.: Fractional order model of micropolar thermoelasticity and 2D half-space problem, *Acta Mechnica*, 234, 535–552, (2023),https://doi.org/10.1007/s00707-022-03399-w.

[130] Singh, B.: Wave propagation in context of Moore–Gibson–Thompson thermoelasticity with Klein–Gordon nonlocality,*Vietnam Journal of Mechanics*, (2024),https://doi.org/10.15625/0866-7136/19728.

[131] Singh, B., and Bijarnia, R.: Nonlocal effects on propagation of waves in a generalized thermoelastic solid half space, *Structural Engineering and Mechanics*, 77, 473–479,(2021), https://doi.org/10.12989/sem.2021.77.4.473.

[132] Singh, B. and Mukhopadhyay, S.:Galerkin-type solution for the Moore–Gibson–Thompson thermoelasticity theory, *Acta Mechanica*, 232(4), 1273-1283, (2021).

[133] Singh, B., and Mukhopadhyay, S.: On fundamental solution of Moore–Gibson–Thompson (MGT) thermoelasticity theory, *Journal of Applied Mathematics and Physics*, 74, (2023), https://doi.org/10.1007/s00033-023-01996-w.

[134] Singh, B., and Mukhopadhyay, S.: Thermoelastic vibration of Timoshenko beam under the modified couple stress theory and the Moore–Gibson–Thompson heat conduction model, *Mathematics and Mechanics of Solids*, (2023), https://doi.org/10.1177/10812865231186127.

[135] Singh, R.V. and Mukhopadhyay, S.:Mathematical significance of strain rate and temperature rate on heat conduction in thermoelastic material due to line heat source, *Journal of Thermal Stresses*, 46(11), 1164-1179, (2023).

[136] Srivastava, A., and Mukhopadhyay, S.: A study of thermoelastic interactions in thin and long radiating rods under Moore–Gibson–Thompson theory of thermoelasticity, *Acta Mechnica*, 234, 4509–4522, (2023).

[137] Sneddon, I. N.: *The Use of Integral Transforms*. Tata McGraw-Hill Publication Co. Ltd., New Delhi, (1979).

[138] Tayel, I.M., and Almuqrin, M.A.: Photothermal effects induced by laser radiation in a 2D axi-symmetric generalized thermoelastic semiconducting half space using MGL model, *Case Studies in Thermal Engineering,* 58, (2024), https://doi.org/10.1016/j.csite.2024.104438.

[139] Thompson ,P.A.: *Compressible fluid dynamics* , New York, McGraw-Hill Publication, (1972).

[140] Thomson, W.: On the thermoelastic and thermo- magnetic properties of matter, *Quarterly Journal of Mathematics*, 1,57–77, (1857).

[141] Tiersten H.F.: Elastic surface waves guided by thin films.*Journal of Applied Physics*, 40, 770-789, (1969).

[142] Tzou, D.Y.: The generalized lagging response in small-scale and high-rate heating, *International Journal of Heat and Mass Transfer*, 38, 17, 3231-3240, (1995).

[143] Voigt, W.: *Lehrbuch der Kristallphysik (Textbook of crystal physics)*,BB Teubner,Leipzig. (1928).

[144] Yadav, A.K.: Thermoelastic waves in a fractional-order initially stressed micropolar diffusive porous medium, *Journal of Ocean Engineering and Science*, 6, 376–388, (2021), https://doi.org/10.1016/j.joes.2021.04.001.

[145] Yadav, A.K.: Reflection of plane waves from the impedance boundary of a magneto-thermo-microstretch solid with diffusion in a fractional order theory of thermoelasticity, *Waves in Random and Complex Media*, 34(1), 404-433, (2024).

[146] Yadav, A.K., Sheoran D., Sangwan M., and Kalkal, K. K.: Effect of nonlocality and internal heat source on an initially stressed thermoelastic medium under MGL model, *Journal of Vibration Engineering and Technologies*, 12(4),(2024), doi: 10.1007/s42417-023-01265-0.

[147] Youssef, H.M.: Theory of two-temperature-generalized thermoelasticity, *Journal of Applied Mathematics (Institute of Mathematics and Its Applications*), 71, (2006), https://doi.org/10.1093/imamat/hxh101.

[148] Youssef, H.M.: State-space approach to two-temperature generalized thermoelasticity without energy dissipation of medium subjected to moving heat source, *Applied Mathematics and Mechanics* , 34, (2013), https://doi.org/10.1007/s10483-013-1653-7.

[149] Youssef, H.M.,and El-Bary, A.A.: Theory of hyperbolic two-temperature generalized thermoelasticity, *Materials Physics and Mechanics*, 40, (2018), https://doi.org/10.18720/MPM.4022018_4 .

[150] Yu, Y.J., Tian X., and Liu, X.R.: Size-dependent generalized thermoelasticity using Eringen's nonlocal model, *European Journal of Mechanics*, 51,96–106, (2015).

[151] Yu, Y.J., Tian, X., and Xiong, Q.: Nonlocal thermoelasticity based on nonlocal heat conduction and nonlocal elasticity, *European Journal of Mechanics*/ A Solids, 60, 238-253, (2016).

[152] Yu, Y.J., Xue, Z.N., and Tian, X.G.: A modified Green–Lindsay thermoelasticity with strain rate to eliminate the discontinuity, *Meccanica,* 53, 2543–2554, (2018), https://doi.org/10.1007/s11012-018-0843-1.

List of Publications

1. Kumar, R., Kaushal, S. and Sharma, G. "Mathematical model for the deformation in a Modified Green–Lindsay thermoelastic medium with nonlocal and two-temperature effects", Journal of Applied Mechanics and Technical Physics, 63, 448–457, (2022). https://doi.org/10.1134/S0021894422030099. (**Scopus,Web of Science (SCIE), UGC CARE LIST IF 0.5).**
2. Kumar, R., Kaushal, S. and Sharma, G. "Axi-Symmetric problem in the thermoelastic medium under Moore-Gibson-Thompson heat equation with hyperbolic two temperature, non-local and fractional order", Mechanics of Solids, 59, 410–430, (2024). https://doi.org/10.1134/S0025654423601891. **(Scopus, Web of Science (SCIE) , UGC CARE LIST, IF 0.6).**
3. Kaushal, S., Kumar, R., Bala, I. and Sharma, G. "Wave propagation at free surface in thermoelastic medium under modified Green-Lindsay model with non-local and two temperature", Structural Engineering and Mechanics, 90(2), 209, (2024), (**Scopus, Web of Science (SCIE), IF 2.2**).
4. Kaushal, S., Kumar, R., Kaur, K. and Sharma, G. "A mathematical model for the deformation problem in a generalized thermoelastic medium under Modified Green–Lindsay Model", International Applied Mechanics, 59, 742–753 (2023), https://doi.org/10.1007/s10778-024-01257-x (**Scopus, UGC CARE LIST, IF0.7).**
5. Kumar R, Kaushal S, and Sharma G, "Response of non-local and heat source in Moore-Gibson-Thompson theory of thermoelasticity with hyperbolic two temperature" WSEAS Transactions on Heat and Mass Transfer, 18,310-24, (2023). (**Scopus, SJR = 0.11**)
6. Kaushal S, Kumar R, Bala I, and Sharma G. "Impact of non-local, two temperature and impedance parameters on propagation of waves in generalized thermoelastic medium under modified Green-Lindsay model" Materials Physics and Mechanics, 2024, 52(1), 1-7. (**Scopus and Web of Science, SJR =0.19**)
7. Kumar, R., Kaushal, S. and Sharma, G. "Plane-wave vibrations in thermoelastic medium under Moore-Gibson-Thompson heat equation" **Communicated.**
8. Sharma, G., Kumar, R. and Kaushal, S. "Thermoelastic modeling under Moore-Gibson-Thompson equation in the frequency domain with fractional order derivative, hyperbolic two-temperature and non-local parameter" **Communicated.**

Conferences Attended/ Paper Presented

1. Presented a research paper titled *"**Mathematical model for the deformation in modified Green-Lindsay thermoelastic medium with two temperature**"* in the international conference on *"**Recent Developments in Mathematical Sciences and Artificial Intelligence and Machine Learning**"* held at Shri Teg Bahadur Khalsa College, Shri Anandpur Sahib, sponsored by **DBT MoST, India** on 14^{th}–15^{th} March 2023.
2. Presented a research paper titled *"**Propagation of waves at an imperfect interface in thermoelastic medium with two temperature**"* in the national conference on *"**Recent Developments in Mathematics**"* held at Kurukshetra University, Kurukshetra, sponsored by **Haryana State Council of Science and Technology** on 26^{th}–27^{th} December 2022.
3. Presented a research paper titled *"**Influence of two temperature on reflection and transmission in temperature rate dependent thermoelasticity**"* in the national conference on *"**Applications of Mathematics in Science and Technology**"* held at Maharaja Agarsen Mahavidyalaya, Jagadhri, sponsored by **Director General Higher Education, Haryana** on 1^{st} February 2020.